Journal of Medicinal Chemistry

pubs.acs.org/jmc

Article

Open Access

This article is licensed under CC-BY 4.0

Refinement of Peptidomimetics toward MUR-2425: A Brain-Penetrant and Selective Caspase-2 Inhibitor with Enhanced Pharmacokinetics

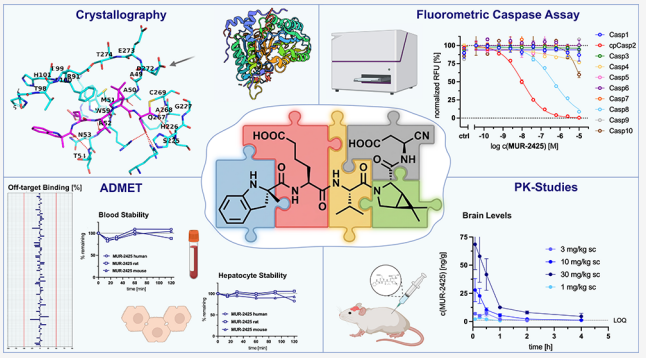
Bernadette Vallaster,[#] Lisa Forster,[#] Merlin Bresinsky, Lukas Wirth, Jessica L. Fuller, Ke Shi, Ian P. Lapcinski, Peng Liu, Deepti Mudaliar, Alexander Hubmann, Jonas Daschner, Herwig Pongratz, Marlisa Ködel, Mu Yang, Karen H. Ashe, Michael A. Walters,* and Steffen Pockes*

Cite This: https://doi.org/10.1021/acs.jmedchem.6c01371

Read Online

ACCESS | Metrics & More | Article Recommendations | Supporting Information

ABSTRACT: Caspase-2 (Casp2) has emerged as a promising target for tau-associated neurodegenerative diseases, yet the development of potent, selective, and drug-like inhibitors remains challenging. Here, we report a systematic structure−activity relationship study of 80 novel covalent-reversible peptidomimetic Casp2 inhibitors, revealing key structural features of the Casp2 S2−S3 binding site and discovering (*S*)-2-methylindoline-2-carboxylic acid (2-Me-Idc) and quinaldic acid (Quin) as versatile and stable P5 scaffolds. One-step conversion of the aldehyde warhead into a nitrile remarkably enhanced selectivity while maintaning potency. The results culminate in MUR-2425 (**87**, (2-Me-Idc)(hE)VP*D-CN), a nanomolar Casp2 inhibitor (pK_i (cpCasp2) = 7.75) with ≥525-fold selectivity over Casp1/3/4/5/6/7/9/10 and 24-fold over Casp8. MUR-2425 prevents the formation of neurotoxic Δtau314 *in vitro*, exhibits stable ADMET properties across human, rat, and mouse species and proves brain penetrance after subcutaneous injection in CD-1 mice. MUR-2425 is confirmed to engage Casp2 covalently by cocrystallization, supporting its further development for Alzheimer's disease and related dementias.



INTRODUCTION

Current therapies for Alzheimer's disease (AD) are largely symptomatic and provide only limited benefit in slowing disease progression.[1] The recent approval of monoclonal antibodies targeting the *β*-amyloid pathway represents an important therapeutic milestone. However, their clinical efficacy remains modest and their use is limited by amyloid-related imaging abnormalities (ARIA), which occur in approximately 20−30% of treated patients.[2] Moreover, these new therapies are suitable only for a subset of patients with early stage AD who present with mild cognitive impairment (MCI) and significant amyloid pathology, while patients carrying the apolipoprotein E (APOE) *ε*4/*ε*4 genotype are generally poor candidates because of their substantially increased risk of ARIA.[3] This limitations leave an unmet need for alternative therapeutic strategies targeting tau-driven neurodegeneration.

Caspase-2 (Casp2) has emerged as a promising therapeutic target for treating tauopathies in recent years. Casp2 is a member of the caspase family, a group of cysteine-dependent aspartate-directed proteases, that cleave substrates on the N-terminal side of aspartic acid residues.[4,5] Although caspases are best known as central mediators of apoptosis,[6] they also regulate nonapoptotic processes such as inflammation, cell differentiation, synaptic plasticity, dendritic development and memory formation in the central nervous system (CNS).[7−9] Structural and biochemical studies have provided detailed insights into caspase architecture, activation mechanisms, and substrate recognition, enabling the rational development of selective inhibitors.[10,11] Beside its abnormally elevated activity levels in a range of pathological conditions, such as fatty liver disease, osteoporosis, and various neurological disorders[12−15] Casp2 is an essential component in the pathological cascade that leads to neuronal damage and cognitive impairment in the CNS.[16−18] In particular, the interaction of Casp2 with the microtubule-associated protein tau has emerged as a key pathogenic mechanism. Under physiological conditions, tau is an unfolded, highly soluble protein that promotes tubulin assembly and microtubule stabilization, thereby maintaining

Received: April 28, 2026
Revised: July 28, 2026
Accepted: August 5, 2026

ACS Publications

© XXXX The Authors. Published by American Chemical Society

Downloaded from pubs.acs.org/jmcmar/article-pdf/doi/10.1021/acs.jmedchem.6c01371/6909867/acs.jmedchem.6c01371.pdf by UNIV REGENSBURG user on 17 November 2026

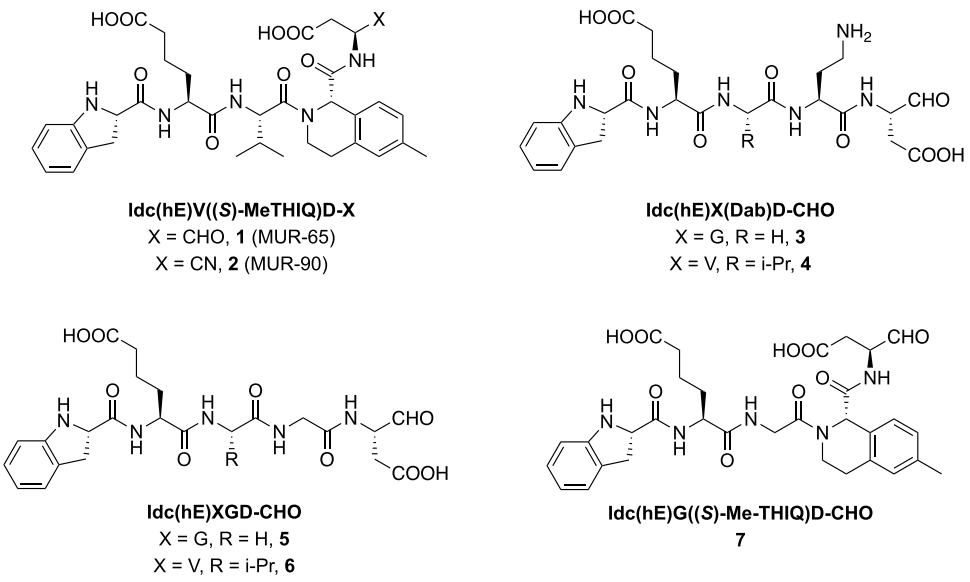


Figure 1. Structures of peptidomimetic compounds **1**−**7** representing highly selective Casp2 inhibitors.

normal neuronal function.[19] In disease, however, tau undergoes pathological post-translational modifications, including hyperphosphorylation and proteolytic truncation, leading to the formation of toxic soluble species, tau fibrils, and their accumulation within neurons.[16,20−22] Casp2 plays a pivotal role in these pathological processes, by cleaving tau at Asp314 (D314) generating the soluble tau fragment Δtau314, which has been linked to synaptic dysfunction and reversible cognitive impairment.[12,16,18] Consistent with this mechanism, elevated levels of both Casp2 and Δtau314 have been detected in post-mortem brain tissue from patients with AD or related tauopathies, such as Lewy body dementia (LBD), Parkinson's disease with dementia (PDD), or Huntington's disease (HD).[4,13,23] It has been shown that the reduction of Casp2 activity improves memory, synaptic function, and neurodegeneration in several mouse models.[7,24,25] Notably, Casp2 depletion in a mouse model of frontotemporal dementia (FTD) reduced Δtau314 and reversed memory deficits within 6 weeks.[16] Although eight of the 12 known caspases are expressed in the brain (caspases-1/-2/-3/-6/-7/-8/-9/-10), Casp2 is unique in generating the 35 kDa tau fragment Δtau314.[16] Therefore, pharmacological inhibition of Casp2 is an attractive approach for therapeutic intervention. However, despite extensive research to develop Casp2 inhibitors,[26−29] several key challenges remain: An orally available, brain-penetrant Casp2 inhibitor has not yet been reported. In addition, a significant overlap in substrate preference is found between Casp2 and caspase-3 (Casp3), which leaves the development of Casp2-specific inhibitors rather challenging but required, since active Casp3 is found in high concentrations in almost all tissues.[28,30]

Our efforts to develop selective Casp2 inhibitors initially focused on the canonical, albeit nonselective, inhibitor AcVDVAD-CHO and the Casp2 cleavage sequence of tau YKPVD314.[28] These studies identified the pentapeptide AcVDV(Dab)D-CHO as a potent inhibitor with improved selectivity over Casp3.[28] We subsequently expanded this approach by investigating peptide sequences derived from Casp2 substrates other than tau.[29] Among these, the inhibitor AcITVKD-CHO, derived from Ral GTPase-activating protein subunit α-1, was the only natural substrate-derived sequence to retain moderate Casp2 inhibitory potency while displaying slight selectivity over Casp3.[29] To address limited selectivity and unfavorable physicochemical properties of the pentapeptidic inhibitors, we next introduced peptidomimetic building blocks and unnatural amino acids identified in earlier structure activity relationship (SAR) studies.[27,31−33] This strategy yielded compound **1** (Idc(hE)V((*S*)-Me-THIQ)D-CHO, MUR-65, Figure 1) with pronounced Casp2 inhibitory potency and remarkable selectivity over Casp3. Replacing the aldehyde with a nitrile afforded compound **2** (Idc(hE)V((*S*)-Me-THIQ)D-CN, MUR-90, Figure 1), which maintained high Casp2 inhibitory potency with a further improved selectivity profile. MUR-90 rescued excitatory neurotransmission in cultured primary rat hippocampal neurons expressing the P301S tau variant linked to FTDP-17 indicating that selective Casp2 inhibition translates into functional neuroprotection.[33] In a recent study by Forster & Vallaster et al., we systematically refined the inhibitor scaffold by increasing lipophilicity, replacing amino acids with linker motifs to reduce molecular weight and hydrogen-bonding capacity and varying individual amino acid side chains.[34] Key findings from this study included the indispensable role of L-homoglutamic acid at position P4 for both Casp2 inhibitory potency and selectivity, as well as favorable effects of 2,4-diaminobutyric acid (Dab) (cf. Idc(hE)G(Dab)D-CHO (**3**) and Idc(hE)V(Dab)D-CHO (**4**), Figure 1) glycine (cf. Idc(hE)GGD-CHO (**5**) and Idc(hE)VGD-CHO (**6**), Figure 1) or (*S*)-Me-THIQ (cf. Idc(hE)G((*S*)-Me-THIQ)D-CHO (**7**), Figure 1) at P2, where Dab and (*S*)-Me-THIQ stand out as being particularly effective for improving selectivity. Glycine was found as a suitable alternative to valine in P3 expanding the accessible chemical space for P2/P3 combinations. Finally, an indoline moiety at P5 increased Casp2 inhibitory potency but suffered from rapid oxidative degradation, limiting its utility for further drug design. Building on the in depth knowledge on favorable line up for positions at P1−P4, the present study focuses on the optimization of the P5 region. Additionally, we want to make optimum use of the unique features in the Casp2 S2−S3 binding pocket and implement nitriles rather than aldehydes as the covalent reactive group. Although there are some examples in drugs and supplements,[35] aldehyde warheads are generally

Downloaded from pubs.acs.org/jmcmar/article-pdf/doi/10.1021/acs.jmedchem.6c01371/6096867/acs.jmedchem.6c01371.pdf by UNIV REGENSBURG user on 17 November 2026

https://doi.org/10.1021/acs.jmedchem.6c01371
J. Med. Chem. XXXX, XXX, XXX−XXX

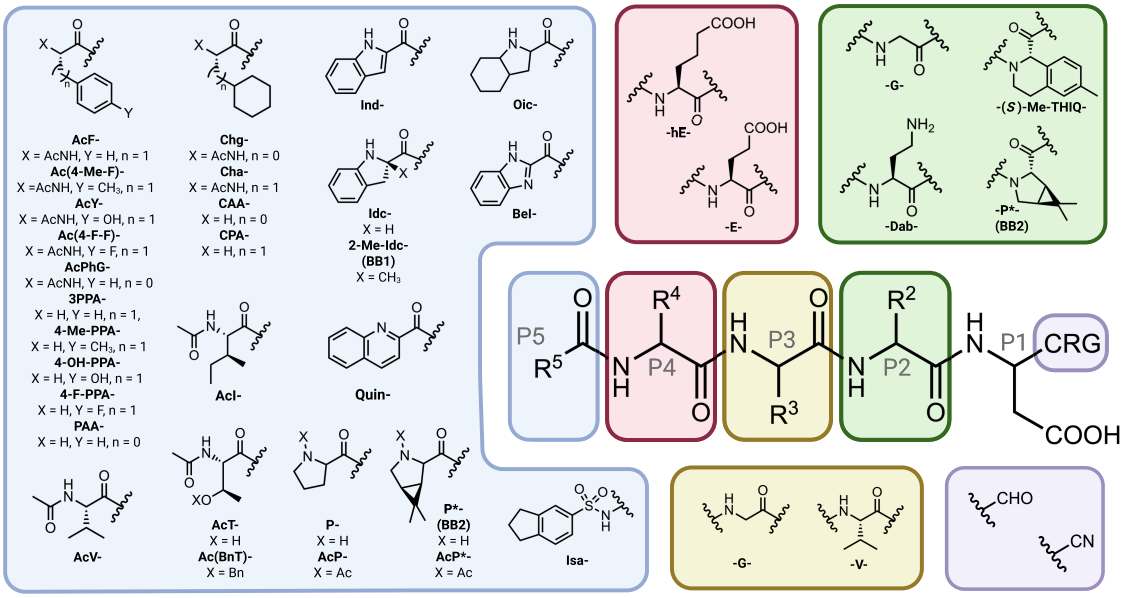


Figure 2. Schematic illustration of modifications that were applied in the design of compounds **8**−**87**. Ac = acetyl, Bn = benzyl, Ph = phenyl, h = homo. Natural amino acids are described with one letter code. Other abbreviations are assigned to the corresponding IUPAC names in the list of abbreviations at the end of the manuscript. Figure was created with BioRender.com.

considered undesirable because of their high intrinsic reactivity which increases the risk for off-target reactions with nucleophilic residues, particularly cysteine thiols.[36] In addition, their redox activity allows for a variety of possible unintended interactions with metabolic enzymes, drugs or proteins.[35] By contrast, nitriles are milder electrophiles that have a well-established track record as covalent-reversible warheads for cysteine protease inhibitors.[37,38] The clinical application of nitriles is exemplified by the antidiabetic drug saxagliptin (dipeptidyl peptidase-4 inhibitor)[39] and the inhibitor of the M^{pro} cysteine protease of SARS-CoV-2 nirmatrelvir.[40] Accordingly, the present work combines optimization of the P5 scaffold and the P2−P3 combinations with evaluation of nitrile warheads to develop selective, chemically stable and brain-penetrant Casp2 inhibitors.

LIGAND DESIGN

Compounds **1**−**7** (Figure 1) served as starting points for optimization of P5. The high inhibitory potency of previously discovered indoline-2-carboxylic acid (Idc) suggests that the Casp2 S5 pocket favors bulky, lipophilic substituents.[34] Crystal structures of the Casp2 binding site further revealed that the S5 pocket is primarily shaped by Pro385 and the aromatic side chain of Tyr383, while the P4−P5 peptide bond contributes to the proper positioning of the P5 residue.[41] In a first approach, we consequently designed novel P5 scaffolds capable of establishing hydrophobic contacts with Pro385 and aromatic π-interactions with Tyr383 while efficiently occupying the available pocket volume. Therefore, we introduced natural and unnatural amino acids at P5 comprising aromatic and saturated ring systems with varying ring sizes, side-chain lengths, and methyl-, hydroxy-, or fluoro- substituents (Figure 2). Particular emphasis was placed on scaffolds with structural resemblance to Idc. To further investigate the contribution of *N*-terminal interactions within the S5 pocket,[27] P5 acetylated analogs and derivatives bearing dialkylated *N*-termini were compared. In addition, the corresponding carboxylic acid analogs were synthesized to determine whether the backbone interactions provided by the P4−P5 peptide bond are required for high Casp2 inhibitory potency.

To further diversify the P5 scaffolds, we introduced quinaldic acid (Quin, Figure 2), a rigid and highly planar aromatic scaffold that had previously proven to be well tolerated at the P6 position in place of the N-terminal acetyl group.[34,42,43] Quin-containing Casp2 inhibitors have already shown favorable safety profiles and indications for improved cell permeability and bioavailability.[42,43] Furthermore, we evaluated (1*R*,2*S*,5*S*)-6,6-dimethyl-3-azabicyclo[3.1.0]hexane-2-carboxylic acid (P*, **BB2**, Figure 2) as a bulky, yet flexible scaffold. This bicyclic motif has already been successfully implemented in approved drugs and, therefore, represents an attractive building block for medicinal chemistry optimization.[44]

A second design strategy specifically addressed the major liability of Idc, namely its oxidative aromatization to indole.[34] We modified Idc and aimed for preventing this specific degradation mechanism by replacing the critical proton in Idc with a methyl group, resulting in (*S*)-2-methylindoline-2-carboxylic acid (2-Me-Idc, Figure 2) as a new P5 scaffold. Furthermore, we assessed the oxidized indole in P5 regarding its inhibitory potency at the target. Both motifs −indole and 2-Me-Idc− have a similar structure to Idc but mechanistically rule out the observed instability. The P5 screening was initially limited to compounds with Dab and G at P2 and later extended to (*S*)-Me-THIQ at P2. (*S*)-Me-THIQ shows most favorable properties for Casp2 inhibitory activity and selectivity from our previous studies[34] but its broad use in screening attempts was limited by commercial availability of the respective building blocks.

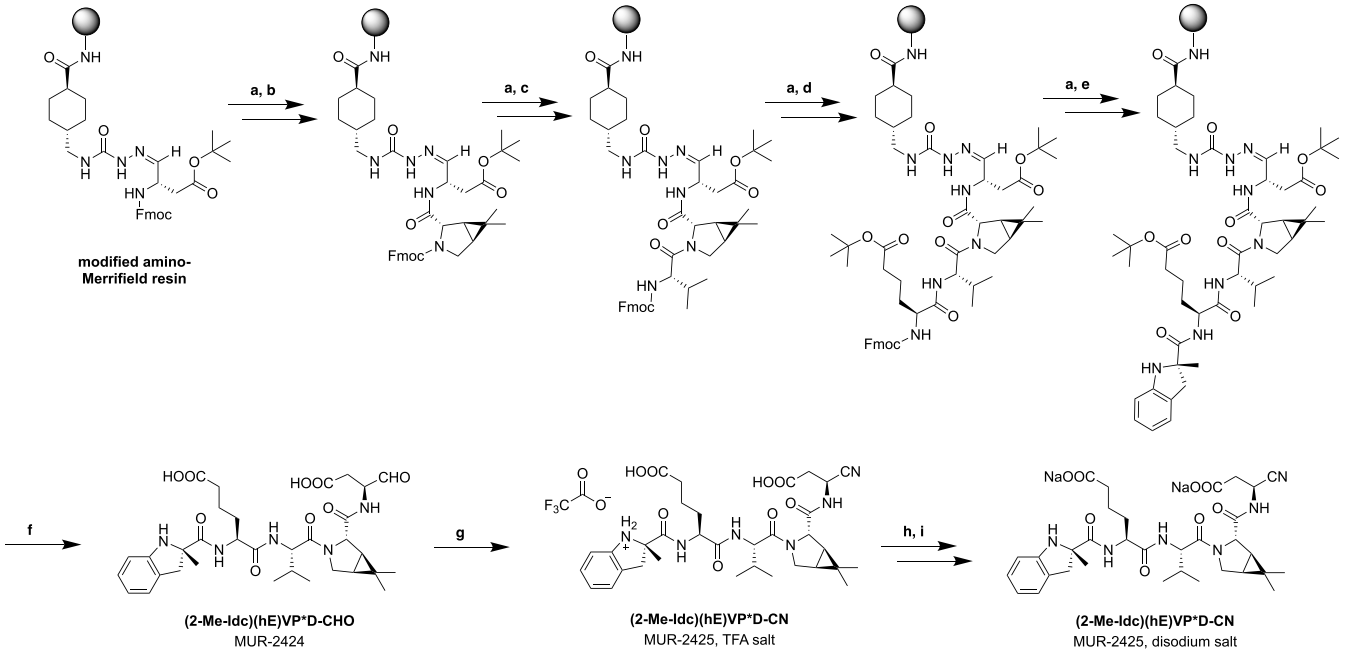
Regarding position P4, we stayed with homoglutamic acid (hE, Figure 2) as an established potency and selectivity enhancer for Casp2 inhibitors[27] and synthesized only a few compounds containing the shortened glutamic acid in P4 as negative controls.

Regarding position P3, we focused on glycine and valine throughout the study (Figure 2). Both residues were

https://doi.org/10.1021/acs.jmedchem.6c01371
J. Med. Chem. XXXX, XXX, XXX−XXX

Downloaded from pubs.acs.org/jmcmar/article-pdf/doi/10.1021/acs.jmedchem.6c01371/6909867/acs.jmedchem.6c01371.pdf by UNIV REGENSBURG user on 17 November 2026

Scheme 1. Synthesis and Salt Conversion of MUR-2425 (87)[a]



[a]Reagents and conditions: (a) piperidine 20% in DMF, 15 min, 35 °C; (b) Fmoc-P*−OH (**BB2**) (2.5 equiv), HATU (3 equiv), DIPEA (3 equiv) DMF/NMP (8/2, v/v), 45 min, 35 °C; (c) Fmoc-Val-OH (5 equiv), HATU (5 equiv), DIPEA (5 equiv) DMF/NMP (8/2, v/v), 45 min, 35 °C; (d) Fmoc-hE(OtBu)−OH (2 equiv), HATU (2.5 equiv), DIPEA (2.5 equiv) DMF/NMP (8/2, v/v), 45 min, 35 °C; (e) 2-Me-Idc−OH (**BB1**) (5 equiv), HATU (5 equiv), DIPEA (5 equiv) DMF/NMP (8/2, v/v), 45 min, 35 °C; (f) TFA/H_2O (9/1, v/v), 20 min, rt; (g) o-phenylhydroxylamine hydrochloride, 50 mM sodium phosphate buffer, rt, overnight; (h) NH_3 (aq), formic acid MeCN/H_2O; (i) 10 mM $NaHCO_3$ (aq), MeCN/H_2O. The modified amino merrifield resin was prepared according to the literature.[28,29] The synthesis of the building blocks **BB1** and **BB2** is described in Scheme S1 in the SI.

systematically combined with different P2 substituents to investigate potential cooperative structure−activity relationships between the S2 and S3 binding pockets.

Regarding position P2 of peptidic Casp2 inhibitors, sterically demanding proline-derived scaffolds were already demonstrated to improve selectivity over Casp3.[32,45] The structure-based rationale for this observation lies in the architecture of the S2 pocket of Casp2 in comparison to that of Casp3: the S2 pocket of Casp3 is partially occluded by Tyr204, resulting in steric clashes with bulky P2 substituents, whereas the corresponding pocket of Casp2 is significantly more spacious.[45] To exploit this unique structural feature of Casp2, we introduced the P* motif in P2 (Figure 2). Its bulky, flexible aliphatic framework was expected to optimally occupy the larger Casp2 S2 cavity. P* was directly compared with our so far most promising residues for P2, namely, Dab, (*S*)-Me-THIQ (Figure 2), and G. In addition, the analog of the canonical but nonselective inhibitor AcVDVAD-CHO with P* in P2 was synthesized.

Up to this point, we employed aldehydes as covalent-reversible warheads because they provide high activity, easy synthetic accessibility via solid-phase peptide synthesis, and thus good feasibility for fast and efficient SAR studies. On the way toward a clinically applicable molecule, however, the metabolically vulnerable aldehyde was replaced with the less reactive nitrile in the most promising compounds. Besides the generally improved safety profile associated with nitrile warheads, this strategy was particularly attractive since our previous work had shown that conversion of the aldehyde inhibitor MUR-65 (**1**, compound 3 in Singh et al.[33]) into its nitrile analog MUR-90 (**2**, compound 1 in Singh et al.[33]) not only maintained high Casp2 inhibitory potency but also markedly improved selectivity, especially over Caspase-1.[33]

CHEMISTRY

Reference compounds **1**−**7** have been reported and characterized in previous studies.[33,34] Peptides **8**−**87** were synthesized in accordance with the standard Fmoc strategy based on established protocols[28,29,33] using solid-phase peptide synthesis (SPPS) on an aspartic acid-loaded amino-Merrifield resin. The conversion of aldehydes to nitriles (**68**−**87**) has been carried out using o-phenylhydroxylamine according to the literature.[46] Using compound **87** (MUR-2425) as a representative example, Scheme 1 illustrates the general procedure for the synthesis of aldehydes and nitriles as further detailed in the Experimental Section. Epimerization during the nitrile conversion yielded two epimers that only differ in the absolute configuration of aspartic acid in P1 and are termed compound **X** (*S*-configuration in P1) and compound (***R***)-**X** (*R*-configuration in P1), respectively. On the basis of X-ray analysis of the cocrystallized inhibitor (**87**, MUR-2425) with JF1 cpCasp2, together with characteristic differences in the NMR spectra of the *R* and *S* epimers, the stereochemical assignments of the remaining nitriles could be established. The assignment procedure is described in detail in the Experimental Section and illustrated in Figures S250−S388 of the Supporting Information (SI). For the compounds (***rac***)**-74**, (***rac***)**-78**, (***rac***)**-82 and** (***rac***)**-83**, the epimers could not be separated. The prefix (***rac***)- indicates the mixture of both epimers in a ratio of approximately 1:1 as estimated by NMR signal integration. The compounds were usually obtained as TFA salts. Additionally, the disodium salts of compounds **79**, (***R***)-

Downloaded from pubs.acs.org/jmcmar/article-pdf/doi/10.1021/acs.jmedchem.6c01371/6909867/acs.jmedchem.6c01371.pdf by UNIV REGENSBURG user on 17 November 2026

https://doi.org/10.1021/acs.jmedchem.6c01371
J. Med. Chem. XXXX, XXX, XXX−XXX

Table 1. Enzyme Inhibitory Potency (pK_i Values) of Compounds 1-87 at cpCasp2 and Casp3

sequence	cmpd	$pK_i \pm$ SEM cpCasp2	N	Casp3	N	K_i (Casp3)/K_i (cpCasp2)
references						
AcVDVAD-CHO		8.00 ± 0.03	34	8.26 ± 0.07	6	0.5
AcDEVD-CHO		6.60 ± 0.32[a,28]	3	8.68 ± 0.26[28]	3	0.008[28]
Idc(hE)V((*S*)-Me-THIQ)D-CHO	**1**	7.40 ± 0.11[33]	≥2	<4.5[33]	≥2	>794[33]
Idc(hE)V((*S*)-Me-THIQ)D-CN	**2**	8.12 ± 0.10[33]	≥2	6.03 ± 0.06	≥2	123[33]
Idc(hE)G(Dab)D-CHO	**3**	7.72 ± 0.11[34]	11	<4.8[34]	8	>832[34]
Idc(hE)V(Dab)D-CHO	**4**	7.46 ± 0.04[34]	4	<4.8[34]	4	>457[34]
Idc(hE)GGD-CHO	**5**	7.92 ± 0.14[34]	10	5.76 ± 0.13	8	145[34]
Idc(hE)VGD-CHO	**6**	7.65 ± 0.07[34]	6	5.17 ± 0.19[34]	4	302[34]
Idc(hE)G((*S*)-Me-THIQ)D-CHO	7	7.95 ± 0.07[34]	9	5.22 ± 0.07[34]	8	537[34]
X(hE)G(Dab)D-CHO						
AcI(hE)G(Dab)D-CHO	**8**	5.94 ± 0.01	3	<5	3	>8.7
AcF(hE)G(Dab)D-CHO	**9**	6.91 ± 0.14	3	<4.8	3	>129
Ac(4-Me-F)(hE)G(Dab)D-CHO	**10**	6.36 ± 0.01	3	<5	3	>23
AcY(hE)G(Dab)D-CHO	**11**	6.86 ± 0.07	3	<4.8	3	>115
Ac(4-F-F)(hE)G(Dab)D-CHO	**12**	6.36 ± 0.05	3	<5	3	>23
(3-PPA)(hE)G(Dab)D-CHO	**13**	6.00 ± 0.06	3	<5	3	>10
(4-Me-PPA)(hE)G(Dab)D-CHO	**14**	6.12 ± 0.02	3	<5	3	>13
(4-OH-PPA)(hE)G(Dab)D-CHO	**15**	5.89 ± 0.02	3	<5	3	>7.8
(4-F-PPA)(hE)G(Dab)D-CHO	**16**	6.16 ± 0.03	3	<5	3	>15
(PAA)(hE)G(Dab)D-CHO	**17**	6.31 ± 0.04	3	<5	3	>20
Ac(Chg)(hE)G(Dab)D-CHO	**18**	6.30 ± 0.04	3	<5	3	>20
Ac(Cha)(hE)G(Dab)D-CHO	**19**	6.54 ± 0.06	3	<5	3	>35
(CAA)(hE)G(Dab)D-CHO	**20**	6.07 ± 0.04	3	<5	3	>12
(CPA)(hE)G(Dab)D-CHO	**21**	6.30 ± 0.06	3	<5	3	>20
P(hE)G(Dab)D-CHO	**22**	5.88 ± 0.01	3	<4.8	3	>12
AcP(hE)G(Dab)D-CHO	**23**	5.60 ± 0.03	3	<5	3	>4.0
(Oic)(hE)G(Dab)D-CHO	**24**	5.63 ± 0.07	3	<5	3	>4.3
X(hE)V(Dab)D-CHO						
AcT(hE)V(Dab)D-CHO	**25**	6.93 ± 0.14	3	<4.8	3	>135
Ac(BnT)(hE)V(Dab)D-CHO	**26**	7.19 ± 0.10	3	<4.8	3	>246
(Isa)(hE)V(Dab)D-CHO	**27**	5.11 ± 0.09	3	<4.8	3	>2.0
(BeI)(hE)V(Dab)D-CHO	**28**	6.50 ± 0.06	3	<4.8	3	>50
X(hE)GGD-CHO						
AcI(hE)GGD-CHO	**29**	5.75 ± 0.05	3	5.52 ± 0.04	3	1.7
Ac(PhG)(hE)GGD-CHO	**30**	6.18 ± 0.01	3	5.50 ± 0.01	3	4.8
AcF(hE)GGD-CHO	**31**	5.93 ± 0.07	3	5.57 ± 0.01	3	2.3
Ac(4F-F)(hE)GGD-CHO	**32**	6.01 ± 0.07	3	5.59 ± 0.06	3	2.6
(PPA)(hE)GGD-CHO	**33**	5.80 ± 0.03	3	5.26 ± 0.01	3	3.5
(4F-PPA)(hE)GGD-CHO	**34**	5.78 ± 0.04	3	5.34 ± 0.06	3	2.8
X(hE)VGD-CHO						
AcI(hE)VGD-CHO	**35**	6.78 ± 0.06	3	5.87 ± 0.03	3	8.1
Ac(PhG)(hE)VGD-CHO	**36**	6.64 ± 0.15	3	5.46 ± 0.04	3	15
AcF(hE)VGD-CHO	**37**	6.85 ± 0.20	3	6.13 ± 0.03	3	5.2
Ac(4F-F)(hE)VGD-CHO	**38**	6.92 ± 0.12	3	5.72 ± 0.15	3	16
(PPA)(hE)VGD-CHO	**39**	6.07 ± 0.07	3	5.39 ± 0.06	3	4.8
(4F-PPA)(hE)VGD-CHO	**40**	6.05 ± 0.05	3	5.35 ± 0.01	3	5.0
(Quin)(hE)-G/V-(Dab)/G-D-CHO						
(Quin)(hE)G(Dab)D-CHO	**41**	7.57 ± 0.05	3	<4.8	3	>589
(Quin)(hE)V(Dab)D-CHO	**42**	7.00 ± 0.09	3	<4.8	3	>159
(Quin)(hE)GGD-CHO	**43**	7.32 ± 0.04	3	5.52 ± 0.15	3	63
(Quin)(hE)VGD-CHO	**44**	7.55 ± 0.08	3	5.63 ± 0.05	3	83
(Quin)E-G/V-(Dab)/G-D-CHO						
(Quin)EV(Dab)D-CHO	**45**	5.43 ± 0.05	3	<4.8	3	>4.3
(Quin)EGGD-CHO	**46**	5.21 ± 0.07	3	5.38 ± 0.06	3	0.7
(Quin)EVGD-CHO	**47**	5.93 ± 0.09	3	6.44 ± 0.05	3	0.3
X(hE)-G/V-((*S*)-Me-THIQ)/P*-D-CHO						
(Quin)(hE)G((*S*)-Me-THIQ)D-CHO	**48**	8.23 ± 0.08	4	5.16 ± 0.02	4	1175
(Quin)(hE)V((*S*)-Me-THIQ)D-CHO	**49**	7.13 ± 0.07	3	<4.8	3	>214

Downloaded from pubs.acs.org/jmcmar/article-pdf/doi/10.1021/acs.jmedchem.6c01371/6909867/acs.jmedchem.6c01371.pdf by UNIV REGENSBURG user on 17 November 2026

https://doi.org/10.1021/acs.jmedchem.6c01371
J. Med. Chem. XXXX, XXX, XXX−XXX

Table 1. continued

sequence	cmpd	pK$_i$ ± SEM cpCasp2	N	Casp3	N	K$_i$ (Casp3)/K$_i$ (cpCasp2)
P*(hE)V((*S*)-Me-THIQ)D-CHO	**50**	5.46 ± 0.07	3	<4.8	3	>4.6
AcP*(hE)V((*S*)-Me-THIQ)D-CHO	**51**	6.19 ± 0.10	3	<4.8	3	>25
AcVDVP*D-CHO	**52**	8.40 ± 0.09	4	8.77 ± 0.09	4	0.4
AcV(hE)VP*D-CHO	**53**	7.57 ± 0.08	3	6.05 ± 0.06	3	33
(Quin)(hE)GP*D-CHO	**54**	8.05 ± 0.06	3	6.61 ± 0.01	3	28
(Quin)(hE)VP*D-CHO	**55**	8.07 ± 0.07	3	5.53 ± 0.07	3	347
Idc(hE)GP*D-CHO	**56**	8.11 ± 0.06	3	6.34 ± 0.05	3	59
Idc(hE)VP*D-CHO	**57**	7.99 ± 0.12	4	5.87 ± 0.09	3	132
Ind(hE)V((*S*)-Me-THIQ)D-CHO	**58**	6.87 ± 0.09	4	4.66 ± 0.04	3	162
Ind(hE)VP*D-CHO	**59**	7.71 ± 0.10	4	5.95 ± 0.03	4	58
(2-Me-Idc)(hE)-G/V-XD-CHO						
(2-Me-Idc)(hE)G(Dab)D-CHO	**60**	8.07 ± 0.06	5	<4.8	4	>1862
(2-Me-Idc)(hE)V(Dab)D-CHO	**61**	7.66 ± 0.04	5	<4.8	4	>724
(2-Me-Idc)(hE)GGD-CHO	**62**	7.80 ± 0.07	4	5.67 ± 0.03	3	135
(2-Me-Idc)(hE)VGD-CHO	**63**	8.02 ± 0.09	5	5.56 ± 0.06	3	288
(2-Me-Idc)(hE)G((*S*)-Me-THIQ)D-CHO	**64**	8.50 ± 0.11	4	5.04 ± 0.03	4	2884
(2-Me-Idc)(hE)V((*S*)-Me-THIQ)D-CHO	**65**	7.96 ± 0.19	4	<4.8	4	>1445
(2-Me-Idc)(hE)GP*D-CHO	**66**	8.49 ± 0.12	3	6.58 ± 0.09	4	81
(2-Me-Idc)(hE)VP*D-CHO	**67**	8.20 ± 0.05	17	5.37 ± 0.02	14	676
Reference nitriles						
AcVDVAD-CN	**68**	7.28 ± 0.06	6	6.82 ± 0.03	6	2.9
AcVDVA((*R*)-D)-CN	**(*R*)-68**	6.11 ± 0.06	3	5.58 ± 0.02	3	3.4
AcV(hE)VP*D-CN	**69**	6.01 ± 0.11	6	<4.8	6	>16
AcV(hE)VP*((*R*)-D)-CN	**(*R*)-69**	<4.8	3	<4.8	3	1.0
Ind(hE)V((*S*)-Me-THIQ)D-CN	**70**	4.93 ± 0.01	3	<4.8	3	>1.3
Ind(hE)V((*S*)-Me-THIQ)((*R*)-D)-CN	**(*R*)-70**	4.69 ± 0.02	3	<4.8	3	>0.8
Ind(hE)VP*D-CN	**71**	6.38 ± 0.07	6	<4.8	6	>38
Ind(hE)VP*((*R*)-D)-CN	**(*R*)-71**	<4.8	3	<4.8	3	1.0
(Quin)(hE)-G/V-XD-CN						
(Quin)(hE)G(Dab)D-CN	**72**	5.89 ± 0.04	6	<4.8	6	>12
(Quin)(hE)G(Dab)((*R*)-D)-CN	**(*R*)-72**	<4.8	3	<4.8	3	1.0
(Quin)(hE)V(Dab)D-CN	**73**	5.65 ± 0.02	3	<4.8	3	>7.1
(Quin)(hE)V(Dab)((*R*)-D)-CN	**(*R*)-73**		6	<4.8	6	1.0
(Quin)(hE)GG((*rac*)-D)-CN	**(*rac*)-74**	<4.85.34 ± 0.02	6	<4.8	6	>3.5
(Quin)(hE)VGD-CN	**75**	5.73 ± 0.01	6	<4.8	6	>8.5
(Quin)(hE)VG((*R*)-D)-CN	**(*R*)-75**	<4.8	3	<4.8	3	1.0
(Quin)(hE)G((*S*)-Me-THIQ)D-CN	**76**	6.72 ± 0.11	7	<4.8	7	>83
(Quin)(hE)G((*S*)-Me-THIQ)((*R*)-D)-CN	**(*R*)-76**	5.10 ± 0.02	3	<4.8	3	>2.0
(Quin)(hE)V((*S*)-Me-THIQ)D-CN	**77**	5.02 ± 0.03	6	<4.8	6	>1.7
(Quin)(hE)V((*S*)-Me-THIQ)((*R*)-D)-CN	**(*R*)-77**	<4.8	3	<4.8	3	1.0
(Quin)(hE)GP*((*rac*)-D)-CN	**(*rac*)-78**	5.77 ± 0.04	3	<4.8	3	>9.3
(Quin)(hE)VP*D-CN	**79**	6.82 ± 0.03	7	<4.8	7	>105
(Quin)(hE)VP*((*R*)-D)-CN	**(*R*)-79**	4.76 ± 0.01	3	<4.8	3	0.9
(2-Me-Idc)(hE)-G/V-XD-CN						
(2-Me-Idc)(hE)G(Dab)D-CN	**80**	6.67 ± 0.08	7	<4.8	7	>74
(2-Me-Idc)(hE)G(Dab)((*R*)-D)-CN	**(*R*)-80**	<4.8	3	<4.8	3	1.0
(2-Me-Idc)(hE)V(Dab)D-CN	**81**	6.65 ± 0.04	7	<4.8	7	>71
(2-Me-Idc)(hE)V(Dab)((*R*)-D)-CN	**(*R*)-81**	< 4.8	3	<4.8	3	1.0
(2-Me-Idc)(hE)GG((*rac*)-D)-CN	**(*rac*)-82**	6.02 ± 0.03	6	<4.8	6	>17
(2-Me-Idc)(hE)VG((rac)-D)-CN	**(*rac*)-83**	6.60 ± 0.08	7	<4.8	7	>63
(2-Me-Idc)(hE)G((*S*)-Me-THIQ)D-CN	**84**	7.31 ± 0.05	11	<4.8	11	>324
(2-Me-Idc)(hE)G((*S*)-Me-THIQ)((*R*)-D)-CN	**(*R*)-84**	5.76 ± 0.01	3	<4.8	3	>9.1
(2-Me-Idc)(hE)V((*S*)-Me-THIQ)D-CN	**85**	5.67 ± 0.05	6	<4.8	6	>7.4
(2-Me-Idc)(hE)V((*S*)-Me-THIQ)((*R*)-D)-CN	**(*R*)-85**	5.06 ± 0.01	3	<4.8	3	>1.8
(2-Me-Idc)(hE)GP*D-CN	**86**	6.70 ± 0.04	7	<4.8	7	>79
(2-Me-Idc)(hE)GP*((*R*)-D)-CN	**(*R*)-86**	5.95 ± 0.02	3	<4.8	3	>14
(2-Me-Idc)(hE)VP*D-CN	**87**	7.72 ± 0.03	41	<4.8	38	>832
(2-Me-Idc)(hE)VP*D-CN	**87 (disodium salt)**	7.75 ± 0.02	53	<4.8	36	>891
(2-Me-Idc)(hE)VP*((*R*)-D)-CN	**(*R*)-87**	5.57 ± 0.02	3	<4.8	3	>5.9

Downloaded from pubs.acs.org/jmcmar/article-pdf/doi/10.1021/acs.jmedchem.6c01371/6909867/acs.jmedchem.6c01371.pdf by UNIV REGENSBURG user on 17 November 2026

https://doi.org/10.1021/acs.jmedchem.6c01371
J. Med. Chem. XXXX, XXX, XXX−XXX

Table 1. continued

sequence	cmpd	pK_i ± SEM cpCasp2	N	Casp3	N	K_i (Casp3)/K_i (cpCasp2)
(2-Me-Idc)(hE)VP*((*R*)-D)-CN	**(*R*)-87 (disodium salt)**	5.22 ± 0.03	5	<4.8	3	>2.6

[a]Data shown are mean values ± SEM of N independent experiments, each performed in duplicate. Data were analyzed by nonlinear regression and best fitted to sigmoidal concentration-inhibition curves. [a]Data represent pK_i values determined with Casp2.

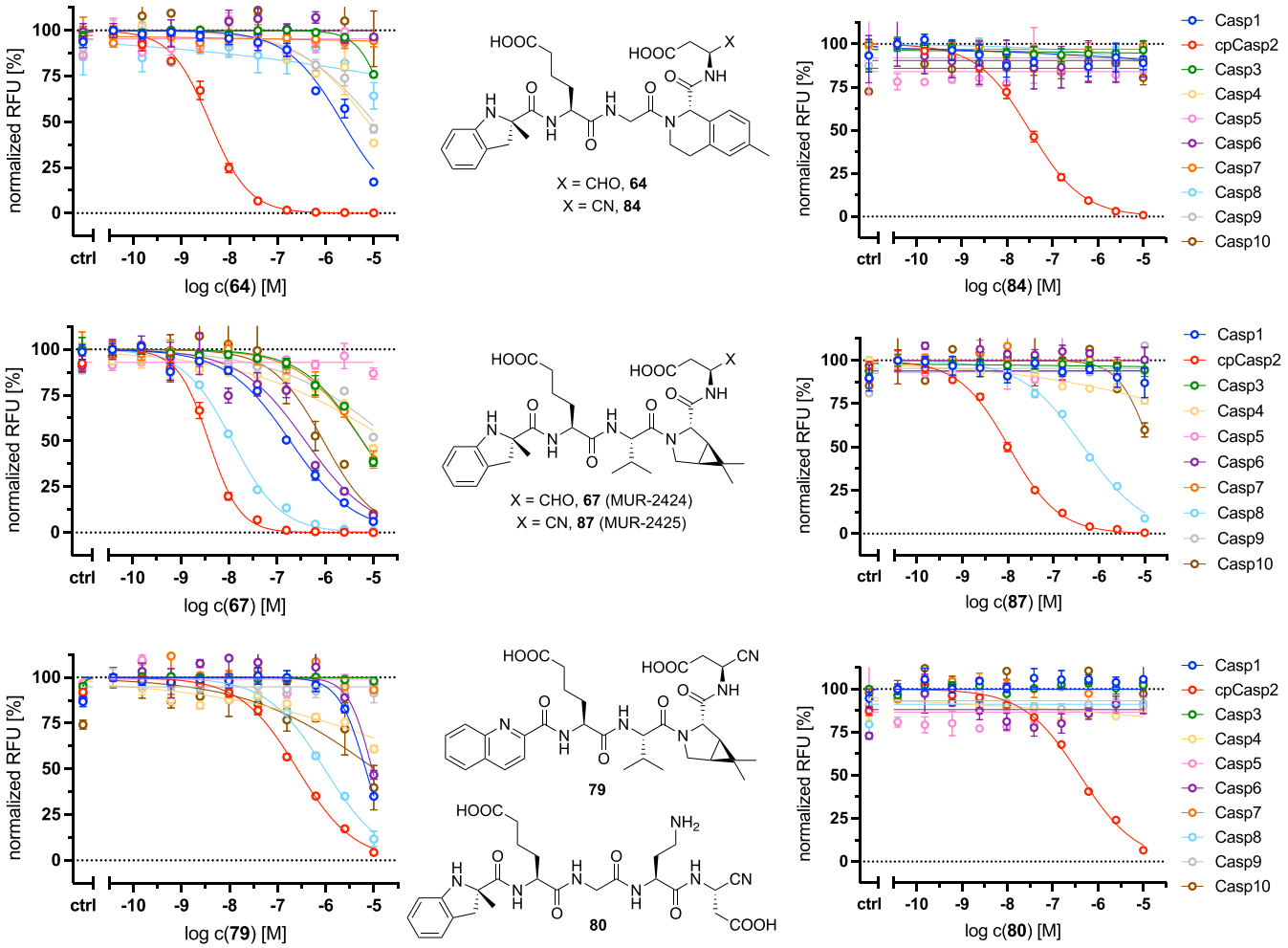


Figure 3. Structures and selectivity profile of potent Casp2 inhibitors **64**, **84**, **67** (MUR-2424), **87** (MUR-2425), **79**, and **80** against caspase-1, -3, -4, -5, -6, -7, -8, -9 and -10 determined in fluorescence-based enzyme inhibition assays. The relative fluorescent units (RFU) are normalized to positive control (ctrl) and depict mean ± standard deviation of one of at least three independent experiments, that were used for calculating the pK_i values as reported in Table 2. Each experiment was performed in duplicate.

79, **80**, (*R*)-**80**, **87**, and (*R*)-**87** were prepared by first generating the free base, followed by treatment with 0.01 M $NaHCO_3$ (aq) (Scheme 1). Experimental details for the synthesis of **BB1-BB2** (Scheme S1), compounds **8**–**63**, **65**–**66**, **68**–**86**, and (*R*)-**87**, calculated physicochemical properties (Tables S1 and S2), chemical stability of compounds **64**, **67** (MUR-2424), **84**, **87** (MUR-2425) (Figure 5 and Figures S2–S7), chemical structures (Figures S20–S122), NMR spectra (Figures S123–S388), and RP-HPLC purity control chromatograms (Figures S389–S492) are provided in the SI.

PHARMACOLOGY

All synthesized peptidomimetics were characterized by their pK_i values in a fluorescence-based enzyme inhibition assay to assess their affinities for circularly permuted caspase-2 (cpCasp2) and Casp3 (Table 1). In contrast to wild-type human Casp2, mutant cpCasp2 has its large and small subunits swapped and connected by a peptide linker, resulting in a constitutively active single-chain enzyme with higher expression yields in *E. coli* and improved storage stability. cpCasp2 was first introduced by Cserjan-Pushmann and coworkers in 2020, who characterized the mutant cpCasp2 regarding substrate specificity and kinetic properties and compared it with the wild-type Casp2.[47] Selected inhibitors were additionally investigated in a panel assay for their selectivity over caspases-1, -4, -5, -6, -7, -8, -9 and -10 (Figure 3 and Table 2). Unless otherwise mentioned, the inhibitors were preincubated for 5 min with the enzyme before the substrate was added to the mixture. Additionally, a selection of highly potent aldehyde and nitrile inhibitors was tested at 60 min preincubation time with cpCasp2, depicting no significant increase in the mean pIC_{50} values for the longer preincubation

Downloaded from pubs.acs.org/jmcmar/article-pdf/doi/10.1021/acs.jmedchem.6c01371/6909867/acs.jmedchem.6c01371.pdf by UNIV REGENSBURG user on 17 November 2026

https://doi.org/10.1021/acs.jmedchem.6c01371
J. Med. Chem. XXXX, XXX, XXX−XXX

Table 2. Enzyme Inhibitory Potency (pK_i Values) of Selected Compounds at Casp1 and Casp4-10[a]

sequence	cmpd	pK_i (Casp1)	N	K_i (Casp1)/ K_i (cpCasp2)	pK_i (Casp4)	N	K_i (Casp4)/ K_i (cpCasp2)	pK_i (Casp5)	N	K_i (Casp5)/ K_i (cpCasp2)	pK_i (Casp6)	N	K_i (Casp6)/ K_i (cpCasp2)	pK_i (Casp7)	N	K_i (Casp7)/ K_i (cpCasp2)	pK_i (Casp8)	N	K_i (Casp8)/ K_i (cpCasp2)	pK_i (Casp9)	N	K_i (Casp9)/ K_i (cpCasp2)	pK_i (Casp10)	N	K_i (Casp10)/ K_i (cpCasp2)
AcVDVAD-CHO		7.06 ± 0.06[18]		8.7		n.d.			n.d.		< 4[18]	2	> 10000	7.08 ± 0.06[18]	2	1.0		n.d.		5.57 ± 0.31[18]	2	31		n.d.	
Ide(hE)V((*S*)-Me-THIQ)D-CHO	**1**	6.41 ± 0.12[13]	≥ 2	9.8		n.d.			n.d.		< 4[13]	≥ 2	> 2512	< 4[13]	≥ 2	> 2512		n.d.		5.12 ± 0.04[13]	≥ 2	191		n.d.	
Ide(hE)V((*S*)-Me-THIQ)D-CN	**2**	< 4[13]	≥ 2	13183		n.d.			n.d.		< 4[13]	≥ 2	> 13183	4.8 ± 0.06[13]	≥ 2	2089		n.d.		< 4.5	≥ 2	> 4169		n.d.	
Ide(hE)G(Dab)D-CHO	**3**	5.09 ± 0.15[34]	3	427	< 5[34]	3	> 525	< 5[34]	3	> 525	< 5[34]	3	> 525	< 5[34]	3	> 525	< 5[34]	3	> 525	< 5[34]	3	> 525	< 5[34]	3	> 525
Ide(hE)GD-CHO	**5**	5.26 ± 0.06[34]	3	457	< 5[34]	3	> 832	< 5[34]	3	> 832	< 5[34]	3	> 832	< 5[34]	3	> 832	< 5[34]	3	> 832	5.00 ± 0.05[34]	3	832	< 5[34]	3	> 832
Ide(hE)G((*S*)-Me-THIQ)D-CHO	**7**	5.77 ± 0.04[34]	3	151	6.08 ± 0.08[34]	3	74	< 5[34]	3	> 891	< 5[34]	3	> 891	< 5[34]	3	> 891	< 5[34]	3	> 891	5.09 ± 0.09[34]	3	724	< 5[34]	3	> 891
(Quin)(hE)G((*S*)-Me-THIQ)D-CHO	**48**	6.99 ± 0.01	3	17		n.d.			n.d.		< 5	3	> 1698	< 5	3	> 1698		n.d.		5.79 ± 0.03	3	275		n.d.	
(Quin)(hE)VP*D-CHO	**55**	7.27 ± 0.09	3	6.3		n.d.			n.d.		6.77 ± 0.15	4	20	5.52 ± 0.03	3	355		n.d.		5.08 ± 0.11	3	977		n.d.	
(2-Me-Ide)(hE)G(Dab)D-CHO	**60**	5.32 ± 0.08	3	563	< 5	3	> 1175	< 5	3	> 1175	< 5	3	> 1175	< 5	4	> 1175	< 5	3	> 1175	< 5	3	> 1175	< 5	3	> 1175
(2-Me-Ide)(hE)V(Dab)D-CHO	**61**	7.53 ± 0.09	3	1.3		n.d.			n.d.		< 5	3	> 457	< 5	3	> 457		n.d.		< 5	3	> 457		n.d.	
(2-Me-Ide)(hE)VGD-CHO	**63**	7.01 ± 0.07	3	10		n.d.			n.d.		< 5	3	> 1047	5.25 ± 0.08	4	589		n.d.		5.11 ± 0.04	3	813		n.d.	
(2-Me-Ide)(hE)G((*S*)-Me-THIQ)D-CHO	**64**	5.83 ± 0.05	4	468	5.29 ± 0.23	3	1622	< 5	3	3162	< 5	3	> 3162	< 5	3	> 3162	< 5	3	> 3162	5.13 ± 0.02	3	2344	< 5	3	> 3162
(2-Me-Ide)(hE)V((*S*)-Me-THIQ)D-CHO	**65**	6.57 ± 0.21	3	25	< 5	3	> 912	< 5	3	> 912	< 5	3	> 912	< 5	3	> 912	5.84 ± 0.02	3	132	5.03 ± 0.08	3	851	< 5	3	> 912
(2-Me-Ide)(hE)GP*D-CHO	**66**	5.58 ± 0.06	3	813	< 5	3	> 3090	< 5	3	> 3090	< 5	3	> 3090	< 5	4	> 3090	5.66 ± 0.65	3	676	< 5	3	> 3090	5.04 ± 0.10	3	2818
(2-Me-Ide)(hE)VP*D-CHO	**67**	6.40 ± 0.19	4	63	5.05 ± 0.07	3	1413	< 5	3	> 1585	6.44 ± 0.09	3	58	5.26 ± 0.03	4	871	7.85 ± 0.13	3	2.2	4.87 ± 0.08	3	2138	6.24 ± 0.13	3	91
(Quin)(hE)G((*S*)-Me-THIQ)D-CN	**76**	< 5	3	> 53		n.d.			n.d.		< 5	4	> 53	< 5	3	> 53		n.d.		< 5	3	> 53		n.d.	
(Quin)(hE)VP*D-CN	**79**	5.53 ± 0.01	3	20	< 5	3	> 66	< 5	3	> 66	5.03 ± 0.04	3	66	< 5	3	> 66	5.99 ± 0.07	3	6.8	< 5	3	> 66	< 5	3	> 66
(2-Me-Ide)(hE)G(Dab)D-CN	**80**	< 5	3	> 47	< 5	3	> 47	< 5	3	> 47	< 5	3	> 47	< 5	3	> 47	< 5	3	> 47	< 5	3	> 47	< 5	3	> 47
(2-Me-Ide)(hE)V(Dab)D-CN	**81**	5.36 ± 0.01	3	20		n.d.			n.d.		< 5	3	> 45	< 5	3	> 45		n.d.		< 5	3	> 45		n.d.	
(2-Me-Ide)(hE)VG((*rac*)-D)-CN	**(*rac*)-83**	5.13 ± 0.04	3	30		n.d.			n.d.		< 5	3	> 40	< 5	3	> 40		n.d.		< 5	3	> 40		n.d.	
(2-Me-Ide)(hE)G((*S*)-Me-THIQ)D-CN	**84**	< 5	3	> 204	< 5	3	> 204	< 5	3	> 204	< 5	7	> 204	< 5	7	> 204	< 5	3	> 204	< 5	3	> 204	< 5	3	> 204
(2-Me-Ide)(hE)GP*D-CN	**86**	< 5	3	> 50	< 5	3	> 50	< 5	3	> 50	< 5	3	> 50	< 5	3	> 50	< 5	3	> 50	< 5	3	> 50	< 5	3	> 50
(2-Me-Ide)(hE)VP*D-CN	**87 (disodium salt)**	< 5	3	> 562	< 5	3	> 562	< 5	3	> 562	< 5	3	> 562	< 5	3	> 562	6.37 ± 0.02	3	24	< 5	3	> 562	5.03 ± 0.04	3	525
(2-Me-Ide)(hE)VP*((*R*)-D)-CN	**(*R*)-87**	< 5	3	> 3.7		n.d.			n.d.		< 5	3	> 3.7	< 5	3	> 3.7		n.d.		< 5	3	> 3.7		n.d.	

[a]Data shown are mean values ± SEM of *N* independent experiments, each performed in duplicate. Data were analyzed by nonlinear regression and best fitted to sigmoidal concentration-inhibition curves.

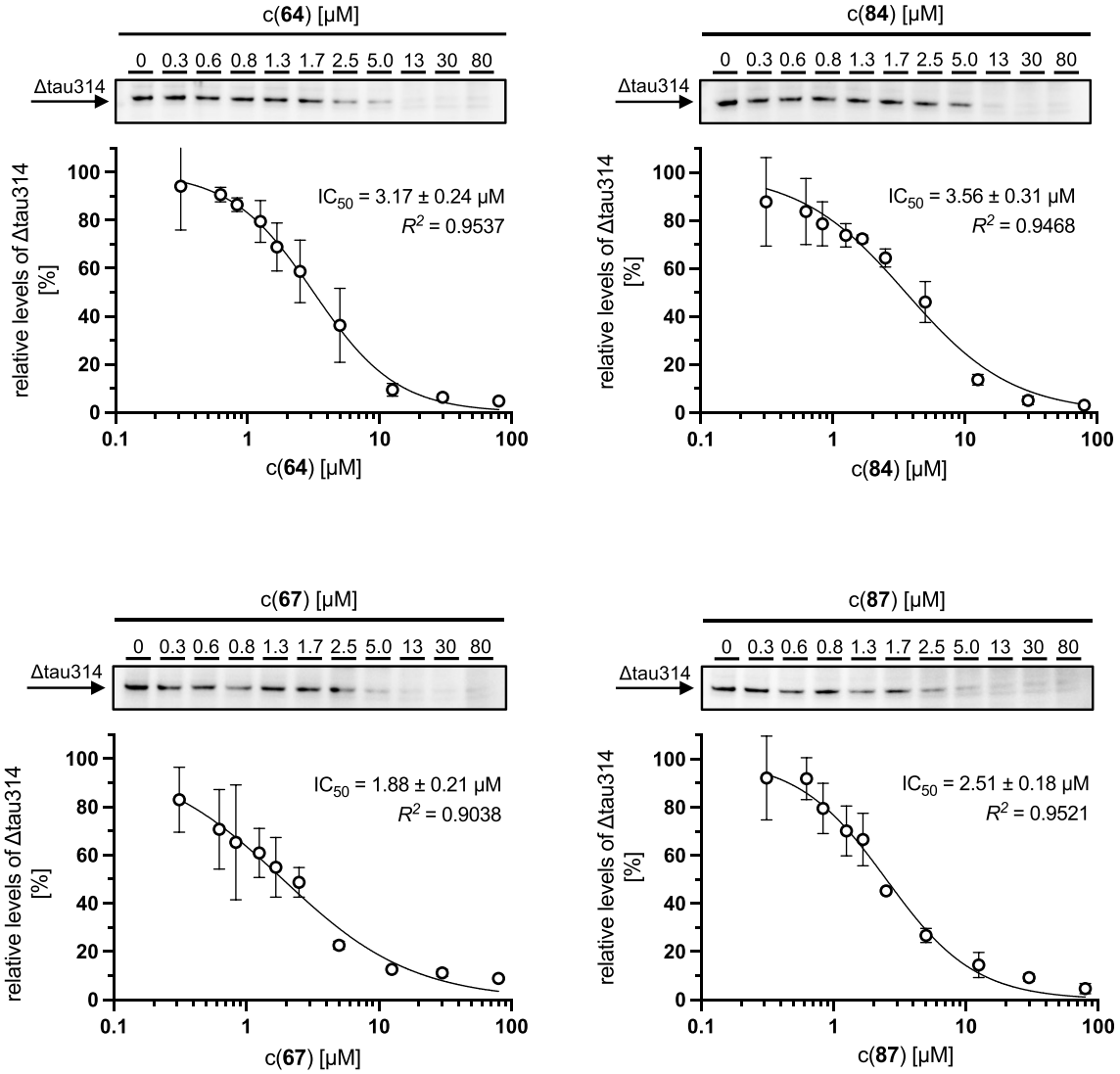


Figure 4. Casp2 selective inhibitors block enzyme catalyzed Δtau314 formation in vitro. For determination of the IC_{50} values of **64**, **84**, **67** (MUR-2424), and **87** (MUR-2425) the level of Δtau314 was quantified by immunoprecipitation (4F3)/Western Blot (tau-5-biotin) and fitted to a dose−response curve against compound concentration. The graphs represent mean ± SD of three individual experiments, each performed in duplicate.

Downloaded from pubs.acs.org/jmcmar/article-pdf/doi/10.1021/acs.jmedchem.6c01371/6909867/acs.jmedchem.6c01371.pdf by UNIV REGENSBURG user on 17 November 2026

https://doi.org/10.1021/acs.jmedchem.6c01371
J. Med. Chem. XXXX, XXX, XXX−XXX

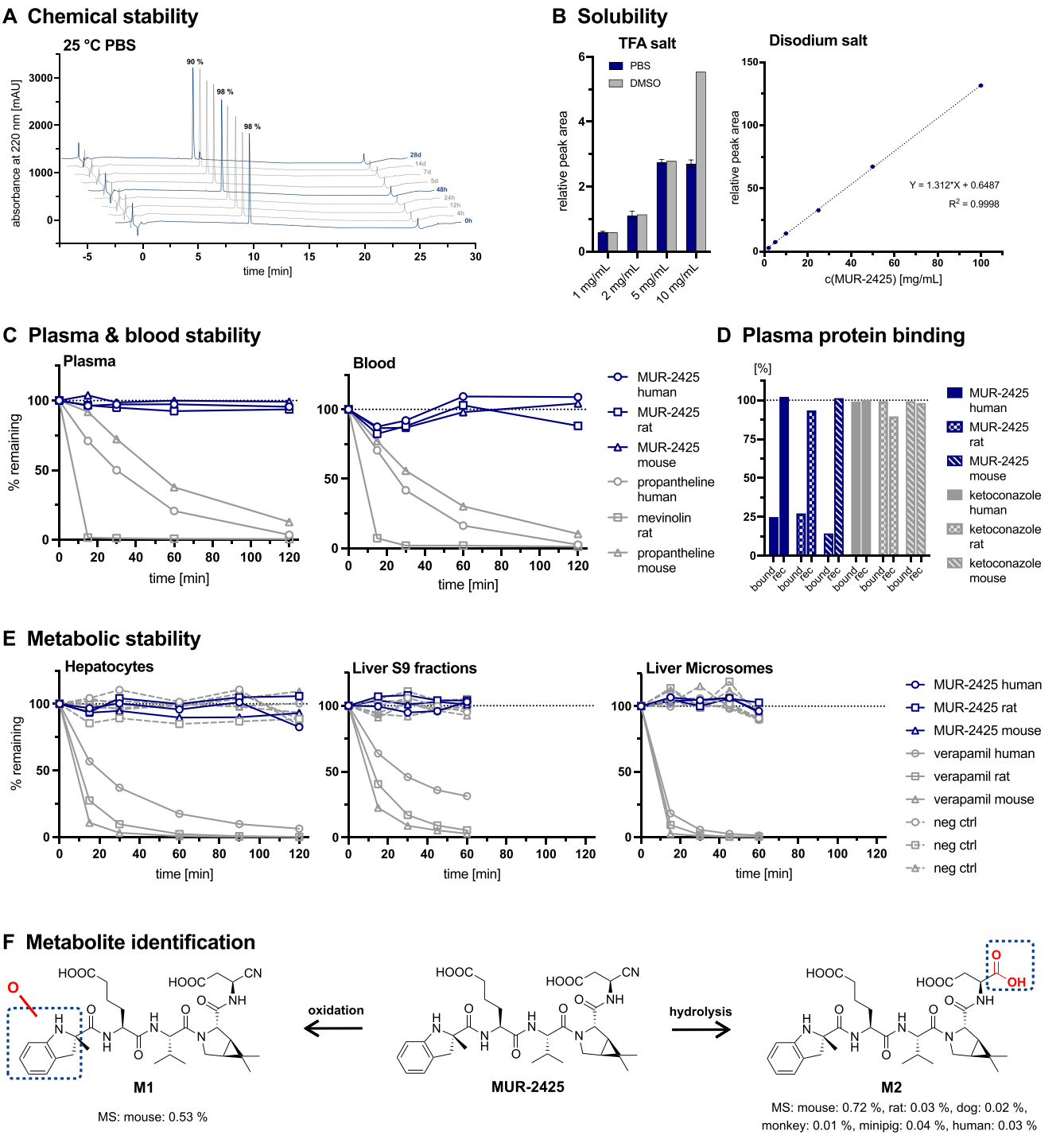


Figure 5. In vitro ADMET data of MUR-2425 (**87**). (A) Chemical stability of MUR-2425 (1 mM) in PBS at pH 7.4 and 25 °C for 28 d (Method D). (B) Solubility of MUR-2425 in PBS at pH 7.4 to a target concentration of 1, 2, 5, and 10 mg/mL (TFA salt) and 2, 5, 10, 25, 50, and 100 mg/mL (disodium salt). The data represent mean ± SD of two independent experiments, each performed at least in triplicate. (C) Plasma protein binding of MUR-2425 and the positive control ketoconazole in human, rat, and mouse plasma. Assay were performed in duplicate. (D) Plasma stability of MUR-2425 and control compounds propantheline and mevinolin in plasma and blood. Assays were performed in duplicate. (E) Metabolic stability of MUR-2425 and controls midazolam, umbelliferone, and verapamil in human, rat, and mouse hepatocytes, liver S9 fractions, and liver microsomes for various time periods at 37 °C. Assays were performed in duplicate. (F) Proposed metabolic pathways of MUR-2425 in human, rat, dog, monkey, minipig, and mouse hepatocytes. The metabolites M1 (oxidation product) and M2 (hydrolysis product) were identified and quantified after 240 min incubation at 37 °C by LC-MS/MS analysis. Plasma/blood stability, metabolic stability and plasma protein binding studies were conducted with the TFA salt form of MUR-2425, chemical stability and metabolite identification were conducted with the disodium salt form of MUR-2425. The results of the respective ADMET experiments are further summarized in Tables S3−S9.

time (results are shown in Table S14). Jump dilution experiments of selected potent aldehyde an nitrile inhibitors were performed at cpCasp2 and are shown in Figure S493. On the basis of fluorometric assay results, a selection of the best-performing aldehydes and nitriles (compounds **64**, **67** (MUR-2424), **84**, and **87** (MUR-2425)) and the negative control

https://doi.org/10.1021/acs.jmedchem.6c01371
J. Med. Chem. XXXX, XXX, XXX−XXX

Downloaded from pubs.acs.org/jmcmar/article-pdf/doi/10.1021/acs.jmedchem.6c01371/6909867/acs.jmedchem.6c01371.pdf by UNIV REGENSBURG user on 17 November 2026

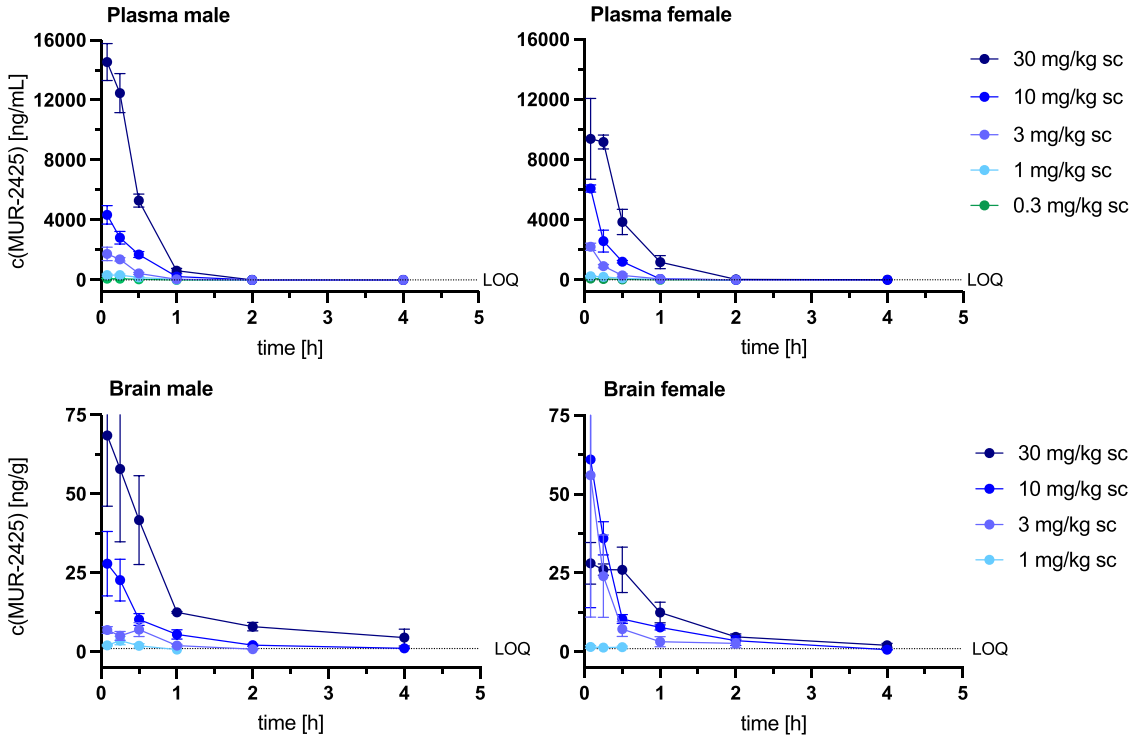


Figure 6. Results from *in vivo* pharmacokinetic studies of **87** (MUR-2425, disodium salt) in male and female CD-1 mice after subcutaneous injection of 0.3, 1, 3, 10, or 30 mg/kg bodyweight. Graphs represent mean ± SD of each study group, consisting of three animals for each administration route, dose and time point. The dashed line marks the limit of quantification (LOQ).

compound (***R***)-**87** (Figure S1) were further characterized for their ability to inhibit the cleavage of the tau protein (Figure 4). The most promising aldehyde and nitrile compounds **67** (MUR-2424) and **87** (MUR-2425), as well as the two nitrile inhibitors **79** and **80**, were characterized regarding their ADMET properties *in vitro* (Figure 5, Figures S8−S16, Tables S3−S9) and their pharmacokinetics in CD-1 mice (Figure 6, Figures S17−S19, Tables S10−S12).

RESULTS AND DISCUSSION

X(hE)G(Dab)D-CHO (8−24) and X(hE)V(Dab)D-CHO (25−28)

At the P5 position of pentapeptides with the general structure X(hE)G(Dab)D-CHO, different natural and unnatural amino acids and corresponding carboxylic acids were investigated. Compound **23** (AcP(hE)G(Dab)D-CHO) exhibited the lowest cpCasp2 inhibitory potency within this series (pK_i = 5.60), which may be attributed to the tertiary nitrogen of the *N*-acetylated proline residue. Previous studies have already shown that *N*-terminal interactions of the nitrogen within the S5 binding pocket of Casp2 are important for effective enzyme inhibition.[27] Consistent with this observation, compound **22** (P(hE)G(Dab)D-CHO), containing a secondary nitrogen at P5, exhibited a slightly improved pK_i value of 5.88. The importance of the P5 nitrogen is emphasized when comparing amino acids at P5 (**9**−**12**; pK_i = 6.31−6.91) with their corresponding carboxylic acid analogs (**13**−**16**; pK_i = 6.00−6.16).

Furthermore, an aromatic substituent in P5 appeared to favor Casp2 binding interactions, as reflected by the higher inhibitory potency of compounds **9** (AcF(hE)G(Dab)D-CHO, pK_i = 6.91) and **17** ((PPA)(hE)G(Dab)D-CHO, pK_i = 6.31) compared with their saturated analogs **19** (Ac(Cha)(hE)G(Dab)D-CHO, pK_i = 6.54) and **20** ((CAA)(hE)G(Dab)D-CHO, pK_i = 6.07). Likewise, other aliphatic P5 residues, including those in **8** (AcI(hE)G(Dab)D-CHO), **18** (Ac(Chg)(hE)G(Dab)D-CHO), and **24** ((Oic)(hE)G(Dab)D-CHO), showed only weak cpCasp2 potency with pK_i values ranging from 5.63 to 6.30. The beneficial effect of the aromatic system was diminished upon increasing the side chain length (**13** ((3-PPA)(hE)G(Dab)D-CHO) pK_i = 6.00 vs **21** ((CPA)(hE)G(Dab)D-CHO) pK_i = 6.30). Conversely, shortening the chain from phenylpropanoic acid to phenylacetic acid, as in compounds **13** ((3-PPA)(hE)G(Dab)D-CHO) and **17** ((PAA)(hE)G(Dab)D-CHO), increased cpCasp2 potency by 0.3 log units. Both aspects suggest that the correct positioning of the aromatic ring within the S5 binding pocket is critical for lipophilic interactions with Tyr383,[41] an amino acid that substantially contributes to the hydrophobic character of the Casp2 S5 binding site.[48] *Para*-substitution of the aromatic ring had only a minor and inconsistent effect on Casp2 inhibitory potency: among the 3-PPA derivatives, the *para*-hydroxyl-substituted analog (**15**) displayed the lowest Casp2 activity, whereas fluorination (**16**) had a slightly positive effect. A different trend was observed for the phenylalanine series: While compound **9**, AcF(hE)G(Dab)D-CHO, pK_i = 6.91), was the most potent analog, both *para*-methylation and *para*-fluorination (**10**, Ac(4-Me-F)(hE)G(Dab)D-CHO and **12**, Ac(4-F-F)(hE)G(Dab)D-CHO) reduced potency (both pK_i = 6.36) while tyrosine retained activity (**11**, AcY(hE)G(Dab)D-CHO) pK_i = 6.86).

The peptidomimetic containing 2,3-dihydroindene-5-sulfonic acid (Isa) at position P5 (**27**, (Isa)(hE)V(Dab)D-CHO) showed only weak cpCasp2 inhibition (pK_i = 5.11). However, compounds **25** (AcT(hE)V(Dab)D-CHO) and **28** ((BeI)(hE)V(Dab)D-CHO) displayed affinities in the three-

Downloaded from pubs.acs.org/jmcmar/article-pdf/doi/10.1021/acs.jmedchem.6c01371/6909867/acs.jmedchem.6c01371.pdf by UNIV REGENSBURG user on 17 November 2026

https://doi.org/10.1021/acs.jmedchem.6c01371
J. Med. Chem. XXXX, XXX, XXX−XXX

digit nanomolar range (pK_i values of 6.93 and 6.50, respectively). Consistent with a previous study reporting that L-benzyl-threonine at P5 yields selective Casp2 inhibitors,[27] compound **26** (Ac(BnT)(hE)V(Dab)D-CHO) demonstrated high cpCasp2 activity (pK_i = 7.19).

X(hE)GGD-CHO (29−34) and X(hE)VGD-CHO (35−40)

In our previous publication, we reported the introduction of a glycine−glycine linker spanning positions P3−P2.[34] We herein compared the glycine−glycine linker with a valine-glycin sequence for P3 and P2 for selected P5 modifications: Inhibitors containing the -V−G- motif in positions P3−P2, e.g., **35** (AcI(hE)VGD-CHO, pK_i = 6.78) and **36** (Ac(Phg)-(hE)VGD-CHO, pK_i = 6.64) demonstrated higher cpCasp2 inhibitory potency than those with a glycine−glycine linker (**29** (AcI(hE)GGD-CHO, pK_i = 5.75) and **30** (Ac(Phg)(hE)-GGD-CHO, pK_i = 6.18)). In general, the -V−G- sequence increased cpCasp2 inhibitory potency by approximately 0.2−1.0 log units. Simultaneously, it had little effect on Casp3 potency, and thus inhibitors of the X(hE)VGD-CHO scaffold exhibited a more favorable cpCasp2 selectivity profile. Following the findings from the X(hE)G(Dab)D-CHO subseries, acetylated amino acids showed enhanced inhibitory potency compared to their carboxylic acid counterparts: **31** (AcF(hE)GGD-CHO, pK_i = 5.93) vs **33** ((PPA)(hE)GGD-CHO, pK_i = 5.80) and **37** (AcF(hE)VGD-CHO, pK_i = 6.85) vs **39** ((PPA)(hE)VGD-CHO, pK_i = 6.07). *Para*-fluorination of the phenyl moiety at P5 had only a minor effect on cpCasp2 inhibitory potency and maintained potency in phenylalanine derivatives while the activity of the corresponding carboxylic acids was slightly enhanced (cf. **31**−**34** and **37**−**40**).

(Quin)(hE)-G/V-(Dab)/G-D-CHO (41−44) and (Quin)E-G/V-(Dab)/G-D-CHO (45−47)

Quinaldic acid (Quin) has previously been shown to be well tolerated in P6 as a replacement for acetylation[34,45] and was introduced at P5 in the present study to potentially improve cellular penetration and bioavailability. Regarding cpCasp2 inhibition, Quin turned out to be the most favorable scaffold of all P5 residues investigated within this series, resulting in **41** ((Quin)(hE)G(Dab)D-CHO, pK_i = 7.57), **44** ((Quin)(hE)-VGD-CHO, pK_i = 7.55) and **43** ((Quin)(hE)GGD-CHO, pK_i = 7.32)). Interestingly, compound **42** ((Quin)(hE)V(Dab)D-CHO, pK_i = 7.00) exhibited a markedly lower inhibitory potency for cpCasp2 than **41**, suggesting that, in combination with Dab at P2, the smaller glycine residue at position P3 is more favorable than valine. Obviously, the planar aromatic system of quinaldic acid fits well into the S5 binding site of Casp2 and seems to be conducive for π-π stacking with Tyr383 in the binding pocket.[41] Since the potency for Casp3 remains unaffected, Quin is amplifying the selectivity that is primarily conferred by the amino acids in P2 (Dab) and P4 (hE).[34] Compared to phenylalanine, Quin in P5 improved selectivity over Casp3 by approximately 5-fold, reaching up to 589-fold (**41**) with Dab in P2 and 83-fold (**44**) with G in P2. Compound **41** exhibited similar inhibitory potency and selectivity to those of reference compound **3**, indicating that Quin at position P5 is as effective as Idc. Replacing hE with glutamic acid (E) at P4 consistently reduced potency (**45**−**47**) with a loss in the range of approximately 1.5−2.1 log units.

X(hE)-G/V-((*S*)-Me-THIQ)/P*-D-CHO (48−59)

The observation that Quin at P5 is equally active as Idc and that the P3−P2 combination of -G(*S*)-Me-THIQ- is more favorable than -V(*S*)-Me-THIQ- with respect to both potency and selectivity were confirmed in this subseries (compare compounds **48** and **49** with pK_i values at cpCasp2 of 8.23 and 7.13 and selectivity factors of 1175-fold and 214-fold over Casp3, respectively).

The bulky proline derivative P* (**BB2**) was introduced into P2 to fill the comparably large S2 pocket of Casp2. For an initial comparison, the P* analog of the canonical inhibitor AcVDVAD-CHO was synthesized, resulting in **52** (AcVDV-(P*)D-CHO). This modification was accompanied by an increase in inhibitory potency for cpCasp2 (pK_i of 8.40 vs 8.00) and Casp3 (pK_i 8.77 vs 8.26), resulting in an impaired selectivity profile. Compound **53** (AcV(hE)V(P*)D-CHO) exhibited a lower cpCasp2 potency with a pK_i value of 7.57, whereas introduction of hE at P4 resulted in the expected decrease in Casp3 activity (pK_i (Casp3) = 6.05), leading to improved selectivity. The transfer of this finding (hE at P4) resulted in consistently high cpCasp2 affinities and good selectivity toward Casp3 for Quin- and Idc- at P5 with respective glycine/valine variation at P3, as demonstrated by compounds **54**−**57** (Table 1). Of particular note is compound **55** ((Quin)(hE)V(P*)D-CHO), which exhibited pK_i values of 8.07 for cpCasp2 and 5.53 for Casp3. Interestingly, unlike the corresponding -V((*S*)-Me-THIQ)- motif, no decrease in cpCasp2 potency was observed for any compound containing the -V−P*- motif in P3−P2. The results suggest that the -V−P*- motif strikes just the right balance to fill the S3−S2 cavity of Casp2 without causing steric hindrance that would compromise activity. Furthermore, the combination appears to exert a beneficial synergistic effect on selectivity over Casp3, resulting in a 6-fold (**55** vs **54**) or 2-fold (**57** vs **56**) increase in selectivity of the -V−P*- motif compared with -GP*-.

Introduction of P* at P5 afforded moderately active inhibitors (P*)(hE)V((*S*)-Me-THIQ)D-CHO (**50**, pK_i = 5.46) and AcP*(hE)V((S)-Me-THIQ)D-CHO (**51**, pK_i = 6.19) with the surprising finding that acetylation to a tertiary nitrogen led to a slight increase in cpCasp2 inhibitory potency in this case.

Inhibitor **58** ((Ind)(hE)V((*S*)-Me-THIQ)D-CHO) is the oxidative degradation product of the previously reported potent inhibitor (Idc)(hE)V((*S*)-Me-THIQ)D-CHO (**1**).[33] The aromatization of Idc to indole (Ind) resulted in a slight reduction of the cpCasp2 inhibitory potency (pK_i of 6.87 instead of 7.40). However, the loss of activity was less pronounced for compound **59** ((Ind)(hE)V(P*)D-CHO, pK_i = 7.71) compared with **57** (pK_i = 7.99) while maintaining consistently low Casp3 inhibitory potency.

(2-Me-Idc)(hE)XXD-CHO (60−67)

To address the stability issues associated with Idc-containing compounds, we introduced (*S*)-2-methylindoline-2-carboxylic acid (2-Me-Idc, **BB1**) as a new P5 scaffold. The subseries (2-Me-Idc)(hE)XXD-CHO (**60**−**67**) covers all systematic combinations of 2-Me-Idc in P5 with glycine or valine at P3 and Dab, glycine, (*S*)-Me-THIQ, or P* at P2.

Without exception, all inhibitors containing 2-Me-Idc at P5 showed higher inhibitory potency at cpCasp2 than the corresponding peptides bearing any other P5 motif investigated in this study. Additionally, the selectivity over Casp3 was consistently improved. These findings also held true when compared with reference compounds **1**−**7** and indicate that 2-Me-Idc successfully enhances both the potency and selectivity for Casp2. The highest inhibitory potencies in the entire

Downloaded from pubs.acs.org/jmcmar/article-pdf/doi/10.1021/acs.jmedchem.6c01371/6909867/acs.jmedchem.6c01371.pdf by UNIV REGENSBURG user on 17 November 2026

https://doi.org/10.1021/acs.jmedchem.6c01371
J. Med. Chem. XXXX, XXX, XXX−XXX

compound series were measured for **64** (2-Me-Idc)(hE)G-((*S*)-Me-THIQ)D-CHO (pK_i = 8.50), **66** (2-Me-Idc)(hE)-GP*D-CHO (pK_i = 8.49), and **67** (2-Me-Idc)(hE)VP*D-CHO (pK_i = 8.20). Selectivity over Casp3 showed a clear dependence on the P2 residue, with THIQ in P2 exhibiting the highest selectivity (**64** (2-Me-Idc)(hE)G((*S*)-Me-THIQ)D-CHO, 2884-fold over Casp3), followed by Dab (**60** (2-Me-Idc)(hE)G(Dab)D-CHO 1862-fold over Casp3), P* (**67** (2-Me-Idc)(hE)VP*D-CHO, 676-fold over Casp3), and G (**63**, (2-Me-Idc)(hE)VGD-CHO 288-fold over Casp3). Once again, the results suggested that valine at P3 pairs best with P* and G in P2, (**63** and **67**) and that (*S*)-Me-THIQ and Dab require glycine at position 3 to achieve optimal results (**64** and **60**). Although the -G−P*- sequence for P3−P2 resulted in high cpCasp2 potency, it was comparatively less selective, due to its relatively high potency at Casp3 (**66**, (2-Me-Idc)(hE)GP*D-CHO, pK_i(Casp3) = 6.58). Consistent trends were observed for the inhibitors containing either Quin or Idc in P5 (**54**, (Quin)(hE)GP*D-CHO, pK_i (Casp3) = 6.61 and **56**, Idc(hE)GP*D-CHO, pK_i (Casp3) = 6.34).

The SAR from the aldehyde subseries can be summarized in the following key findings: Quin and 2-Me-Idc are equivalent and superior alternatives to the unstable Idc in P5, combining high inhibitory potency for cpCasp2 with strong selectivity over Casp3. The outstanding performance of Quin and 2-Me-Idc and the comparably poor results obtained for the other P5 scaffolds suggest that a plane and aromatic system in combination with a cyclic nitrogen is advantageous, most likely because it enables favorable $\pi-\pi$ stacking interactions with Tyr383 in the Casp2 subsite. At P2, cyclic and sterically bulky groups, particularly THIQ and P*, are the preferred choice exhibiting high inhibitory potency for Casp2 and good selectivity (**1**, **7**, **48**, **49**, **64**, **65** and **56**, **57**, **54**, **55**, **66**, **67**). Dab in P2 (**3**, **4**, **41**, **42**, **60**, **61**) also conferred good selectivity but exhibited slightly lower overall potency than the two cyclic scaffolds. Glycine in P2 was generally less favorable owing to its lower selectivity (**5**, **6**, **43**, **44**, **62**, **63**). The results further indicate a structural interplay between P2 and P3 to ensure optimal binding to the Casp2 S2−S3 subsite, as the preferred amino acid at P3 varies depending on the substituent at P2. Inhibitors with larger P2 substituents, such as (*S*)-Me-THIQ and Dab, exhibit higher cpCasp2 potency and selectivity with glycine at P3 (**1**, **7**, **48**, **49**, **64**, **65**, and **3**, **4**, **41**, **42**, **60**, **61**). In contrast, if the proline derivative P* or glycine occupies the P2 position, valine is the preferred P3 amino acid, especially regarding selectivity (**56**, **57**, **54**, **55**, **66**, **67** and **5**, **6**, **43**, **44**, **62**, **63**).

Reference Nitriles (68−71)

Aldehyde inhibitors with the general structure (Quin)-hE-G/V-X-D-CHO and (2-Me-Idc)-hE-G/V-X-D-CHO were selected for the additional synthesis of the corresponding peptides containing a nitrile warhead instead. In addition, nitrile analogs of the reference compound AcVDVAD-CHO and their derivatives were synthesized, as well as some nitrile compounds containing indole (Ind) in P5, the oxidatively degraded form of Idc.

Compound **68** (AcVDVAD-CN) showed strong Casp2 activity but lacked selectivity over Casp3. Replacement of the aldehyde warhead by a nitrile reduced cpCasp2 inhibitory potency (pK_i = 7.28 vs 8.00) but slightly improved selectivity (selectivity factor 2.9 vs 0.50). Similar trends were observed for inhibitor **53**, which was converted into its nitrile analog AcV(hE)VP*D-CN (**69**). In our previous work, we reported the discovery of the potent and selective, but unstable, Casp2 inhibitor **2** (MUR-90, (Idc)(hE)V((*S*)-Me-THIQ)-CN, pK_i = 8.12).[33] To investigate whether the favorable activity of **2** could be retained upon oxidative degradation, we synthesized the oxidized form Ind(hE)V((*S*)-Me-THIQ)D-CN (**70**), which exhibited negligible cpCasp2 inhibitory potency (pK_i = 4.93). The analog with P* in P2 (**71**, Ind(hE)VP*D-CN) showed a reduced cpCasp2 potency by 1.61 log units (pK_i = 6.38) compared to the corresponding aldehyde (**59**, Ind(hE)-VP*D-CHO, pK_i = 7.71) with no detectable Casp3 activity. The respective (*R*)-forms of **68**−**71** displayed no inhibitory potency for cpCasp2 and Casp3, with the exception of AcVDVA((*R*)-D)-CN ((***R***)-**68**), which exhibited moderate inhibition (pK_i (cpCasp2): 6.11, pK_i (Casp3): 5.58) but had a lower pK_i value compared to the corresponding (*S*)-form (**68**).

(Quin)hE-G/V-XD-CN & (2-Me-Idc)hE-G/V-XD-CN (72−87)

With the exception of AcVDVAD-CN and AcVDVA((*R*)-D-CN) (**68** and (***R***)-**68**), none of the nitrile peptidomimetics showed any detectable activity against Casp3. In general, the conversion of the aldehyde to the nitrile was accompanied by a loss of inhibitory potency at cpCasp2, consistent with the higher intrinsic reactivity of the aldehyde. The potency loss ranged from 0.48 (MUR-2425, **87**) to 2.29 log units (**85**). The inhibitors with (*R*)-configuration at P1 consistently showed significantly reduced activity at cpCasp2, with (nearly) inactive pK_i values ranging from 5.95 (**86**) to <4.8. In accordance with the results of the aldehyde series, the compounds with Quin in P5 were generally less potent than the 2-Me-Idc analogs (**72**-**79** vs **80**-**87**). Moreover, the decrease in cpCasp2 inhibitory potency upon conversion from aldehyde to nitrile was generally more pronounced for Quin-containing compounds than for their 2-Me-Idc counterparts. The only exception for this observation is the comparison of the nitrile compounds **77** ((Quin)(hE)V((S)-Me-THIQ)D-CN; loss of 2.11 log units) and **85** ((2-Me-Idc)(hE)V((S)-Me-THIQ)D-CN; loss of 2.29 log units) with their corresponding aldehydes **49** and **65**. These findings further highlight 2-Me-Idc as the most advantageous P5 scaffold for nitrile-based inhibitors. Compound **87** (MUR-2425) with the sequence (2-Me-Idc)(hE)-VP*D-CN clearly emerges as the most potent nitrile inhibitor with a pK_i value of 7.75 and >800-fold selectivity over Casp3, followed by (2-Me-Idc)(hE)G((*S*)-Me-THIQ)D-CN (**84**, pK_i = 7.31). The best compound with Dab in P2 is (2-Me-Idc)(hE)G(Dab)D-CN (**80**, pK_i = 6.67). The highest inhibitory potency among inhibitors with glycine in P2 was observed for (2-Me-Idc)(hE)VG((rac)-D)-CN ((***rac***)-**83**, pK_i = 6.60). Regarding the latter, it should be noted that the reported value reflects the mixture of the (*R*) and (*S*) epimer at P1, since separation of the epimers after the nitrile conversion was particularly difficult for compounds containing G in P2. Consequently, a direct comparison of compounds containing racemic (*rac*)-D-CN with those bearing the pure (*S*)-D-CN configuration should be interpreted with caution. Nevertheless, since the epimeric ratio is approximately 1:1, the reported potency provides a reasonable estimate, as the calculated pK_i values would theoretically differ by only a factor of two. Among the Quin-containing inhibitors, (Quin)(hE)VP*D-CN (**79**) was the most potent with a pK_i of 6.82 at cpCasp2 and 105-fold selectivity over Casp3. Compared with MUR-2425 (**87**), this corresponds to an approximately 8-fold reduction in cpCasp2 inhibitory potency. Jump dilution experiments of

Downloaded from pubs.acs.org/jmcmar/article-pdf/doi/10.1021/acs.jmedchem.6c01371/6909867/acs.jmedchem.6c01371.pdf by UNIV REGENSBURG user on 17 November 2026

https://doi.org/10.1021/acs.jmedchem.6c01371
J. Med. Chem. XXXX, XXX, XXX−XXX

selected potent aldehydes and nitriles on cpCasp2 confirmed the reversible binding nature of both warhead scaffolds and are shown in Figure S493 (SI). While the residence time τ of the aldehydes is generally in the range of < 50 min, the corresponding nitriles show a clear trend toward faster dissociation from cpCasp2 (residence times < 10 min), reflecting the reduced intrinsic electrophilic reactivity of the nitrile. Of particular note are compounds **64** and **67**, which stand out among the reversible aldehydes with slightly prolonged residence times (τ = 110 min (**64**) and τ = 91 min (**67**)). However, inhibitor **52** (AcVDVP*D-CHO, τ = 492 min) approaches the irreversible reference compound emricasan ($\tau \geq$ 800 min) under the selected conditions.

Caspase Panel Assay

To investigate the effects of structural changes on the selectivity within the caspase family, selected aldehydes (**48**, **55**, **60**, **61**, **63**−**67**) and nitriles (**76**, **79**, **80**, **81**, (*rac*)-**83**, **84**, **86**, **87**, (***R***)-**87**) were additionally evaluated for their affinities toward Casp1, Casp6, Casp7, and Casp9 (Table 2). Compounds of particular interest (**60**, **64**-**67**, **79**, **80**, **84**, **86**, **87**) were also tested in an extended panel against Casp4, Casp5, Casp8, and Casp10 (Table 2). Comparison of aldehyde inhibitors generally showed that, compared to Quin in P5, 2-Me-Idc not only offers an advantage in terms of selectivity toward Casp3 (see Table 1) but also improves selectivity toward caspase-1, −6, −7, and −9 (e.g., **48** vs **64** and **55** vs **67**, Table 2). With respect to the P3 residue, valine, compared with glycine, increased activity toward Casp1 as demonstrated for compounds **60** (562-fold selective) and **61** (1.3-fold selective) with Dab in P2, for **64** (468-fold selective) and **65** (25-fold selective) with THIQ in P2, and for **66** (813-fold selective) and **67** (63-fold selective) with P* in P2. When comparing the combination -G−P*- in P3−P2 (**66**) with -V−P*- (**67**) in terms of selectivity, **66** with G in P3 consistently exhibits superior selectivity against Casp6, Casp7, and Casp9 (more than 3090-fold, Table 2) whereas the -V−P*- motif impaired particularly the selectivity against Casp6 (**55** and **67**). The opposite trend was observed for Casp3 , where compound **67** exhibited a higher selectivity factor of 676 than compound **66** (selectivity factor of 81). With pK_i values < 5.8, none of the compounds in the series exhibited significant inhibition of Casp7 and Casp9. Indeed remarkable was the effect of switching the warhead from the aldehyde to a nitrile, which completely eliminated potential selectivity issues with respect to Casp1, 3, 6, 7, and 9: None of the nitrile inhibitors showed notable inhibitory potency against these caspases. With regard to Casp8 and Casp10, inhibitor **67** (2-Me-Idc)(hE)VP*D-CHO) displayed comparably high pK_i values (pK_i = 7.85 for Casp8 and pK_i = 6.24 for Casp10), but could be significantly improved for the nitrile inhibitor **87** (pK_i of 6.37 at Casp8 and sub-micromolar potency at Casp10). Overall, the markedly improved selectivity across all tested caspases, combined with their lower intrinsic reactivity, makes the nitrile inhibitors more attractive candidates for drug development than their aldehyde counterparts. Consequently, compounds **80** (2-Me-Idc)(hE)-G(Dab)D-CN), **84** (2-Me-Idc)(hE)G((*S*)-Me-THIQ)D-CN, and **87** (2-Me-Idc)(hE)VP*D-CN) emerge as most promising inhibitors of this series (Figure 3). Compounds **80** and **84** are highly selective for cpCasp2, but not as potent as **87** pK_i = 7.75 for **87**, vs pK_i = 7.31 for **84**, and pK_i = 6.67 for **80**). Bearing the hydrophilic Dab residue in P2, compound **80** is expected to have a lower propensity to cross the BBB than the other two inhibitors and it has demonstrated lower chemical stability (Figure S5, SI). Compound **84** with the THIQ motif in P2 was considered to be metabolically vulnerable. In addition, the commercial availability of the building block for the 6-methyl-THIQ motif was restricted, which is a considerable liability with respect for future upscaling procedures. Consequently, compound **87** was chosen as the most promising lead compound, being the most potent inhibitor with a favorable Caspase selectivity profile (> 832-fold over Casp3, > 525 fold over Casp1, Casp4, Casp5, Casp6, Casp7, Casp9, and Casp10 and 24 fold selectivity over Casp8), and having the drug-like P* motif in P2. Compound (***R***)-**87** (the P1 epimer of MUR-2425) depicted only weak activity at Casp2 (pK_i = 5.22) and no activity at Casp1, Casp3, Casp6, Casp7, and Casp9, suggesting that it could serve as a negative control for MUR-2425 (**87**) in *in vivo* studies.

In Vitro Caspase-2-Catalyzed tau Cleavage Assay

The nitrile inhibitors **84** (2-Me-Idc)(hE)G((*S*)-Me-THIQ)D-CN) and **87** (MUR-2425, (2-Me-Idc)(hE)V(P*)D-CN), which exhibited the highest inhibitory potency at cpCasp2 in the fluorometric enzyme assay, were evaluated together with their aldehyde analogs **64** ((2-Me-Idc)(hE)G((*S*)-Me-THIQ)-D-CHO) and **67** (MUR-2424, (2-Me-Idc)(hE)V(P*)D-CHO) for their ability to block caspase-2-mediated cleavage of full-length human tau protein *in vitro* (Figure 4). The presence of Δtau314, the truncated tau fragment ending C-terminally at D314,[16] was assessed by Western Blotting. All four compounds inhibited Δtau314 formation with an IC_{50} in the low micromolar range. Consistent with the results of the fluorometric enzyme inhibition assay, the aldehyde inhibitors (**64**, **67**) showed slightly lower IC_{50} values than their nitrile analogs (**84**, **87**). The inhibitors with THIQ in P2 (**64**, **84**) were less effective in preventing the production of Δtau314 than the ones with P* in P2 (**67**, **87**). As expected from the fluorometric Casp2 inhibition assay, compound (***R***)-**87** was found to be ineffective in preventing tau cleavage (IC_{50} value of >100 μM; Figure S1) and thus once again confirmed its suitability as a negative control for **87** (MUR-2425).

Physicochemical Properties and Chemical Stability

We calculated the CNS MPO score (central nervous system multiparameter optimization score) as an established parameter to estimate and compare the blood-brain barrier (BBB) permeability of the peptidomimetic inhibitors (Table S1). The lipophilicity (ClogP), the calculated partition coefficient at pH = 7.4 (ClogD), the molecular weight (MW), the topological polar surface area (TPSA), the number of hydrogen bond donors (HBDs), and the pK_a of the most basic center are combined and weighted equally in the calculation. CNS MPO score ranges from 0 to 6, with higher values being more desirable for passive BBB diffusion.[49] All compounds of the series show a CNS MPO score of 3.0 besides the ones with Dab in P2, which scored 2.3. As a value of > 4 is generally considered indicative for successful crossing of the blood−brain barrier, Dab in P2 appeared disadvantageous from this perspective, although the present study confirmed the motif to be an effective Casp2 selectivity enhancer. The lower molecular weight for the compounds with G in P2 was not accompanied by an improved CNS MPO score. Overall, the structural modifications applied in the peptide series described in this study did not result in a significant improvement of the CNS MPO score compared to our previously published results.[34] A detailed list of calculated physicochemical

Downloaded from pubs.acs.org/jmcmar/article-pdf/doi/10.1021/acs.jmedchem.6c01371/6909867/acs.jmedchem.6c01371.pdf by UNIV REGENSBURG user on 17 November 2026

https://doi.org/10.1021/acs.jmedchem.6c01371
J. Med. Chem. XXXX, XXX, XXX−XXX

properties for selected inhibitors **64**, **67** (MUR-2424), **79**, **80**, **84**, and **87** (MUR-2425) can be found in the Supporting Information (Table S2).

Chemical Stability of Compounds 64, 67 (MUR-2424), 79, 80, 84, and 87 (MUR-2425)

2-Methyl indoline carboxylic acid (2-Me-Idc) proved to be the most favorable motif at position P5, providing higher selectivity and inhibitory potency than the other motifs investigated. The scaffold was designed to prevent the oxidation of indoline (Idc) to indole (Ind) by introduction of a methyl group in alpha position to the carbonyl group (Figure 1). This strategy worked out successfully, resulting in excellent chemical stability of highly potent Casp2 inhibitors bearing both aldehyde (**64**, **67**) and nitrile warheads (**84**, **87**). When stored in PBS or DMSO at 25 °C, less than 5% degradation (based on UV absorption at 220 nm) was detected within 7 days (aldehydes) or 14 days (nitriles) (Figure 5A and Figures S2−S7). Importantly, no oxidation to the corresponding indole derivative was detected. In contrast, in our previous study,[34] approximately 50% oxidation of Idc to Ind (estimated on UV absorption at 220 nm) was observed after 7 days at room temperature in DMSO. The aldehydes with 2-Me-Idc in P5 (**64** and **67**) were more stable in DMSO than in PBS. Storage appeared to affect the equilibrium between the aldehyde form and the hemiacetal form of aspartic acid in P1 as reflected by narrowing of the respective peak in the chromatogram. LC/MS analysis of the nitriles **84** and **87** revealed that hydrolysis of the nitrile to the corresponding amide was the predominant degradation pathway, although this process occurred only to a minor extent. Amide formation proceeded more rapidly in DMSO than in PBS. Compounds **64** and **84** exhibited inhibitory potency and selectivity comparable to those of compounds **67** (MUR-2424) and **87** (MUR-2425) while displaying even lower degradation, which supports the general suitability of 2-Me-Idc as a chemically stable P5 scaffold. Based on the cpCasp2 assays results, Quin was identified as a second potent motif for P5. We assessed the stability of **79** ((Quin)(hE)GPD-CHO) - the Quin analog of **87**- confirming that Quin is as stable as 2-Me-Idc. Compound **80**, the most active nitrile with Dab in P2, was examined as a representative for Dab containing inhibitors and showed enhanced degradation compared the other nitriles (88% purity after 14d storage at 25 °C). Chromatograms from LC-MS stability analysis of **64**, **67**, **79**, **80**, **84**, and **87** (MUR-2425) at 25, −20, and −80 °C are provided in Figures S2−S7.

ADMET and Pharmakokinetic Profile of Compounds 67 (MUR-2424), 79, 80, and 87 (MUR-2425)

Considering all of the previous results, compound **87** (2-Me-Idc)(hE)VP*D-CN (MUR-2425) emerged as an optimized potent and selective Casp2 inhibitor. Together with the corresponding aldehyde **67** (2-Me-Idc)(hE)VP*D-CN (MUR-2424), **87** (MUR-2425) was subjected to its *in vitro* properties regarding absorption, distribution, metabolism, excretion, and toxicity (ADMET) and regarding its *in vivo* pharmacokinetic properties (PK) in CD-1 mice. Compounds **79** (best nitrile inhibitor with Quin in P5) and **80** (best nitrile inhibitor with Dab in P2) were investigated for comparison with **87** (MUR-2425) with respect to their ADMET and PK profile, to estimate the effect of these structural modifications on the pharmacokinetic performance.

***In Vitro* ADMET Profile.** In general, MUR-2425 (**87**) and MUR-2424 (**67**) exhibited a rather hydrophilic compound profile with experimentally determined logD values of ≤ 2.59 (MUR-2425) and −1.75 (MUR-2424) (shake flask method, cf. Table S4). Both compounds also displayed good aqueous solubility of the TFA salts in PBS (pH 7.4) reaching 5 mg/mL or 6.51 mM for MUR-2425 and ≥ 77 mg/mL or ≥ 100 μM for MUR-2424. The conversion of MUR-2425 from the TFA salt into the disodium salt marks an important step in terms of biocompatibility and dramatically increased the solubility by 20-fold to > 100 mg/mL (> 143.53 mM, Figure 5B, Figure S8 and Table S3, SI). The polar character of MUR-2425 favored solubility but in combination with the high molecular weight (Mw = 652.32 g/mol), it lead to poor membrane penetration. This was confirmed in MDCK-MDR1 permeability studies by low permeability coefficients both from apical to basolateral compartment ($(P_{app(A\text{-}B)}$= 0.27 * 10^{-6} cm/s) and vice versa ($P_{app(B\text{-}A)}$ = 0.22 × 10^{-6} cm/s, Table S5, SI). The low permeability together with an efflux ratio of 0.81 further indicated that MUR-2425 is no substrate of MDR1-mediated transport. MUR-2425 showed excellent stability under physiological conditions in human, rat and mouse plasma and whole blood samples with recovery rates of 88% to ≥ 100% after 120 min incubation at 37 °C, Figure 5C and Table S6, SI. Moderate plasma protein binding of 14−27% was observed across all three species (Figure 5D and Table S7, SI). The lowest recovery rate was found in rat whole blood (88%) which also showed the highest plasma protein binding (27%). Furthermore, MUR-2425 was barely affected by metabolic degradation in human, rat, and mouse hepacotocytes, liver S9 fractions and liver microsomes (recovery rates ≥ 90% after 60 min incubation at 37 °C, Figure 5E and Table S8, SI). LC-MS-based metabolite identification in human, rat, mouse, dog, monkey, and minipig hepatocytes confirmed the high metabolic resilience of MUR-2425 (recovery rates of > 95% after 240 min incubation at 37 °C in all species) and proposed two possible metabolites M1 and M2 of MUR-2425 (Figure 5F and Table S9, SI). M1 is the product of an oxidation process of 2-Me-Idc in P5 (0.53%) and was only detected in mouse hepatocytes. M2 arised from hydrolysis of the nitrile warhead to the corresponding amide (0.03% (human), 0.72% (mouse), 0.03% (rat), 0.02% (dog), 0.01% (monkey), 0.04% (minipig)). No unique metabolite was detected in human. The metabolic turnover of MUR-2425 was too low to enable CYP phenotyping in human liver microsomes. Consequently, the responsible CYP isoform(s) could not be identified, (91−98% of the parent compound remained after incubation regardless of whether selective CYP inhibitors were present).

The corresponding aldehyde MUR-2424 (**67**) was evaluated only in human and mouse species (Tables S3−S8 and Figures S9−S11 (SI)). Remarkably, MUR-2424 displayed membrane permeability and stability in plasma, whole blood, hepatocytes, liver S9 fractions, and liver microsomes comparable to those of the nitrile analog. These findings demonstrated that despite the higher intrinsic reactivity of the aldehyde warhead, aldehyde-based peptidomimetics are not inherently less stable under physiological conditions.

The inhibitors **79** and **80** showed ADMET profiles largely comparable to those of MUR-2425 with high solubility of at least 300 μM (disodium salts), negative logD values (−2.02 (**79**) and −3.21 (**80**)), low membrane penetrance ($(P_{app(A\text{-}B)}$(**79**) = 0.39 * 10^{-6} cm/s, ($(P_{app(B\text{-}A)}$(**79**) = 0.69 * 10^{-6} cm/s; ($(P_{app(A\text{-}B)}$(**80**) = 0.64 * 10^{-6} cm/s, ($(P_{app(B\text{-}A)}$(**80**) = 0.62 * 10^{-6} cm/s)) and high stability in human, rat, and mouse plasma, blood, hepatocytes, liver S9 fractions, and liver

Downloaded from pubs.acs.org/jmcmar/article-pdf/doi/10.1021/acs.jmedchem.6c01371/6909867/acs.jmedchem.6c01371.pdf by UNIV REGENSBURG user on 17 November 2026

https://doi.org/10.1021/acs.jmedchem.6c01371
J. Med. Chem. XXXX, XXX, XXX−XXX

microsomes (Figures S9, S11, Tables S3−S6 and S8, SI). Of note is the decreased half-life of compound **79** in whole blood samples ($t_{1/2}$ = 99 min (human), $t_{1/2}$ = 156 min (rat), $t_{1/2}$ = 131 min (mouse), Figure S11, Table S8, SI). The three compounds mainly differ in their binding to plasma proteins (Figure S10 and Table S7, SI): **79** showed elevated bound fractions (69%, 79%, 49%; human, rat, mouse) whereas **80** showed lower bound fractions (4%, 3%, 8%; human, rat mouse) compared to MUR-2425 (25%, 27%, 14%; human, rat, mouse), which is as expected from the higher hydrophilicity brought into **80** by Dab in P2. The overall amount of metabolites of MUR-2425, **79**, and **80** that were identified in mouse, rat, dog, monkey, minipig, and human hepatocytes remained below 3% in each case (Table S9, SI). Interestingly, the proposed metabolic pathways differed between the three compounds: Whereas MUR-2425 primarily underwent nitrile hydrolysis and oxidation of the P5 scaffold (Figure 5F), compound **79** formed two glucuronide conjugates, while **80** underwent cysteine conjugation followed by stepwise cleavage of the peptide backbone (Figure S12, SI).

MUR-2425 was further evaluated for potential drug−drug interactions and safety aspects. At concentrations of 1 and 10 μM, no induction of the CYP isoforms CYP1A2, CYP2B6, and CYP3A4 was observed in human hepatocytes (Figure S13, SI), nor was inhibition of the CYP isoforms CYP1A2, CYP2A6, CYP2B6, CYP2C8, CYP2C9, CYP2C19, CYP2D6, CYP2E1, and CYP3A4 detected in human liver microsomes (Figure S14, SI). The compound did not affect cell viability of human hepatocytes under these conditions. Additionally, no inhibition of the critical human Ether-à-go-go related gene (hERG) channel could be seen in a concentration of 30 μM using two independent techniques (patch clamp system and FLIPR assay, Figure S15, SI). Finally, MUR-2425 did not show activity ($\geq$ 50% inhibition or stimulation for 10 μM compound concentration) against 116 relevant safety off-targets that were investigated using the Eurofins SafetyScreenPlus Panel (Figure S16, SI).

Overall, the *in vitro* ADMET profile of MUR-2425 is characterized by an excellent aqueous solubility and high chemical and metabolic stability. There is no evidence for any critical interaction, off-target effect, or toxic degradation product of MUR-2425 in this data set.

***In Vivo* Pharmacokinetics (PK).** Pharmacokinetic studies comparing plasma and brain levels of MUR-2424 (**67**), **79**, **80**, and MUR-2425 (**87**) following different routes of administration and dosages were conducted in male and female CD1 mice. The aldehyde MUR-2424 was evaluated in a dose of 10 mg/kg by intravenous (iv) and subcutaneous (sc) injections of the TFA salt. The nitrile MUR-2425 was administered subcutaneously at doses of 3, 10, and 30 mg/kg in both the TFA or the disodium salt form, whereas the disodium salt was additionally given sc in doses of 0.3 and 1 mg/kg, and the TFA salt was additionally given orally (po) with 10 mg/kg and 50 mg/kg. Compounds **79** and **80** were administered subcutaneously at 3, 10, and 30 mg/kg using the disodium salt form. The in vivo PK data of MUR-2424 are summarized in Table S10 and Figure S17 (SI), the data of MUR-2425 are summarized in Figure 6 (disodium salt), Figure S19 (TFA salt), and Table S12 (SI). The in vivo PK data of **79** and **80** are summarized in Table S11 and Figure S18 (SI).

In our previously reported peptide series, compound **1** (MUR-65) did not reach measurable concentrations in the brain following subcutaneous (sc) injection.[34] In contrast, the refined aldehyde MUR-2424 successfully enters the brain after iv and sc injection of 10 mg/kg (Figure S17, SI). The calculated brain/plasma ratios ((AUC_{last}brain)/(AUC_{last}plasma)) were comparable for the two different administration routes (0.0067 (iv) and 0.013 (sc)) indicating that transport across the blood−brain barrier rather than systemic exposure is the limiting factor for brain distribution. Thus, the higher plasma levels following iv injection (C_{max}(iv) = 31913 ng/mL, AUC_{last}/dose(iv) = 15149 h*ng/mL) compared to sc injection (C_{max}(sc) = 1837 ng/mL, AUC_{last}/dose(sc) = 65.2 h*ng/mL) were not accompanied with a proportionally higher brain exposure, but instead resulted in a slightly lower brain/plasma ratio (Table S10, SI). When comparing MUR-2424 with MUR-2425 (10 mg/kg; sc; TFA salt, Figure S17 with S19 and Table S10 with S12, SI), MUR-2425 achieves slightly higher plasma levels ($c_{0.25h}$= 3053 ng/mL (male), $c_{0.25h}$= 3623 ng/mL (female) and AUC_{last}/dose = 189 h*ng/mL (male), AUC_{last}/dose = 214 h*ng/mL (female)) than MUR-2424 ($c_{0.25h}$= 1863 ng/mL (female), AUC_{last}/dose = 65.2 h*ng/mL (female)). Meanwhile, the brain plasma ratio remained comparable (0.011 and 0.0075 (male and female) for MUR-2425; 0.013 for MUR-2424).

Following subcutaneous administration of MUR-2425 at doses ranging from 0.3 to 30 mg/kg, plasma exposure increased in a clear dose-dependent manner (Figure 6 and Figure S19, SI). Despite the relatively low brain/plasma ratio of 0.007−0.032 (Table S12, SI), measurable concentrations of MUR-2425 were detected in the brain even after administration of 1 mg/kg, which is remarkable due to the size and polarity of this pentapeptidic molecule. No significant differences were observed between male and female animals or between the TFA salt and disodium salt form.

After oral administration of MUR-2425 at 10 mg/kg or 50 mg/kg, dose-dependent peak plasma levels show systemic bioavailability (AUC_{last}/D) of 0.1% compared to the sc application (Figure S19 and Table S12, SI). Given the low systemic exposure and the brain/plasma ratio of 0.007−0.037 (determined from sc administration), it is not surprising that brain concentrations remained below the limit of quantification following oral dosing. Nevertheless, these findings demonstrate that gastrointestinal absorption of MUR-2425 is possible in principle. The development of a suitable formulation could hold considerable promise for an improvement.

Replacement of 2-Me-Idc by Quin in P5 leads from MUR-2425 to the inhibitor **79**, which showed a similar PK profile as MUR-2425 but higher C_{max} values in the male cohort (Figure 6, Figure S18 and Tables S11−S12, SI). When hydrophilic Dab was used in P2, the CNS-MPO score switched to 2.3 for compound **80**, compared to 3.0 for MUR-2425 and **79**. Surprisingly, the *in vivo* PK data show even slightly higher C_{max} values of **80** in both plasma and brain compared to MUR-2425. In addition, the maximum concentrations both in brain and plasma were detected at a later time point (Figure 6, Figure S18 and Tables S1−S12, SI). The data indicates that a higher polarity of **80** - reflected in the lower CNS MPO score - does not reduce the overall extent of absorption or brain penetration but rather slows the kinetics of transport from the subcutaneous interstitium into the bloodstream and subsequently across the blood−brain barrier. One possible explanation for this effect could be the formation of an intramolecular salt bridge between the primary amino group of the Dab side chain and the carboxyl group of either hE at P4 or the C-terminal aspartic acid residue, which may influence

Downloaded from pubs.acs.org/jmcmar/article-pdf/doi/10.1021/acs.jmedchem.6c01371/6909867/acs.jmedchem.6c01371.pdf by UNIV REGENSBURG user on 17 November 2026

https://doi.org/10.1021/acs.jmedchem.6c01371
J. Med. Chem. XXXX, XXX, XXX−XXX

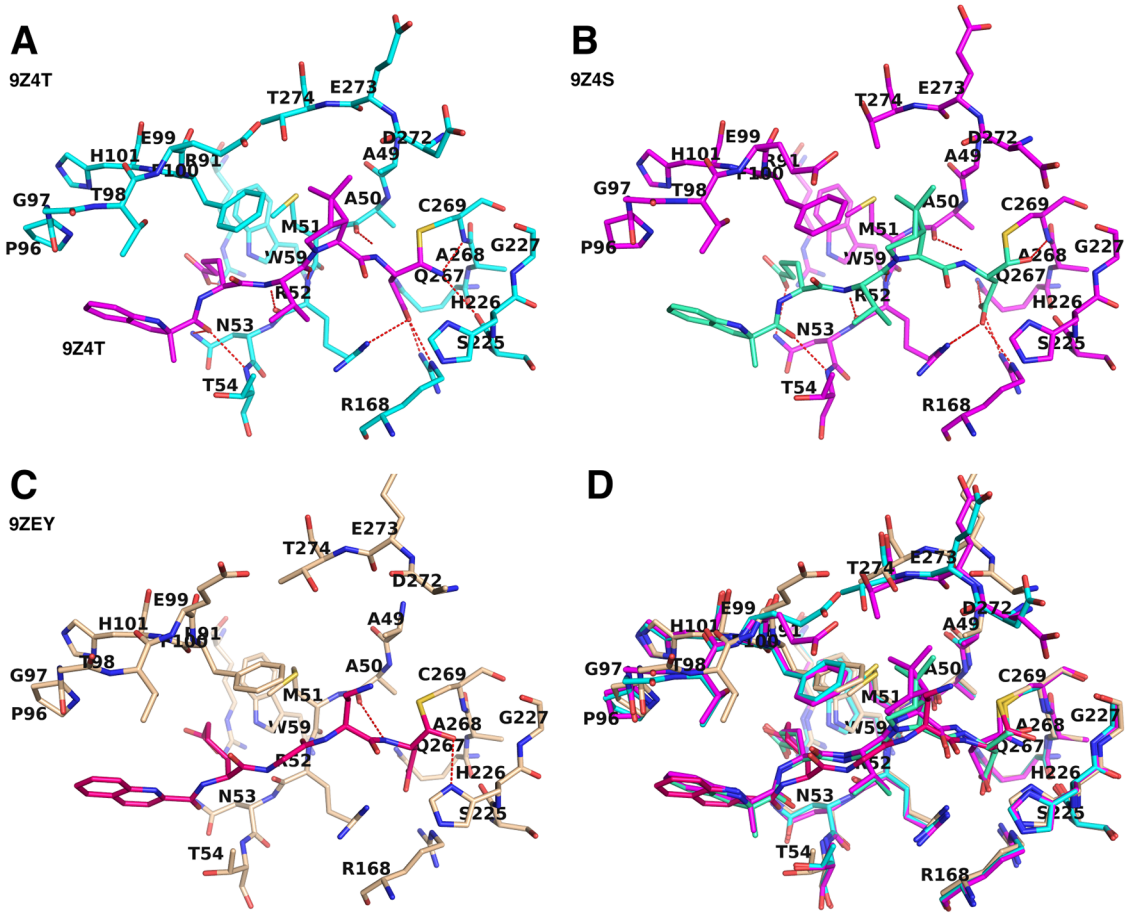


Figure 7. Comparison of JF1cpCasp2 crystal structures in complex with **87** (MUR-2425, (2-Me-Idc)(hE)VP*D-CN), **67** (MUR-2424, (2-Me-Idc)(hE)VP*D-CHO), and **41** ((Quin)(hE)G(Dab)D-CHO). (A) Hydrogen bond (H-bond) interactions of MUR-2425 bound to JF1cpCasp2 (PDB ID: 9Z4T). (B) H-bond interactions of MUR-2424 bound to JF1cpCasp2 (PDB ID: 9Z4S). (C) H-bond interactions of (Quin)(hE)G(Dab)D-CHO bound to JF1cpCasp2 (PDB ID: 9ZEY). (D) Structural alignment of the three JF1cpCasp2 complexes (PDB IDs: 9Z4T, 9Z4S, and 9ZEY). The RMSD values for the alignments of 9Z4S and 9ZEY with 9Z4T are 0.21 and 0.40 Å, respectively.

membrane penetration. All three investigated nitrile inhibitors show comparable brain/plasma ratios of roughly 0.01 (ranges from 0.0047 to 0.0093 (**79**), 0.0074−0.020 (**80**), and 0.006−0.037 (MUR-2425) Tables S11−S12, SI). MUR-2425 exhibits a pharmacokinetic profile comparable to or better than those of **79** and **80** and is characterized by higher potency and selectivity for cpCasp2.

Crystallography

Complexes of the three inhibitors (Quin)(hE)G(Dab)D-CHO (**41**, PDB ID: 9ZEY), (2-Me-Idc)(hE)VP*D-CHO (**67**, MUR-2424, PDB ID: 9Z4S), and (2-Me-Idc)(hE)VP*D-CN (**87**, MUR-2425, PDB ID: 9Z4T) bound to JF1 cPCasp2 (cf. Figure 7) were obtained under identical conditions using reagents repurchased from the ECO-PACT crystallization screen (Molecular Dimensions). Crystals selected for data collection were grown in 0.1 M Tris (pH 8.0), 0.2 M NaCl, and 20% (w/v) PEG6000. Crystals appeared within 24 h and reached full size within 3 days. Among the three species, JF1cpCasp2−**41** crystallized in space group $P2_1$, with unit cell parameters a = 61.67 Å, b = 128.12 Å, c = 76.24 Å, α = 90.00°, β = 108.18°, γ = 90.00°, and two homodimers in the asymmetric unit. Conversely, JF1cpCasp2−MUR-2424 and JF1cpCasp2−MUR-2425 belonged to the orthorhombic crystal system (space group $P2_12_12_1$) and had two molecules (one homodimer) in the asymmetric unit. Their unit cell parameters were a = 75.75 Å, b = 81.74 Å, c = 112.60 Å and a = 74.29 Å, b = 79.45 Å, c = 112.36 Å, respectively.

JF1cpCasp2−MUR-2425 exhibited the highest resolution at 1.53 Å. In contrast, JF1cpCasp2−**41** diffracted to 2.25 Å, the lowest resolution among the three. JF1cpCasp2−MUR-2424 diffracted to 1.61 Å. The B-factors follow a consistent trend: MUR-2425 shows significantly higher stability, with an average ligand B-factor of 38.02 Å^2 (compared with the overall structure average: 25.58 Å^2). This is notably lower than **41** (ligand: 57.51 Å^2, structure: 29.80 Å^2) and MUR-2424 (ligand: 53.02 Å^2, structure: 27.91 Å^2). Data are summarized in Table S13 (SI).

Despite differences in crystallographic statistics, the three structures are remarkably similar. All inhibitors bind within the active site pocket and form covalent S−C bonds with the catalytic sulfur atom. The root-mean-square deviation (RMSD) between Chain A of 9Z4T (Figure 7A) and 9Z4S (Figure 7B) is only 0.21 Å over 252 Cα atoms, while the RMSD between 9ZEY (Figure 7C) and 9Z4T is 0.40 Å over 237 Cα atoms. Structural alignment of the three JF1cpCasp2 complexes are shown in Figure 7D.

In the 9ZEY structure, H-bonds (distances <3.2 Å are shown) are primarily localized at the P1 and P2 positions. In contrast, in 9Z4S and 9Z4T, the H-bonding network extends along the entire inhibitor chain. Because 9ZEY features a

https://doi.org/10.1021/acs.jmedchem.6c01371
J. Med. Chem. XXXX, XXX, XXX−XXX

Downloaded from pubs.acs.org/jmcmar/article-pdf/doi/10.1021/acs.jmedchem.6c01371/6909867/acs.jmedchem.6c01371.pdf by UNIV REGENSBURG user on 17 November 2026

flexible Dab (diaminobutyric acid) side chain at the P2 position, the Phe100 side chain collapses slightly into the binding pocket, effectively reducing its volume. Conversely, both MUR-2424 and MUR-2425 possess larger, more rigid P2 side chains that interact more effectively with the pocket architecture. Notably, the P1 nitrile group (C≡N) of MUR-2425 adopts a significantly different orientation than the carbonyl (C=O) in 9ZEY and 9Z4S. The nitrogen atom of the nitrile group moves over 1.0 Å toward the His226 side chain, forming two hydrogen bonds: one with the backbone nitrogen of Cys269 and another with the carbonyl oxygen of His226.In comparison, the carbonyl oxygen of the aldehyde inhibitors primarily forms a single hydrogen bond with the backbone nitrogen of Cys269.

SUMMARY AND CONCLUSION

We designed and synthesized a new series of covalent-reversible pentapeptidic Casp2 inhibitors which were tested in a fluorescence-based assay to determine their inhibitory potency for cpCasp2 and their selectivity over Casp1, Casp3, Casp4, Casp5, Casp6, Casp7, Casp8, Casp9 and Casp10. Based on our findings from previous studies, where we reported Idc as potent but chemically unstable P5 scaffold,[34] we focused on overcoming the chemical instability of this P5 residue. The resulting SAR revealed that an aromatic system in combination with a nitrogen capable of hydrogen-bond interactions is preferred for effective Casp2 inhibition. Following this design strategy, we successfully established 2-methyl-indoline-carboxylic acid (2-Me-Idc) as a new P5 scaffold that enhances inhibitory potency and selectivity for cpCasp2 while providing high chemical stability. Quinaldic acid (Quin) also proved to be a suitable alternative, exhibiting only slightly lower potency and selectivity than 2-Me-Idc while even improving chemical stability. Furthermore, systematic SAR throughout the whole peptide series showed that P2 and P3 must be considered together to achieve an optimal fit within the S2−S3 pocket of Casp2, and that these two positions can play a decisive role in conferring selectivity over other caspases once this fit is established. With the aim of reducing the risk of porential undesired off-target effects, we established a protocol to convert the aldehyde warhead of our most potent pentapeptidic inhibitors from a highly reactive aldehyde to the milder nitrile. Although this warhead replacement reduced potency for cpCasp2 to varying degrees, it also led to an excellent selectivity profile, reducing the potency or completely removing the interaction with the other members of the human caspases. The aldehyde inhibitors **64**, **67** (MUR-2424), and nitrile inhibitors **84** and **87** (MUR-2425) were confirmed to block the formation of the pathophysiological tau cleavage product Δtau314 in an *in vitro* efficacy assay. Inhibitor **87** (MUR-2425) was selected as the optimized lead compound and evaluated in humans, rats, and mice with regard to its *in vitro* ADMET profile. These studies demonstrated good solubility, a long plasma half-life, high metabolic stability, and the absence of any safety concerns in terms of off-target effects, CYP interactions, or critical degradation products. Pharmacokinetic studies in CD-1 mice further showed that MUR-2425 penetrates the brain after subcutaneous injection of 1, 3, 10, and 30 mg/kg with a brain/plasma ratio of 0.006−0.037. In contrast, no detectable brain concentrations were observed after oral administration. Comparable *in vitro* ADMET and *in vivo* PK results for the aldehyde analog **67** (MUR-2424) indicate that the modifications in P1−P5 regardless of the warhead change to a nitrile, already represent a successful improvement over the former lead compound **1** (MUR-65). MUR-2424 reached measurable brain concentrations after subcutaneous administration and exhibited ADME properties stable as those of MUR-2425. ADMET and *in vivo* PK profiling of nitrile compounds **79** and **80** demonstrated that there is scope for structural modifications within the peptide series without compromising pharmacokinetic properties and brain penetrance. Nevertheless, MUR-2425 remains overall superior to **79** or **80** owing to its high specific potency for Casp2. Cocrystals of compounds **67** (MUR-2424) and **87** (MUR-2425) bound to JF1cpCasp2 have similar structures (RMSD 0.21 Å) but show noticeable differences of the P1 aldehyde and nitrile warhead positioning affecting overall interactions along the peptide backbone. Overall, this study combines ligand-based drug design, a systematic SAR analysis incorporating structural biology, ADMET and pharmacokinetic evaluations to propose MUR-2425 as a brain-penetrant, selective Casp2 inhibitor for further clinical development in the treatment of neurodegenerative tauopathies.

EXPERIMENTAL SECTION

Chemistry

Commercially available chemicals, solvents and the building blocks *N*-(9-Fluorenylmethoxycarbonyl)-L-alanine (Fmoc-Ala-OH), 1*H*-Benzimidazole-2-carboxylic acid, *N*-(9-flluorenylmethoxycarbonyl)-*O*-benzyl-L-threonine (Fmoc-Thr(OBn)−OH), cyclohexaneacetic acid, 3-cyclohexyl-2-{[(9*H*-fluoren-9-ylmethoxy)carbonyl]amino}propionic acid (Fmoc-Cha−OH), (*S*)-2-((((9*H*-fluoren-9-yl)methoxy)-carbonyl)amino)-2-cyclohexylacetic acid (Fmoc-Chg−OH), 3-cyclohexylpropionic acid, *N*-(9-fluorenylmethoxycarbonyl)-L- aspartic-acid-4-*tert*-butylester (Fmoc-Asp(OtBu)−OH), N_{α}-Fmoc-N_{γ}-*tert*-butyloxycarbonyl-L-2,4-diaminobutyric acid (Fmoc-Dab(Boc)−OH), N_{α}-(9-fluorenylmethyloxycarbonyl)-L-glutamic-acid-γ-t-butyl ester (Fmoc-Glu(OtBu)−OH), Fmoc-L-α-homoglutamic acid 6-*tert*-butyl ester (Fmoc-hE(OtBu)−OH), *N*-(9-fluorenylmethoxycarbonyl)-L-phenylalanine (Fmoc-Phe-OH), *N*-[(9*H*-fluoren-9-ylmethoxy)carbonyl]-4-fluor-L-phenylalanine (Fmoc-Phe-(4-F)−OH), *N*-[(9*H*-fluoren-9-ylmethoxy)carbonyl]-4-methyl-L-phenylalanine (Fmoc-Phe(4-Me)−OH), *N*-(9-fluorenylmethoxycarbonyl)glycine (Fmoc-Gly-OH), *N*-(9-fluorenylmethoxycarbonyl)-L-isoleucine (Fmoc-Ile-OH), (*S*)-*N*-α-(9-fluorenylmethyloxycarbonyl)-2-indolinecarboxylic acid (Fmoc-Idc−OH), (*S*)-2-methylindoline-2-carboxylic acid hydrochloride (Fmoc-Idc−OH), indan-5-sulfonyl-chloride, (2*S*,3a*S*,7a*S*)-1-Fmoc-octahydroindol-2-carboxylic acid (Fmoc-Oic−OH), *N*-(9-fluorenylmethoxycarbonyl)-L-proline (Fmoc-Pro-OH), phenylacetic acid, Fmoc-L-α-phenylglycine (Fmoc-Phg−OH), 3-phenylpropionic acid, 3-(4-fluorphenyl)propionic acid, 3-(4-methylphenyl)propionic acid, 3-(4-hydroxyphenyl)propionic acid, quinaldic acid (Quin−OH), (*S*)-1-(((9*H*-fluoren-9-yl)methoxy)carbonyl)-6-methyl-1,2,3,4-tetrahydroquinoline-2-carboxylic acid (Fmoc-(*S*)-Me-THIQ−OH), *N*-(9-fluorenylmethoxycarbonyl)-*O*-*tert*-butyl-L-threonine (Fmoc-Thr(OtBu)−OH), *N*-(9-fluorenylmethoxycarbonyl)-L-valine (Fmoc-Val-OH), *N*-(9-fluorenylmethoxycarbonyl)-*O*-*tert*-butyl-L-tyrosine (Fmoc-Tyr(OtBu)−OH) were purchased from standard commercial suppliers (abcr (Karlsruhe, Germany), Acros Organics (Geel, Belgium), Alfa Aesar (Karlsruhe, Germany), BLD Pharmatech (Reinbek, Germany), Carbolution (St. Ingbert, Germany), Iris Biotech (Marktredwitz, Germany), Merck (Darmstadt, Germany), Sigma-Aldrich (Munich, Germany), TCI Europe (Zwijndrecht, Belgium)) and were used as received. Fmoc protection of enantiopure (S)-6-methyl-1,2,3,4-tetrahydroisoquinoline-1-carboxylic acid to achieve (S)-2-(((9*H*-fluoren-9-yl)methoxy)carbonyl)-6-methyl-1,2,3,4-tetrahydroisoquinoline1-carboxylic acid (Fmoc-(*S*)-Me-THIQ−OH) was performed as described previously.[33,34] Deuterated solvents for nuclear magnetic

Downloaded from pubs.acs.org/jmcmar/article-pdf/doi/10.1021/acs.jmedchem.6c01371/6909867/acs.jmedchem.6c01371.pdf by UNIV REGENSBURG user on 17 November 2026

https://doi.org/10.1021/acs.jmedchem.6c01371
J. Med. Chem. XXXX, XXX, XXX−XXX

resonance (^{1}H NMR and ^{13}C NMR) spectra were purchased from Deutero GmbH (Kastellaun, Germany). All reactions carried out with dry solvents were accomplished in dry flasks under nitrogen or argon atmosphere. For the preparation of buffers, HPLC eluents and stock solutions Millipore water was used. Column chromatography was accomplished using Merck silica gel Geduran 60 (0.063−0.200 mm). Flash chromatography was performed using an Advion Interchim puriFlash XS 520 Plus purification system (Advion, Ithaca, NY; Interchim, Montluçon, France) with SI-HP 30 μm puriFlash columns from Interchim (Montlucon, France). Reactions were monitored by thin layer chromatography (TLC) on Merck silica gel 60 F254 aluminum sheets and spots were visualized under UV light at 254 nm, by potassium permanganate or ninhydrin staining. Lyophilization was done with a Labogene CoolSafe 100−9 Pro equipped with a Welch CRV Pro 2 vacuum pump (Labogene, Allerød, Denmark). Nuclear magnetic resonance (^{1}H NMR and ^{13}C NMR) spectra were recorded on a Bruker (Karlsruhe, Germany) Avance 300 (^{1}H: 300 MHz, ^{13}C: 75 MHz), 400 (^{1}H: 400 MHz, ^{13}C: 101 MHz), 500 (^{1}H: 500 MHz, ^{13}C: 126 MHz) or 600 (^{1}H: 600 MHz, ^{13}C: 151 MHz) spectrometer using perdeuterated solvents. The chemical shift δ is given in parts per million (ppm). Multiplicities were specified with the following abbreviations: s (singlet), d (doublet), t (triplet), q (quartet), and m (multiplet) as well as combinations thereof. ^{13}C NMR-Peaks were determined by DEPT 135 and DEPT 90 (distortionless enhancement by polarization transfer). NMR spectra were processed with MestReNova 15.0 (Mestrelab Research, Compostela, Spain). High-resolution mass spectrometry (HRMS) was performed on an Agilent 6540 UHD Accurate-Mass Q-TOF LC/MS system (Agilent Technologies, Santa Clara, CA) using an ESI source. A preparative HPLC system from Thermo Fisher Scientific consisting of an UltiMate 3000 HPG-3200BX PUMP and a VWD-3400RS UV/vis-detector were used for compound purification (Thermo Fisher Scientific, Waltham, MA). A Phenomenex Gemini 5 μm NX-C18 column (110 Å, 250 × 21.2 mm, Phenomenex Ltd., Aschaffenburg, Germany) served as stationary phase. As mobile phase, 0.1% TFA in Millipore water and acetonitrile (MeCN) was used. The temperature was 25 °C, the flow rate 20 mL/min and UV detection was performed at 220 nm. Analytical purity and stability control was performed on an 1100 HPLC system from Agilent Technologies equipped with an Instant Pilot controller, a G1312A binary pump, a G1329A ALS autosampler, a G1379A vacuum degasser, a G1316A column compartment, and a G1315B diode array detector (DAD) or on a Vanquish Core HPLC system from Thermo Fisher Scientific equipped with a Binary Pump C, a Split Sampler CT, Column Compartment C, a Diode Array Detector CG and an ISQ EC Single Quadrupole Mass Spectrometer (Thermo Fisher Scientific, Waltham, MA). The column was a Gemini 5 μm NX-C18 column (110 Å, 250 × 4.6 mm) or Gemini 3 μm NX-C18 column (110 Å, 150 × 3 mm) (Phenomenex Ltd., Aschaffenburg, Germany) tempered at 30 °C. As mobile phase, mixtures of MeCN and aqueous TFA or mixtures of MeCN and aqueous formic acid were used (Method A: Gemini 5 μm, linear gradient: MeCN/TFA(0.05%) (v/v) 0 min: 10:90, 25−35 min: 95:5, 36−45 min: 10:90, flow rate = 1.00 mL/min, t_0 = 2.90 min; Method B: Gemini 3 μm, linear gradient: MeCN/TFA (0.05%) (v/v) 0 min: 10:90, 15−21 min: 95:5, 21.5−27 min: 10:90, flow rate = 0.50 mL/min t_0 = 1.58 min; Method C: Gemini 3 μm, linear gradient: 0.025% formic acid in MeCN/formic acid (0.05%) (v/v) 0 min: 10:90, 15−21 min: 95:5, 21.5−27 min: 10:90, flow rate = 0.50 mL/min, t_0 = 1.58 min; Method D: Gemini 3 μm, linear gradient: 0.025% formic acid in MeCN/formic acid (0.05%) (v/v) 0 min: 5:95, 15−21 min: 95:5, 21.5−27 min: 5:95, flow rate = 0.50 mL/min, t_0 = 1.58 min). Capacity factors were calculated according to $k = (t_R - t_0)/t_0$. Furthermore, a filtration of the stock solutions with PTFE filters (25 or 15 mm, 0.2 μm, Phenomenex Ltd., Aschaffenburg, Germany) was carried out before testing. Compound purities determined by HPLC were calculated as the peak area of the analyzed compound in % relative to the total peak area (UV detection at 220 nm). All compounds are >95% pure by HPLC.

Synthesis and Analytical Data

General Procedure for the Synthesis of Aldehydes (8−67). The peptidomimetic aldehydes were obtained by solid-phase peptide synthesis in 10 mL syringes by alternately coupling and deprotecting the respective N-terminal F-moc-protected amino acids or carboxylic acids on an aspartic acid-loaded semicarbazide-amino Merrifield resin (100−500 mg) synthesized as previously reported.[28] The general procedure is described below for an exemplary batch size of 300 mg resin (0.19 mmol, 1 equiv). In the first step, deprotection of the aspartic acid on the resin was performed with 20% piperidine in dimethylformamide (DMF) (v/v) for 15 min at 35 °C. After aspirating the excess reagents, the remaining resin was washed with dimethylformamide (DMF, 2 × 8 mL). Building up the peptides from the C- to the N-terminus, 2−5 equiv of the respective amino acid/carboxylic acid were dissolved in 3 mL DMF and *N*-methyl pyrrolidone (NMP) (8/2) and drawn into the syringe. Subsequently, *O*-(7-Azabenzotriazol-1-yl)-*N*,*N*,*N*′,*N*′-tetramethyluronium-hexafluorphosphat (HATU, 2.5−5 equiv) and *N*,*N*-diisopropylethylamine (DIPEA, 2.5−5 equiv) were mixed in 3 mL of DMF/NMP (8/2) and aspirated into the syringe, too. When using 5 equiv of the acid, then 5 equiv HATU (357 mg, 0.94 mmol), and 5 equiv DIPEA (164 μL, 0.94 mmol) were added. When using 2.5 equiv or 3 equiv of the acid, then 3 equiv HATU (214 mg, 0.56 mmol), and 3 equiv DIPEA (98 μL, 0.56 mmol) were added. When using 2 equiv of the acid, then 2.5 equiv HATU (179 mg, 0.47 mmol), and 2.5 equiv DIPEA (82 μL, 0.47 mmol) were added, respectively. Coupling was performed for 45 min at 35 °C and followed by washing step as described for the deprotection. When using 7 equiv of the acid, then 10 equiv HATU (714 mg, 1.88 mmol), and 10 equiv DIPEA (196 μL, 1.12 mmol) were added and the reaction time was prolonged to 2 h at 35 °C. The coupling and deprotection steps were repeated until the desired peptidomimetic was constructed. For N-terminally acetylated compounds, an additional acetylation step was carried out after the last deprotection step using acetic anhydride (178 μL, 1.88 mmol, 10 equiv) and DIPEA (328 μL, 1.88 mmol, 10 equiv) in 6−8 mL DMF for 30 min at 35 °C. After washing the resin with DMF (2 × 8 mL), methanol (2 × 8 mL), dichloromethane (2 × 8 mL), and diethyl ether (2 × 8 mL), the final peptidomimetic was cleaved off the resin and side chain protecting groups were stripped in trifluoroacetic acid (TFA)/water (9/1, 6−8 mL) for 20 min at room temperature. Additional water and solvents were removed by freeze-drying to achieve the crude product, which was then purified via preparative HPLC. Final compounds were yielded as white lyophilizates.

Comments on NMR Spectra of Aldehydes (8−67). For the aldehyde warhead containing peptides, the formation of an intramolecular hemiacetale between the carboxylic acid in the side chain of aspartic acid and the aldehyde at the C-terminus of the peptide was observed both in NMR spectroscopy (signal splitting) and HPLC chromatography (broadening of peaks). There are two possible diastereomers for the cyclic form caused by the formation of an additional chiral center at the former aldehyde carbon. The equilibrium between the open-stranded form and the cyclic hemiacetale was considered for interpretation of the NMR spectra, whereby the signal splittings of aspartic acid, as these are the most pronounced, are described as follows: In ^{1}H spectra, the open stranded form shows the signal of the aldehyde function (C**H**O) at 9.3 ppm (DMSO-d_6). The proton of the carboxylic acid is expected at ∼12 ppm (DMSO-d_6) but can be distinguished from COO**H** of homoglutamic acid only in very few instances. The hemiacetale form shows up in the C**H** signals at ∼5.5 ppm (DMSO-d_6) and the corresponding O**H** at ∼5.7 ppm (DMSO-d_6). The integration ratio of 2−3/8−7 between the signal at 9.3 ppm (aldehyde) and 5.5 ppm (hemiacetale) shows that the cyclic form is favored in most of the peptides. Peaks and integrals of the neighboring C$\mathbf{H}_2$ in the aspartic acid side chain are split in the range of ∼2.2−3.2 ppm and were only labeled for the prominent hemiacetale isomer. In ^{13}C spectra, peaks at ∼200−210 ppm (**C**HO), at ∼103 ppm (**C**−OH) and at ∼90 ppm (**C**−OH) are aligned with the neighboring C$\mathbf{H}_2$ at ∼55, ∼53, and ∼48 ppm, respectively. For reasons of clarity, only the signal pair for

Downloaded from pubs.acs.org/jmcmar/article-pdf/doi/10.1021/acs.jmedchem.6c01371/6909867/acs.jmedchem.6c01371.pdf by UNIV REGENSBURG user on 17 November 2026

https://doi.org/10.1021/acs.jmedchem.6c01371
J. Med. Chem. XXXX, XXX, XXX−XXX

the most pronounced diastereomer of the hemiacetal form was picked for peak report. The aldehyde carbon atom (**C**HO) was additionally marked if it was particularly visible. A splitting of the signals in the ^{1}H and ^{13}C spectra can also be observed for other C and H atoms, but superposition makes a precise separation and alignment difficult.

(*S*)-6-((2-((*S*)-1-(((*S*)-1-Carboxy-3-oxopropan-2-yl)-carbamoyl)-6-methyl-3,4-dihydroisoquinolin-2(1*H*)-yl)-2-oxoethyl)amino)-5-((*S*)-2-methylindoline-2-carboxamido)-6-oxohexanoic Acid Hydrotrifluoroacetate (64). The title compound was synthesized according to the general procedure using 300 mg resin (0.19 mmol, 1 equiv), Fmoc-(*S*)-Me-THIQ−OH (155 mg, 0.38 mmol, 2 equiv), Fmoc-Gly-OH (279 mg, 0.94 mmol, 5 equiv), Fmoc-hE(OtBu)−OH (207 mg, 0.47 mmol, 2.5 equiv), and (2-Me-Idc)−OH (201 mg, 0.94 mmol, 5 equiv) with the corresponding amounts of HATU and DIPEA yielding a fluffy white solid (50.1 mg, 35%): RP-HPLC: 98%, (Method D: t_R = 9.38, k = 4.95). ^{1}H NMR (500 MHz, DMSO-d_6) δ 12.04 (brs, 1H), 9.29 (s, 0.2H, CHO), 8.82 (d, J = 3.6 Hz, 1H), 8.31 (t, J = 5.3 Hz, 1H), 7.82 (d, J = 8.3 Hz, 1H), 7.38−7.27 (m, 1H), 7.03 (t, J = 10.7 Hz, 3H), 6.97 (t, J = 7.6 Hz, 1H), 6.65−6.59 (m, 2H), 5.71 (m, 0.6H), 5.50 (d, J = 12.1 Hz, 0.5H), 5.26 (d, J = 1.5 Hz, 1H), 4.42−4.38 (m, 1H), 4.17−4.07 (m, 2H), 4.06−4.00 (m, 1H), 3.97−3.88 (m, 1H), 3.59−3.48 (m, 1H), 3.10 (d, 1H), 3.02−2.94 (m, 1H), 2.90 (d, 1H), 2.86−2.63 (m, 2H), 2.45−2.29 (m, 1H), 2.26 (s, 3H), 2.16 (t, J = 7.4 Hz, 2H), 1.74−1.64 (m, 1H), 1.58−1.49 (m, 1H), 1.48−1.38 (m, 2H), 1.32 (s, 3H). ^{13}C NMR (126 MHz, DMSO-d_6) δ 175.01, 174.91, 174.25, 171.49, 170.97, 168.20, 149.79, 136.68, 135.16, 129.01, 128.63, 127.32, 127.18, 127.01, 126.42, 124.65, 118.45, 109.72, 102.40, 66.84, 57.14, 52.47, 51.72, 42.16, 41.04, 40.93, 33.25, 33.10, 32.37, 28.09, 24.20, 20.66, 20.60. HRMS (ESI-MS): m/z [M + H]$^+$ calculated for $C_{33}H_{40}N_5O_9^+$: 650.2821, found 650.2822; $C_{33}H_{39}N_5O_9 \times C_2HF_3O_2$ (763.72).

(*S*)-6-(((*S*)-1-((1*R*,2*S*,5*S*)-2-(((*S*)-1-Carboxy-3-oxopropan-2-yl)carbamoyl)-6,6-dimethyl-3-azabicyclo[3.1.0]hexan-3-yl)-3-methyl-1-oxobutan-2-yl)amino)-5-((*S*)-2-methylindoline-2-carboxamido)-6-oxohexanoic Acid Hydrotrifluoroacetate (67). The title compound was synthesized according to the general procedure using 300 mg resin (0.19 mmol, 1 equiv), Fmoc-P*−OH (177 mg, 0.47 mmol, 2.5 equiv), Fmoc-Val-OH (319 mg, 0.94 mmol, 5 equiv), Fmoc-hE(OtBu)−OH (207 mg, 0.47 mmol, 2.5 equiv), and (2-Me-Idc)−OH (201 mg, 0.94 mmol, 5 equiv) with the corresponding amounts of HATU and DIPEA yielding a fluffy white solid (44.4 mg, 31%): RP-HPLC: 96%, (Method D: t_R = 9.36, k = 4.93). ^{1}H NMR (500 MHz, DMSO-d_6) δ 12.00 (brs, 1H), 9.40 (d, J = 5.4 Hz, 0.2H, CHO), 8.57 (dd, J = 27.5, 6.6 Hz, 1H), 8.32 (d, J = 8.1 Hz, 1H), 7.77 (d, J = 8.2 Hz, 1H), 7.02 (d, J = 7.3 Hz, 1H), 6.98 (t, J = 7.6 Hz, 1H), 6.66−6.61 (m, 2H), 5.77−5.68 (m, 0.3H), 5.46 (d, J = 1.2 Hz, 0.7H), 4.37 (ddt, J = 10.7, 8.3, 4.0 Hz, 1H), 4.25 (d, J = 20.0 Hz, 0H), 4.16−4.11 (m, 1H), 4.08−4.02 (m, 1H), 3.86−3.73 (m, 2H), 3.02 (dd, 2H), 3.04−2.94 (m, 1H), 2.30 (dt, J = 17.9, 1.9 Hz, 1H), 2.11 (t, J = 7.2 Hz, 2H), 1.97−1.87 (m, 1H), 1.60−1.51 (m, 1H), 1.50−1.45 (m, 1H), 1.44−1.31 (m, 4H), 1.30 (s, 3H), 0.98 (d, J = 4.0 Hz, 3H), 0.91−0.84 (m, 6H), 0.81 (s, 3H). ^{13}C NMR (126 MHz, DMSO-d_6) δ 175.21, 174.83, 174.16, 171.24, 171.06, 169.51, 149.54, 127.35, 126.50, 124.69, 118.64, 109.93, 102.52, 66.86, 59.77, 56.11, 52.46, 51.29, 47.00, 42.22, 33.27, 32.92, 32.61, 30.66, 29.76, 27.03, 25.88, 24.07, 20.47, 18.95, 18.78, 18.74, 12.57. HRMS (ESI-MS): m/z [M + H]$^+$ calculated for $C_{33}H_{46}N_5O_9^+$: 656.3259, found 656.3300; $C_{33}H_{45}N_5O_9 \times C_2HF_3O_2$ (769.77).

General Procedure for the Synthesis of Nitriles (68−87). The compounds with nitrile warhead were synthesized from the corresponding aldehydes in a one-step overnight reaction, adopted from Cheewawisuttichai et al.[46] The aldehyde peptidomimetic (10−100 mg; 1 equiv) was dissolved in 50 mM sodium phosphate buffer (222 mg $Na_2HPO_4 \times 2H_2O$ and 172 mg $NaH_2PO_4 \times H_2O$ in 50 mL Millipore water, adjusted with 0.1 M NaOH to pH = 6.8). o-Phenylhydroxylamine hydrochloride (2 equiv) was added and the reaction stirred for 12−18 h at room temperature. The crude reaction mixure was filtered over a 0.22 μM PTFE filter and purified via preparative HPLC to yield the final compound as white lyophilizate.

Comments on (R)-/(S)-Epimers of the Nitriles (Figures S250−S388, SI). Epimerization during the nitrile conversion of one aldehyde results in the formation of two nitrile epimers that only differ in their absolute configuration of aspartic acid in P1 and are termed as compound **X** ((*S*)-configuration of D in P1) and compound (*R*)-**X** ((*R*)-configuration of D in P1). Based on the X-ray confirmed absolute configuration of **87** (MUR-2425) with JF1cpCasp2, consistent differences in ^{1}H and ^{13}C NMR spectra between the (*R*) and (*S*) forms allow us to deduce the (*R*)/(*S*)-assignment for the other nitriles as discussed in the following sections. Figures S250−S388 (SI) concisely illustrate some of the striking differences in the stacked spectra of the (*R*)- and (*S*)-epimer. Important ^{1}H signals covered in the discussion are numbered 1−7 and outlined in red. Important ^{13}C signals covered in the discussion are highlighted in red. The correct assignment of particular signals to specific C or H atoms was obtained by using DEPT135, DEPT90, HSQC, HMBC, COSY, and NOESY NMR (not shown).

^{1}H NMR. The N**H** proton forming the peptide bond between D and the amino acid in P2 (signal #1) shows tendency to be shifted downfield in the (*R*)-epimer whereas the prominence of this effect ranges and is strongest for THIQ in P2. For G in P2, the effect is barely noticeable, whereas here the downfield shift ((*R*)-epimer) of N**H** of the amide bond between P2 and P3 (signal #6) or P3 and P4 (signal #7) is more pronounced. The α-C**H** of D (P1) is a highly conserved quartett at ∼4.8−4.9 ppm (signal #2) and deshielded in the (*R*)-epimer of compounds with P*, Dab or G in P2 whereas it is highfield-shifted in the (*R*)-form of compounds with THIQ in P2. The lower coupling constant J of the C**H**$_2$ protons in the side chain of D in P1 (signal #4) is a distinct feature of the (*R*)-epimer. Due to the overlap with other methylene groups in compounds with THIQ in P2 or G in P2, the effect is not clearly discernible in these molecules. Meanwhile, for the (*R*)-epimer of compounds with THIQ and also for compounds with Dab in P2, a higher coupling constant of C**H**$_2$ of G in P3 is obvious (signal #5). The α-C**H** of the amino acid in P2 (signal #3) appears at lower ppm value for the (*R*)-epimer irrespective of the pentapeptide sequence. Although this latter effect is not always the most obvious, it is consistent across the entire peptide series and therefore a central pillar around which the other indicators are grouped in a confirmatory manner.

^{13}C NMR. The most prominent difference shows up in the carbonyl atoms of the aspartic acid in P1: For the (*R*)-epimer, the methylene group of D in P1 (signal at ∼36 ppm) shifts to a lower field, while the signal of the α-C**H** of D in P1 (signal at ∼37 ppm) shifts to a higher field. This characteristic pattern is confirmed in all nitriles of the series and therefore, alongside signal #3 in the ^{1}H NMR, it is the second important cornerstone for complete traceability of (*R*)-/(*S*)-identification. In addition, the nitrile carbon at around 118−119 ppm shows tendency to be shifted to a higher ppm value in the (*R*)-form, but this is only clearly noticeable for compounds having THIQ in P2 and barely recognizable when G is the amino acid in P2. For the latter, the shift of the α-**C** atom of G in P2 at ∼42 ppm is more pronounced and was therefore selected to be shown instead of the **C**N. Also the carbonyl atoms at ∼168−175 ppm change their position in the spectrum. The presumed assignment of these signals based on the HMBC spectrum of **87** reveals, in many cases, a highfield shift for the **C**OOH of D in P1 (∼170.1 ppm) and a low field shift for the α-**C**H of D in P1 (∼170.0 ppm) in the (*R*)-epimer. However, since the differences are marginal and the assignment of the carbonyl signals cannot be made with certainty, these results are of minor importance and were overruled in favor of more clearly determinable characteristics in cases of apparent discrepancy.

Special Aspects in NMR Spectra of the Free Base of Compounds 72, (R)-72, 80, (R)-80, 81, and (R)-81. Compounds **72**, (*R*)-**72**, **80**, (*R*)-**80**, **81**, and (*R*)-**81** contain Dab in P2. NMR spectra were measured both of the TFA and of the free bases for these compounds. Whereas the differences in the (*R*)- and (*S*)-epimers of the TFA salt are in line with statements summarized in the sections above, the interpretation of the free-base spectra requires some special comments:

Downloaded from pubs.acs.org/jmcmar/article-pdf/doi/10.1021/acs.jmedchem.6c01371/6909867/acs.jmedchem.6c01371.pdf by UNIV REGENSBURG user on 17 November 2026

https://doi.org/10.1021/acs.jmedchem.6c01371
J. Med. Chem. XXXX, XXX, XXX−XXX

^{1}H NMR. In contrast to the TFA salt, the α-C**H** of the amino acid in P2 (signal #3) is shifted downfield for the (*R*)-epimer when G is in P3. In addition, the C**H**$_2$ of D in P1 (signal #2) results in a messy multiplet for the (*R*)-epimer which rules out a reliable comparison of coupling constants. Nevertheless, the signal of the (*R*)-form has always a similar shape unlike with the (*S*)-form.

^{13}C NMR. The order of the **C**H and **C**H$_2$ of D in P1 is the otherway round for the TFA salts: In the freebase spectra, the methylene group of D in P1 is the signal at ∼38.5 ppm and shifts to a lower field in the (*R*)-epimer, whereas the α-**C**H of D in P1 corresponds to the signal at ∼38.0 ppm and changes only very little to higher field or not markable. Finally, for both the (*R*)- and the (*S*)-epimer, all carbonyl atoms seem to be shifted to higher ppm values in the free base compared to the TFA salt.

(*S*)-6-((2-((*S*)-1-(((*S*)-2-Carboxy-1-cyanoethyl)carbamoyl)-6-methyl-3,4-dihydroisoquinolin-2(1*H*)-yl)-2-oxoethyl)amino)-5-((*S*)-2-methylindoline-2-carboxamido)-6-oxohexanoic Acid Hydrotrifluoroacetate (84). The title compound was synthesized according to the general procedure starting from **64** (50.0 mg, 0.07 mmol, 1 equiv) and o-phenylhydroxylamine hydrochloride (19.1 mg, 0.14 mmol, 2 equiv) yielding a fluffy white solid (15.0 mg, 30%): RP-HPLC: 96%, (Method C: t_R = 10.37, k = 5.57). ^{1}H NMR (500 MHz, DMSO-d_6) δ 9.04 (d, J = 7.3 Hz, 1H), 8.30 (t, J = 5.4 Hz, 1H), 7.83 (d, J = 8.4 Hz, 1H), 7.34 (d, J = 7.8 Hz, 1H), 7.09−7.01 (m, 3H), 6.98 (td, J = 7.6, 1.3 Hz, 1H), 6.67−6.61 (m, 2H), 5.63 (s, 1H), 4.83 (q, J = 7.2 Hz, 1H), 4.44−4.38 (m, 1H), 4.12 (d, J = 5.3 Hz, 2H), 3.92−3.85 (m, 1H), 3.61−3.53 (m, 1H), 3.11 (d, J = 16.1 Hz, 1H), 2.96−2.77 (m, 5H), 2.27 (s, 3H), 2.16 (t, J = 7.4 Hz, 2H), 1.73−1.64 (m, 1H), 1.58−1.49 (m, 1H), 1.48−1.39 (m, 2H), 1.33 (s, 3H). ^{13}C NMR (126 MHz, DMSO-d_6) δ 174.90, 174.21, 171.46, 170.49, 169.99, 168.33, 149.45, 136.79, 135.05, 128.64, 128.58, 127.45, 127.31, 127.10, 126.54, 124.65, 118.64, 118.55, 109.89, 66.89, 56.60, 51.71, 42.07, 41.00, 40.92, 37.04, 36.04, 33.22, 32.28, 27.86, 24.15, 20.64, 20.58. HRMS (ESI-MS): m/z [M + H]$^+$ calculated for $C_{33}H_{39}N_6O_8^+$: 647.2824, found 647.2830; $C_{33}H_{38}N_6O_8 \times C_2HF_3O_2$ (760.72).

(*S*)-6-(((*S*)-1-((1*R*,2*S*,5*S*)-2-(((*S*)-2-Carboxy-1-cyanoethyl)-carbamoyl)-6,6-dimethyl-3-azabicyclo[3.1.0]hexan-3-yl)-3-methyl-1-oxobutan-2-yl)amino)-5-((*S*)-2-methylindoline-2-carboxamido)-6-oxohexanoic Acid (87). *(S)-6-(((S)-1-((1R,2S,5S)-2-(((S)-2-Carboxy-1-cyanoethyl)carbamoyl)-6,6-dimethyl-3-azabicyclo[3.1.0]hexan-3-yl)-3-methyl-1-oxobutan-2-yl)amino)-5-((S)-2-methylindoline-2-carboxamido)-6-oxohexanoic Acid Hydrotrifluoroacetate*. The title compound was synthesized according to the general procedure starting from **67** (95.0 mg, 0.12 mmol, 1 equiv) and o-phenylhydroxylamine hydrochloride (35.9 mg, 0.25 mmol, 2 equiv) yielding a fluffy white solid (14.3 mg, 15%): RP-HPLC: 98%, (Method C: t_R = 9.71, k = 5.15). ^{1}H NMR (500 MHz, DMSO-d_6) δ 8.89 (d, J = 7.2 Hz, 1H), 8.32 (d, J = 8.3 Hz, 1H), 7.78 (d, J = 8.3 Hz, 1H), 7.03 (d, J = 7.3 Hz, 1H), 6.99 (td, J = 7.6, 1.2 Hz, 1H), 6.67−6.62 (m, 2H), 4.83 (q, J = 7.1 Hz, 1H), 4.37 (td, J = 8.1, 5.0 Hz, 1H), 4.18 (s, 1H), 4.14 (t, J = 8.8 Hz, 1H), 3.87−3.78 (m, 2H), 2.99 (dd, J = 89.3, 16.1 Hz, 2H), 2.89−2.77 (m, 2H), 2.11 (t, J = 7.2 Hz, 2H), 1.92 (dp, J = 9.0, 6.6 Hz, 1H), 1.60−1.53 (m, 1H), 1.53−1.49 (m, 1H), 1.43−1.32 (m, 3H), 1.30 (s, 3H), 1.23 (d, J = 7.6 Hz, 1H), 1.00 (s, 3H), 0.90 (d, J = 6.7 Hz, 3H), 0.86 (d, J = 6.7 Hz, 3H), 0.81 (s, 3H). ^{13}C NMR (126 MHz, DMSO-d_6) δ 174.80, 174.15, 171.24, 170.88, 170.09, 169.57, 149.53, 127.36, 126.56, 124.70, 118.91, 118.75, 110.01, 66.88, 59.48, 56.13, 51.30, 46.96, 42.20, 37.05, 36.03, 33.26, 32.59, 30.46, 29.74, 26.96, 25.89, 24.05, 20.47, 18.96, 18.82, 18.73, 12.50. HRMS (ESI-MS): m/z [M + H]$^+$ calculated for $C_{33}H_{45}N_6O_8^+$: 653.3293, found 653.3304; $C_{33}H_{44}N_6O_8 \times C_2HF_3O_2$ (766.77).

Disodium (S)-6-(((S)-1-((1R,2S,5S)-2-(((S)-2-Carboxy-1-cyanoethyl)carbamoyl)-6,6-dimethyl-3-azabicyclo[3.1.0]hexan-3-yl)-3-methyl-1-oxobutan-2-yl)amino)-5-((S)-2-methylindoline-2-carboxamido)-6-oxohexanoate. The TFA salt of **87** (39.9 mg, 0.05 mmol, 1 equiv) was dissolved in a mixture of 2 mL 0.1% NH_3 (aq) and 1 mL 0.1% NH_3 in MeCN and injected to $HPLC_{prep}$ using 0.1% formic acid in mH_2O and MeCN as mobile phase. After freeze-drying in order to remove residual TFA, the free base was achieved as white lyophilizate (31.1 mg, 95%). ^{1}H NMR (500 MHz, DMSO-d_6) δ 8.89 (d, J = 7.2 Hz, 1H), 8.32 (d, J = 8.3 Hz, 1H), 7.74 (d, J = 8.4 Hz, 1H), 7.01 (d, J = 7.2 Hz, 1H), 6.97 (td, J = 7.6, 1.2 Hz, 1H), 6.65−6.57 (m, 2H), 5.98 (s, 1H), 4.83 (q, J = 7.1 Hz, 1H), 4.37 (td, J = 8.1, 5.2 Hz, 1H), 4.18 (s, 1H), 4.14 (t, J = 8.8 Hz, 1H), 3.91−3.77 (m, 2H), 2.97 (dd, J = 92.3, 16.1 Hz, 2H), 2.86−2.77 (m, 2H), 2.11 (t, J = 7.2 Hz, 2H), 1.98−1.88 (m, 1H), 1.60−1.54 (m, 1H), 1.53−1.49 (m, 1H), 1.45−1.31 (m, 3H), 1.29 (s, 3H), 1.23 (d, J = 7.6 Hz, 1H), 1.00 (s, 3H), 0.91 (d, J = 6.6 Hz, 3H), 0.86 (d, J = 6.6 Hz, 3H), 0.81 (s, 3H). ^{13}C NMR (126 MHz, DMSO-d_6) δ 174.94, 174.12, 171.22, 170.84, 170.07, 169.54, 150.05, 127.28, 126.25, 124.60, 118.73, 118.27, 109.59, 66.71, 59.46, 56.11, 51.23, 46.94, 42.26, 37.05, 36.05, 33.25, 32.61, 30.44, 29.72, 26.94, 25.87, 24.12, 20.43, 18.94, 18.80, 18.72, 12.48.

The free base of **87** (32.1 mg, 0.05 mmol, 1 equiv) was dissolved in 1 mL MeCN and cooled to 0 °C before 0.01 M $NaHCO_3$ aq (9.84 mL, 0.10 mmol, 2 equiv) was added dropwise. The mixture was stirred for 2 min at 0 °C and freeze-dried, yielding the disodium salt as a white powder (34.3 mg, 100%): RP-HPLC: 99%, (Method C: t_R = 9.74, k = 5.17). ^{1}H NMR (500 MHz, DMSO-d_6) δ 9.08 (d, J = 7.1 Hz, 1H), 8.54 (d, J = 8.1 Hz, 1H), 7.97 (d, J = 7.8 Hz, 1H), 6.99 (d, J = 7.3 Hz, 1H), 6.95 (td, J = 7.6, 1.2 Hz, 1H), 6.62−6.56 (m, 2H), 6.07 (s, 1H), 4.76 (q, J = 6.8 Hz, 1H), 4.29 (q, J = 6.9 Hz, 1H), 4.13 (s, 1H), 4.10 (d, J = 8.7 Hz, 1H), 3.88−3.76 (m, 2H), 2.96 (dd, J = 124.8, 16.1 Hz, 2H), 2.40−2.27 (m, 2H), 2.00−1.91 (m, 1H), 1.91−1.79 (m, 2H), 1.53−1.48 (m, 1H), 1.46−1.34 (m, 3H), 1.30 (s, 3H), 1.23 (d, J = 7.6 Hz, 1H), 0.99 (s, 3H), 0.91 (d, J = 6.7 Hz, 3H), 0.88 (d, J = 6.6 Hz, 3H), 0.81 (s, 3H). ^{13}C NMR (126 MHz, DMSO-d_6) δ 176.83, 174.75, 171.73, 170.85, 170.38, 169.96, 150.10, 127.22, 126.31, 124.54, 120.42, 118.03, 109.34, 66.76, 59.86, 56.27, 51.72, 46.93, 41.94, 40.11, 38.41, 37.34, 33.33, 30.41, 29.52, 27.15, 25.84, 24.46, 21.98, 18.97, 18.84, 18.82, 12.53. HRMS (ESI-MS): m/z [M + H]$^+$ calculated for $C_{33}H_{45}N_6O_8^+$: 653.3293, found 653.3305; $C_{33}H_{42}N_6Na_2O_8$ (696.71).

Fluorescent Enzyme Assay Protocols

Biochemical Reagents. Human recombinant Casp1, 4, 5, 6, 7, 8, 9, and 10 were purchased from Enzo (Lörrach, Germany). AFC fluorogenic substrates (AcYVAD-AFC, Z-VDVAD-AFC, AcDEVD-AFC, AcWEHD-AFC, Z-VEID-AFC, AcIETD-AFC, and AcLEHD-AFC) and control peptides (AcYVAD-CHO, AcVDVAD-CHO, AcDEVD-CHO, AcWEHD-CHO, AcVEID-CHO, AcIETD-CHO, and AcLEHD-CHO) were purchased from Bachem (Babendorf, Bubendorf, Switzerland) and MedChemExpress (Monmouth Junction, New Jersey, US). Recombinant cpCasp2, Casp3, and tau were produced in house as described in the following.

Expression and Purification of Recombinant Caspase-2 and tau. The pET23b vector-encoding human caspase-2 was a gift from Prof. Dr. Michelle Arkin at University of California, San Francisco.[50] The htau0N4R-pET28a plasmid[16] was used as the initial template that encodes wild-type human microtubule-associated protein tau N4R isoform (containing four microtubule-binding domains but no amino-terminal inserts) ORF. Briefly, the Casp2 plasmid was transformed into *Escherichia coli* Lemo21 DE3 cells with 2 mM rhamnose that were cultured at a 1 L scale in shake flasks at 37 °C. When the culture reached an OD_{600} = 0.3, incubation temperature was reduced to 28 °C. When the OD_{600} reached 0.6−0.8, protein expression was induced with 0.1 mM isopropyl-β-D-thiogalactopyranoside (IPTG) and allowed to shake at 250 rpm and 28 °C overnight. Sixteen h after induction, cells were harvested through centrifugation (5000 rpm for 20 min at 4 °C), lysed by French press (2 passes at 1000 psi), and centrifuged again for 30 min at 20,000 rpm at 4 °C. The supernatant was resuspended in buffer (100 mM Tris pH 8.0, 100 mM NaCl, 20 mM imidazole). Purification was performed on a Cytiva ÄKTA Pure system (Marlborough, MA) by nickel-affinity chromatography on a HisTrap FF crude column (Cytiva) followed by ion-exchange chromatography on a HiTrap Q FF column (Cytiva). Protein was diluted to 0.5 mg/mL and stored at −80 °C in 100 mM MES (pH 6.5), 150 mM NaCl, 0.1% CHAPS, 1.5% sucrose, and 10 mM DTT. Typical yield for the expression, isolation, and purification

Downloaded from pubs.acs.org/jmcmar/article-pdf/doi/10.1021/acs.jmedchem.6c01371/6909867/acs.jmedchem.6c01371.pdf by UNIV REGENSBURG user on 17 November 2026

https://doi.org/10.1021/acs.jmedchem.6c01371
J. Med. Chem. XXXX, XXX, XXX−XXX

was approximately 0.1 mg/L. Expression of recombinant Casp2 and tau proteins was induced using 150 μM IPTG (Promega, Madison, WI) in the BL21(DE3) *E. coli* strain (Millipore Sigma) at 16 °C for 14 h, while shaking at 250 rpm. Cells were then harvested via centrifugation at 6000*g*, 4 °C for 15 min, followed by lysis via sonication. Proteins were initially purified using HisPur Ni-NTA resin (Thermo Fisher Scientific, Waltham, MA) followed by metal chelating chromatography [5 mL HiTrap Chelating HP columns (GE Healthcare Life Sciences, Piscataway, NJ)]. Further purification was carried out using either anion exchange chromatography [5 mL HiTrap Q HP columns (GE Healthcare Life Sciences)] for Casp2 or cation exchange chromatography [5 mL HiTrap SP HP columns (GE Healthcare Life Sciences)] for tau. Proteins were stored in 1X phosphate-buffered saline (pH 7.4) at 10 mg/mL [concentration determined using a BCA assay (Thermo Fisher Scientific)], −80 °C until further use.

Expression and Purification of Recombinant Circularly Permutated Caspase-2 (cpCasp2). A circularly permutated caspase-2 (cpCasp2) based on modifications to Casp2 (UniProt P42575) suggested by Cserjan-Puschmann et al. was expressed.[47] The gene encoding 6H-Casp2$_{334-452}$-GS-Casp2$_{170-333}$ with a $D_{347} \rightarrow A_{347}$ mutation was inserted into a pET30a(+) vector (GenScript, Piscataway, NJ, USA) using NdeI and EcoRV restriction sites. The transformation into Lemo21 cells was performed as recommended by the vendor (New England Biolabs, Ipswich, MA, USA), and the plates were incubated overnight at 37 °C. A single colony was picked for primary culture using a sterile tip, added to sterile Luria broth (LB) media containing antibiotics, and incubated overnight at 37 °C and 270 rpm. The primary culture was then diluted 1:100 into 1 L shake flasks containing sterile LB and the proper antibiotics. The liter cultures were incubated at 37 °C and 270 rpm, and the OD was monitored until it reached between 0.6 and 0.8. Once the desired OD was reached, the cells were induced overnight with 0.1 mM IPTG at 28 °C and 270 rpm. After induction, the cells were harvested through centrifugation at 5000*g* for 20 min. Typical yield was about a 3.5 g cell pellet per liter. The pellets were stored at −20 °C until purification. The pellets were resuspended in lysis buffer (buffer A with 2.5 μM Leupeptin, 5 μM Pepstatin, 0.5 μM DNase, 1 mM PMSF, and 10 mM $MgCl_2$) and lysed through sonification. The lysate was clarified through centrifugation at 20,000*g* for 30 min. The supernatant was filtered through a 0.45 μm filter before it was purified on a BioRad Biologic DuoFlow Chromatography System. For nickel-affinity chromatography a 5 mL HisTrap FF column was equilibrated with 100% buffer A (100 mM Tris, pH 8.0, 100 mM NaCl, 20 mM imidazole). A gradient of buffer B (100 mM Tris, pH 8.0, 100 mM NaCl, 400 mM imidazole) was then applied from 0 to 50% to wash and elute the protein. cpCasp2 was eluted at about 20% buffer B. Final purification was achieved on a Hi-Trap Q anion exchange column in 25 mM Tris, pH 8.0 utilizing a gradient of 0−1 M NaCl. cpCasp2 was eluted at about 150 mM NaCl. The final yield was 8−10 mg of cpCasp2 per liter. After adding 10% glycerol, the protein was stored at −80 °C.

Expression and Purification of Recombinant Caspase-3. The pET23b vector encoding human caspase-3 was a gift of Dr. Michelle Arkin at University of California, San Francisco. Expression and purification of Casp3 was guided by previously described protocols.[51] Briefly, the plasmid was transformed into *E. coli* Rosetta 2 pLyss DE3 cells that were cultured at 1 L scale in shake flasks at 37 °C. Five hours post induction with IPTG, cells were harvested through centrifugation (5000*g* for 15 min at 4 °C), lysed by sonication, and centrifuged again for 30 min at 20,000*g*. Supernatant was resuspended in buffer (100 mM Tris pH 8.0, 500 mM NaCl). Purification was performed on a Cytiva ÅKTA Pure system (Marlborough, MA) by nickel-affinity chromatography on a HisTrap FF crude column (Cytiva) followed by ion-exchange chromatography on a HiTrap Q FF column (Cytiva). Protein was diluted to 0.5 mg/mL and stored at −80 °C in 100 mM Tris, pH 8.0 supplemented with 10% glycerol. The typical yield for the expression, isolation, and purification was approximately 3 mg/L.

Fluorometric Enzyme Assay

K_M of the respective AFC-labeled standard peptides values were determined experimentally for every enzyme batch that was used to be the following: Casp1: 11.5 μM (batch 1) and 0.79 μM (batch 2); cpCasp2: 13.6 μM (batch 1) and 19.0 μM (batch 2); Casp3: 17.2 μM (batch 1) and 5.6 μM (batch 2); Casp4: 46.6 μM; Casp5: 110.4 μM; Casp6: 53.5 μM; Casp7: 26.4 μM; Casp8: 29.8 μM; Casp9:79.2 μM (batch 1) and 10.0 μM (batch 2); Casp10: 344.5 μM. Enzymes were diluted in aqueous buffer consisting of 100 mM MES (pH 6.5) for Casp2 and 100 mM HEPES (pH 7.0) for all other caspases, plus 150 mM NaCl, 0.1% CHAPS, 1.5% sucrose. Dithiothreitol (DTT) was added from frozen stock solution (stored at −20 °C) freshly to buffer immediately prior to performing the assay resulting in a final assay concentration of 10 mM. Enzyme concentrations were 0.1 U/well for Casp1, Casp6 and Casp7, 20 nM/well for Casp2, 2 nM/well for Casp3 and 0.05 U/well for Casp4, Casp5, Casp8, Casp9 and Casp10. Fourteen μL/well of enzyme solution were placed in a black 384-well Corning assay plate. Starting from DMSO stock solutions, test compounds were serially diluted in assay buffer without DTT and 2 μL/well were plated into the assay plate in duplicate. Final DMSO assay concentration was kept below 0.16%. Compound and enzyme mixture was preincubated at 37 °C for 5 min before 4 μL of the AFC substrate (final assay concentrations: 5 μM AcYVAD-AFC for Casp1 (batch1), 1 μM AcYVAD-AFC for Casp1 (batch2), 10 μM Z-VDVAD-AFC for Casp2, 5 μM AcDEVD-AFC for Casp3, 10 μM AcWEHD-AFC for Casp4, 25 μM AcWEHD-AFC for Casp5, 5 μM Z-VEID-AFC for Casp6, 5 μM AcDEVD-AFC for Casp7, 10 μM AcIETD-AFC for Casp8, 30 μM AcLEHD-AFC for Casp9 (batch1), 5 μM AcLEHD-AFC for Casp9 (batch2), and 50 μM AcIETD-AFC for Casp10) were added for a total assay volume of 20 μL/well. Fluorescence from free AFC was read at 37 °C at 10 time points over 40 min using a Clariostar plate reader (BMG Labtech) (λ_{ex} = 400 nm, λ_{em} = 505 nm). The 21 min time point was considered for the assessment of enzyme inhibitory potency reported as pIC_{50} and the ensuing pK_i value. Selected inhibitors were additionally tested for 60 min preincubation of the inhibitor with cpCasp2. These results are summarized in Table S14.

Jump Dilution Assay

The reference compounds emricasan, AcVDVAD-CHO and selected inhibitors were incubated in a concentration corresponding to 10 x IC_{50} with 10 nM cpCasp2 at 37 °C for 30 min in aqueous Casp2 assay buffer containing 100 mM MES (pH 6.5), 150 mM NaCl, 0.1% CHAPS, 1.5% sucrose, and 10 mM freshly added dithiothreitol (DTT). After incubation, the enzyme-inhibitor mixture was diluted 1:100 in assay buffer containing the substrate Z-VDVAD-AFC to a final concentration of 0.1 nM cpCasp2, 0.1 x IC_{50} of the inhibitor, and 10 μM AcVDVAD-AFC. Residual enzyme activity was measured at a CLARIOstar plate reader (BMG Labtech) at λ_{ex} = 400 nm and λ_{em} = 505 nm over 60 min. The residence time τ was defined as the reciprocal of the dissociation constant koff of the binary enzyme-inhibitor complex, and was calculated as described in the literature using the following equation: $[P] = v_s * t + (v_i - v_s)*(1\text{-e-}k_{off}*t)/k_{off}$ where [P] is the concentration of product formed by substrate cleavage, v_s is the steady-state velocity of enzyme activity (expected to be 0.9091 × v_0), and v_i is the initial velocity (expected to be 0.091 × v_0), with v_0 representing the velocity of the uninhibited control sample (positive ctrl).[42] Mean residence times were calculated from at least three independent experiments, each performed in duplicate. The progress curves and calculated residence times are shown in Figure S493 in the SI.

In vitro Caspase-2-Catalyzed tau Cleavage Assay

Procedure. Purified recombinant Casp2 was subjected to an extensive preincubation period to ensure binding with the inhibitory compounds. The enzyme, at a final concentration of 67 μM during this phase, was mixed with various test concentrations of the compounds. This mixture was held at 4 °C for 90 h. Following this, the pretreated enzyme was introduced to purified recombinant full-length Tau at a 1:1 molar ratio in a 1x reaction buffer (25 mM

Downloaded from pubs.acs.org/jmcmar/article-pdf/doi/10.1021/acs.jmedchem.6c01371/6909867/acs.jmedchem.6c01371.pdf by UNIV REGENSBURG user on 17 November 2026

https://doi.org/10.1021/acs.jmedchem.6c01371
J. Med. Chem. XXXX, XXX, XXX−XXX

HEPES, pH 7.5; 0.1% (w/v) CHAPS; 10 mM DTT) to start the cleavage reaction. The reaction was incubated at 37 °C for 6 h, then instantaneously terminated by adding 0.1% (v/v) protease inhibitor cocktail.

Immunoprecipitation/Western Blotting. Immunoprecipitation was conducted according to a previously published protocol.[23] Briefly, after the Casp2 cleavage reaction was terminated, the enzyme and cleavage products were diluted into 400 μL of immunoprecipitation (IP) buffer (50 mM Tris-HCl, pH 7.4; 150 mM NaCl, 0.1 mM phenylmethylsulfonyl fluoride, 0.2 mM 1,10-phenanthroline monohydrate, and a protease inhibitor cocktail (MilliporeSigma)). Next, this diluted mixture was incubated for 14−16 h at 4 °C with 10 μg of Δtau314-specific monoclonal antibody 4F3 and 50 μL of Protein G Sepharose 4 Fast Flow resin (GE Healthcare). Following this overnight incubation, the resin was extensively washed to remove nonspecifically bound proteins, and the precipitated proteins were eluted from the resin. Finally, Western blotting (WB) analysis was performed on the eluted material using biotin-conjugated 4F3 based on a protocol detailed in a prior publication to visualize and quantify the resulting cleavage products.[13] The levels of proteins were determined from two independent experiments.

In Vitro ADMET Studies for 67 (MUR-2424), 79, 80, and 87 (MUR-2425)

I*n vitro* ADME and *in vivo* PK studies of **67** (MUR-2424) were conducted by Cyprotex Discovery Ltd. (Framingham, USA), *in vitro* ADME studies CYP and hERG experiments and *in vivo* PK studies of **79**, **80** and MUR-2425 (**87**)-apart from solubility determinations of MUR-2425 - were conducted by Pharmaron Co. Ltd. (Bejjing, China) according to the protocols as described in the following.

General Bioanalytical Method (Pharmaron). For the studies that were conducted by Pharmaron Co. Ltd., LC-MS/MS analysis was performed on a Shimadzu Triple Quad 4500, 5500, or 6500 instrument from AB Inc. (Canada) equipped with an ESI interface in positive multiple reaction monitoring (MRM+) mode at 500 °C with an ion spray voltage of 5500 V. A XSelect HSS T3 XP column (100 Å, 2.5 μ, 2.1 × 50 mm; Waters, Milford, USA) with a flow rate of 0.65 mL/min (Pharmaron Bioanalytical Method A) or a XSelect HSS T3 XP column (100 Å, 2.5 μ, 2.1 × 30 mm; Waters, Milford, USA) with a flow rate of 1.00 mL/min (Pharmaron Bioanalytical Method B) was used. The column was tempered to 40 °C and a linear gradient of 0.1% formic acid in mH_2O and 0.1% formic acid in MeCN was applied.

Turbidimetric Solubility (67 (MUR-2424)). Serial dilutions of MUR-2424 and controls (reserpine and tamoxifen as low solubility controls, verapamil as high solubility control) were prepared in DMSO at 100-fold of the final concentration (1.6, 3.1, 6.25, 12.5, 50, 100, 200 μM for MUR-2424; 3.9, 7.8, 31.25, 62.5, 125, 250, 500 μM for controls). Test compounds were diluted 100-fold into buffer (PBS, pH 7.4) in a 96-well plate and mixed. After 2 h, the presence of precipitate was detected by turbidity (absorbance at 540 nm). An absorbance value of greater than 'mean +3x standard deviation of the blank' (after subtraction of the background) was considered an indication of turbidity. The solubility limit was reported as the highest experimental concentration with no evidence of turbidity. The results are summarized in Table S3 (SI).

Kinetic Solubility Method A (79, 80). The test compound (**79**, **80**) or the control progesterone (15 μL, 10 mM in DMSO) were added to 485 μL PBS (pH 7.4) in a 96-well rack. Vials were sealed and incubated at 25 °C while shaking at 1100 rpm for 2 h. After incubation, the samples were transferred to a second filter plate and filtered using a Vacuum Manifold. Ten μL of the filtrate were diluted with 10 μL DMSO and 980 μL MeCN:H_2O (1:1) containing the internal standards tolbutamine, labetalol and ketoprofen. The samples were quantified against 3 μM standards (STD) via LC-MS/MS analysis according to Pharmaron Bioanalytical Method A. For preparation of the standards, a 10 mM compound stock solution was diluted with DMSO to 300 μM of which 10 μL were diluted with 980 μL acetonitrile and 10 μL PBS (pH 7.4). The study was performed in duplicate and the solubility of the test compound in the sample was calculated from [sample] = (A_{sample} * V_{STD} * DF_{sample} * [STD])/(A_{STD} * V_{sample}) where A is the peak area ratio (test compound/internal standard), V is the injection volume (3 μL) and DF is the dilution factor. Any value close or above 300 μM indicates that the compound may have a solubility at or above 300 μM. The results are summarized in Table S3 (SI).

Kinetic Solubility Method B (87 (MUR-2425)). MUR-2425 was dissolved in PBS to a target concentration of 1, 2, 5, and 10 mg/mL (TFA salt; equal to 1.3, 2.6, 6.52, and 13.04 mM) and 2, 5, 10, 25, 50, and 100 mg/mL (Disodium salt; equal to 2.87, 7.17, 14.35, 35.88, 71.77, and 143.53 mM). After shaking for 15 min at 25 °C with 1200 rpm, the samples were filtered over a 0.22 μM PTFE filter. The filtrate was diluted with PBS, spiked with 2 mM Rhodamine B (2 mM in DMSO) as internal standard and quantified via LC/MS on a Vanquish Core HPLC equipped with an ISQ EC Single Quadrupole Mass Spectrometer (Thermo Fisher Scientific, Waltham, MA) on a Gemini 3 μm NX-C18 column (110 Å, 150 × 3 mm) (Phenomenex Ltd., Aschaffenburg, Germany) tempered at 30 °C and 0.05% formic acid in H_2O and 0.025% formic acid in MeCN with a flow rate of 0.5 mL/min as mobile phase. Additionally, the TFA salt form of MUR-2425 was dissolved in 100% DMSO to 0.5, 1, 2, 5, 8, 10 mg/mL (equal to 0.65, 1.30, 2.60, 5.22, 10.43, 13.04 mM), spiked with rhodamine B as internal standard and measured as calibration curve, assuming 100% solubility of MUR-2425 under these conditions. The relative peak area of MUR-2425 referred to the internal standard rhodamine B at 220 nm was used for quantification of amount that was completely dissolved. The data are summarized in Figure 5B, Figure S8 and Table S3 (SI). Data represent mean ± SD of two independent measurements, each performed with at least three replicates.

LogD

Method A (67 (MUR-2424)). Test compound (MUR-2424; DMSO stock) or controls (ketoconazole, tolbutamide) were spiked in octanol that was presaturated with 0.1 M phosphate buffer (pH 7.4) and shaken for 30 min at 1000 rpm. 0.1 M phosphate buffer (pH 7.4) that was presaturated with octanol was added to the octanol solution and shaken at 350 rpm for 60 min at room temperature. The mixed samples were then centrifuged at 1000 rpm for 5 min at 22 °C. Aliquots of the octanol layer and the aqueous layer were removed, diluted with acetonitrile and analyzed by LC-MS using Cyprotex generic conditions. LogD was calculated using the following equation: logD = log(c_{oct}/c_{aq}), where c_{oct} = peak area ratio (analyte/internal standard) in octanol layer (corrected for dilution) and c_{aq} = peak area ratio (analyte/internal standard) in aqueous layer (corrected for dilution). The results are summarized in Table S4 (SI).

Method B (79, 80, and 87 (MUR-2425)). Fifteen μL of test compound (**79**, **80**, MUR-2425) or the control progesterone (10 mM in DMSO) were placed into 96-well deep-well plate. After addition of 500 μL phosphate buffer saturated 1-octanol, the plate was vortexed for 2 min at 1000 rpm followed by the addition of 500 μL 1-octanol saturated phosphate buffer (pH 7.4). The plate was then sealed and shaken with 2000 rpm at 25 °C for 2 h using an Eppendorf Thermomixer Comfort plate shaker. Afterward, the plate was centrifuged for 30 min at 25 °C and 3220*g* to separate the phases. 50 μL aliquots of the upper phase were diluted twice with 450 μL acetonitrile containing internal standards (IS) labetalol, tolbutamide, and ketoprofen. Finally, 30 μL aliquots were diluted with 120 μL of acetonitrile containing IS, 120 μL of ultrapure water and 30 μL of 1-octanol saturated phosphate buffer. 50 μL aliquots from the lower phase were diluted with 249.5 μL acetonitrile containing IS, 200 μL of ultrapure water and 0.5 μL of phosphate buffer (pH 7.4) saturated 1-octanol. Several dilution steps including the addition of the respective opposite phase were carried out to achieve appropriate peak shape and size for subsequent quantification via LC-MS/MS according to Pharmaron Bioanalytical Method A. The assay was performed in duplicate. The relative peak area of the test compound referred to the internal standard was determined from the extracted ion chromatogram and gives the LogD value as LogD = log($AreaRatio_{octanol}$*

Downloaded from pubs.acs.org/jmcmar/article-pdf/doi/10.1021/acs.jmedchem.6c01371/6909867/acs.jmedchem.6c01371.pdf by UNIV REGENSBURG user on 17 November 2026

https://doi.org/10.1021/acs.jmedchem.6c01371
J. Med. Chem. XXXX, XXX, XXX−XXX

$DF_{octanol}/AreaRatio_{buffer}$ * DF_{buffer}) where DF is the dilution factor. The results are summarized in Table S4 (SI).

MDCK-MDR1 Permeability

Method A (67 (MUR-2424)). Darby Canine Kidney (MDCK) epithelial cells stably transfected with the human MDR gene were seeded on a Multiscreen plate (Millipore, MA, USA) and formed a confluent monolayer over 4 to 5 days prior to the experiment. The MDCK-MDR1 cell monolayer integrity was assessed by fluorometric measurement of Lucifer Yellow leakage.

For apical to basolateral (A−B) permeability, the test compound (MUR-2424) in the absence or presence of 2 μM elacridar (a P-gp inhibitor) was added to the apical (A) side and the amount of permeation was determined on the basolateral (B) side; for basolateral to apical (B−A) permeability, the test compound in the absence or presence of 2 μM elacridar was added to the B side and the amount of permeation was determined on the A side. The A-side buffer contained 100 μM lucifer yellow dye in Transport Buffer (1.98 g/L glucose in 10 mM HEPES, 1x Hank's Balanced Salt Solution; pH 7.4), while the B-side buffer was Transport Buffer at pH 7.4. MDCK-MDR1 cells were incubated with 10 μM of test compound (MUR-2424) or controls (prazosin, a P-gp substrate and antipyrine, a high permeability marker) in these buffers for 60 min, and at the end of the assay, donor and receiver side solution samples were collected, quenched by 100% methanol containing an internal standard and centrifuged at 5000 rpm for 10 min at 4 °C. Following centrifugation, the supernatant of donor and receiver side samples were analyzed by LC-MS/MS using Cyprotex generic conditions. The permeability coefficient (P_{app}) of the test compound in the absence and presence of the P-gp inhibitor was calculated from the following equation: $P_{app} = ((dQ/dt)/(c_0*A))$, where dQ/dt is the rate of permeation of the test compound across the cells, c_0 is the donor compartment concentration at time 0 min and A is the area of the cell monolayer. The efflux ratio (ER) was calculated from mean A-B and B-A data according to the following equation: $ER = P_{app(B-A)}/P_{app(A-B)}$. An ER > 2 indicates a potential substrate for P-gp efflux transporter protein. The results are summarized in Table S5 (SI).

Method B (79, 80, and 87 (MUR-2425)). For experiments with **79** and **80**, MDCKII-MDR1_NKI cells, obtained from The Netherlands Cancer Institute were used. For experiments with MUR-2425, MDCK-MDR1 cells were used. Cells were cultured in DMEM (Gibco) containing FBS (AusGenex, City of Gold Cost, Australia) and penicillin/streptomycin (Solarbio, Beijing, China) at 37 °C, 5% CO_2 and 95% relative humidity. Cells were diluted to 1.56×10^6 cells/mL with culture medium and 50 μL cell suspension/well were dispensed into a 96-well HTS Transwell plate (Corning, New York, USA) and incubated for 3−8 days. Cell culture medium was replaced every other day, beginning no later than 24 h after initial plating Monolayer integrity was assessed by measuring transepithelial electrical resistance (TEER) using a Millicell Epithelial Volt-Ohm measuring system (Millipore, USA). A TEER value greater than 42 $\Omega*cm^2$ indicates monolayer integrity. 10 mM stock solutions of test compound (**79**, **80**, MUR-2425) and controls (metoprolol, prazosin, imatinib) were prepared in DMSO and diluted with HBSS (10 mM HEPES, pH 7.4) to a final concentration of 1 μM and a final DMSO concentration of 0.5%. Thirty min before the assay, the buffer in the MDCK-MDR1 plate was exchanged with prewarmed HBSS (10 mM HEPES, pH 7.4) and incubated at 37 °C. To determine the rate of drug transport from the apical to basolateral direction (A-B), 125 μL of 1 μM working solution of test or control compound was added to the transwell insert (apical compartment) and a 50 μL sample (D_0 sample) was immediately transferred from the apical compartment to a new 96-well plate. Then the wells in the receiver plate (basolateral compartment) were filled with 235 μL of HBSS (10 mM HEPES, pH7.4). To determine the rate of drug transport from the basolateral to the apical compartment (B-A), 285 μL of 1 μM working solution of test or control compound was added to the receiver plate wells and a 50 μL sample (D_0 sample) was immediately transferred from the basolateral compartment to a new 96-well plate. Then the transwell inserts were filled with 75 μL of HBSS (10 mM HEPES, pH 7.4). After incubation at 37 °C for 2 h, 50 μL aliquots from donor and acceptor sides were diluted with 4 volumes of cold methanol containing internal standards (IS) ketoprofen, labetalol, tolbutamide and diclofenac. D_0 samples and samples after 2 h were vortexed for 5 min, centrifuged at 3200g for 30−40 min, diluted with ultrapure water (1/1) and analyzed by LC-MS/MS according to Pharmaron Bioanalytical Method B with the modification of applying a negative multiple reaction monitoring mode with an ion spray voltage of −4500 V for **79**. The assay was performed in duplicate. Lucifer Yellow (LY) leakage after 2 h transport period was determined according to the following procedure: A stock solution of Lucifer yellow was prepared in water and diluted with HBSS (10 mM HEPES, pH 7.4) to reach the final concentration of 100 μM. 100 μL of this solution were added to the transwell insert and the receiver plate wells were filled with 300 μL of HBSS (10 mM HEPES, pH7.4). The plates were incubated at 37 °C for 30 min. 80 μL samples were removed from the apical and basolateral compartment to measure the LY fluorescence signal in a fluorescence plate reader at 485 nM excitation and 530 nM emission. The LY leakage was calculated as $LY\ leakage = [LY]_{acceptor}/([LY]_{donor} + [LY]_{acceptor})$ where $[LY]_{acceptor}$ is the fluorescence intensity in the acceptor well (0.3 mL), and $[LY]_{donor}$ is the fluorescence intensity in the donor well (0.1 mL). A LY leakage of <1% was considered acceptable. The apparent permeability coefficient P_{app} was calculated as $P_{app} = (V_A*[drug]_{acceptor})/(Area*t*[drug]_{initial,\ donor})$ where V_A is the volume in the acceptor well [mL], Area is the surface area of the membrane (0.143 cm^2) and t is the total transport time [s]. The efflux ratio was calculated as $ER = P_{app(B-A)}/P_{app(A-B)}$ and the recovery was calculated as $Rec[\%] = (V_A \times [drug]_{acceptor} + V_D*[drug]_{donor})/(V_D \times [drug]_{initial,donor})$ where V_A is the volume [mL] in the acceptor well and V_D is the volume [mL] in the donor well. The results are summarized in Table S5 (SI).

Stability in Human, Mouse, and Rat Plasma and Blood

Method A (67 (MUR-2424)). The test compound MUR-2424 and controls (propantheline as positive control, warfarin as negative control) were incubated in final concentrations of 5 μM in singlicate with human and mouse plasma or blood (pH 7.4 ± 0.1) at 37 °C. At different time points (0, 15, 30, 60, and 120 min), an aliquot was removed from each experimental reaction and mixed with ice-cold stop solution (acetonitrile or methanol containing an internal standard). In case of plasma samples, stopped reactions were kept on ice for at least 10 min and subsequently filtered by centrifugation for 1 min at 500 rcf and 4 °C. The blood samples were subjected to three freeze−thaw cycles and 20 min sonication at 0 °C before they were centrifuged at 6102 rcf for 20 min at 4 °C to precipitate the proteins. All supernatants were analyzed by LC-MS/MS using Cyprotex generic conditions. Data were calculated as % remaining parent compound by assuming 0 min time point peak area ratio (analyte/internal standard) as 100%. Data were fit to a first-order decay model to calculate slope k as in the following equation: elimination rate constant (k) = (−gradient). The *in vitro* half-life was calculated according to the following equation: $t_{1/2} = 0.693/k$. The results are summarized in Figure S9 and Table S6 (SI).

Method B (79, 80, and 87 (MUR-2425)). Pooled, gender mixed human plasma and blood (K_2EDTA) from healthy Asian volunteers was collected in domestic hospital with ethical approval. Pooled, gender mixed rat and mouse plasma and blood (K_2EDTA) from CD-1 mice was purchased from SPF Biotechnology Co., Ltd. (Bejing, China). 1 mM working solutions of test compound (**79**, **80**, MUR-2425) (in DMSO) or control compound mevinolin (in DMSO) and propantheline (in acetonitrile) were spiked into preincubated plasma/blood in a final concentration of 5 μM and a final solvent concentration of 0.5% and incubated at 37 °C while shaking at 60 rpm. After incubation periods of 0, 15, 30, 60, and 120 min, the reaction was stopped by adding 400 μL of room temperature quench solution (acetonitrile containing internal standards labetalol, tolbutamide, and ketoprofen). Samples were vortexed for 5 min and centrifuged at 3220g for 40 min at 4 °C to precipitate proteins. Subsequently, 100 μL of the supernatant were transferred to a new 96-well plate and diluted with 100 μL water. Quantification was

Downloaded from pubs.acs.org/jmcmar/article-pdf/doi/10.1021/acs.jmedchem.6c01371/6909867/acs.jmedchem.6c01371.pdf by UNIV REGENSBURG user on 17 November 2026

https://doi.org/10.1021/acs.jmedchem.6c01371
J. Med. Chem. XXXX, XXX, XXX−XXX

performed by LC-MS/MS analysis according to Pharmaron Bioanalytical Method A (plasma and blood samples of MUR-2425; plasma samples of **79**) and according to Pharmaron Bioanalytical Method B (blood samples of **79**; plasma and blood samples of **80**) with the modification of applying a negative multiple reaction monitoring mode with an ion spray voltage of −4500 V for the blood samples of **79**. The relative peak area of the test compound referred to the internal standard was determined from the extracted ion chromatogram and gives the percentage of remaining compound as the ratio of the relative peak area at the respective time point and the relative peak area at the time point 0 min. The slope value k was obtained by linear fit of the natural logarithm of remaining percentage plotted against incubation time. The *in vitro* half-life ($t_{1/2}$) was determined from the slope value as $t_{1/2} = -0.693/k$. The results are summarized in Figure 5C, Figure S9 and Table S6 (SI).

Plasma Protein Binding

Method A (67 (MUR-2424)). MUR-2424 or warfarin (control) were added in duplicate to human or mouse plasma (pH 7.4) to reach a final concentration of 5 μM in case of MUR-2424 or 2 μM in the case of warfarin. Samples were dialyzed in a RED device (Rapid Equilibrium Dialysis, Pierce) against PBS on an orbital shaker for 4 h. At the end of the incubation, aliquots from both plasma and PBS sides were collected, and matrix−matrix matched with an appropriate amount of PBS and blank plasma, respectively. Three volumes of acetonitrile containing an analytical internal standard were added to release the test compound and precipitate proteins. After filtration, the supernatant was analyzed by LC-MS/MS using Cyprotex generic conditions. Based on the peak area ratio (analyte/internal standard), the percentage of bound compound was calculated as follows: % bound = 100% − % free with % free = (Peak Area Ratio$_{\text{buffer chamber}}$/Peak Area Ratio$_{\text{plasma chamber}}$) * 100%. The results are summarized in Figure S10 and Table S7 (SI).

Method B (79, 80, and 87 (MUR-2425)). Pooled, gender mixed human plasma (K_2EDTA) from healthy asian volunteers was collected in a domestic hospital with ethical approval. Pooled, gender mixed mouse plasma (K_2EDTA) from CD-1 mice was purchased from BioIVT LCC (Westbury, USA). Pooled, gender mixed rat plasma from SD rats was obtained from a local supplier. Working stock solutions of test compound (**79**, **80**, MUR-2425) and positive control ketoconazole were spiked into preincubated plasma to a final concentration of 1 μM (final DMSO concentration 0.5%). After membrane dialysis against PBS for 6 h at 37 °C and 150 rpm with 5% CO_2, 20 μL aliquots from both buffer and plasma chambers were transferred into a buffer and plasma case plate separately. 80 μL of blank plasma was added to the buffer case plate, and 80 μL of PBS was added to the plasma case plate. 480 μL of a quench solution (acetonitrile containing the internal standards labetalol, tolbutamide, and ketoprofen) was added to precipitate the proteins, followed by vortexing for 15 min. After centrifugation at 3220*g* for 30 min at 4 °C, 100 μL of the supernatant were diluted with 100 μL water and analyzed via LC-MS/MS according to Pharmaron Bioanalytical Method A with the modification of applying a negative multiple reaction monitoring mode with an ion spray voltage of −4500 V for **79**. The assay was performed in duplicate, and the concentration of the test compound in buffer and plasma chambers was determined from peak area ratio referred to the internal standard. The percentage of bound compound was calculated as follows: % bound = 100% − % free with % free = (Peak Area Ratio$_{\text{buffer chamber}}$/Peak Area Ratio$_{\text{plasma chamber}}$) * 100%; % recovery = (Peak Area Ratio$_{\text{buffer chamber}}$ + Peak Area Ratio$_{\text{plasma chamber}}$)/Peak Area Ratio$_{\text{total sample}}$ * 100%; % stability = Peak Area Ratio$_{\text{6h sample}}$/Peak Area Ratio$_{\text{0h sample}}$ * 100%. The results are summarized in Figure 5D, Figure S10 and Table S7 (SI).

Metabolic Stability in Human and Mouse Hepatocytes

Method A (67 (MUR-2424)). MUR-2424 and a control (midazolam, umbelliferone) were incubated with pooled cryopreserved human or mouse hepatocytes at 37 °C. The cells were thawed, viable cells counted, and equilibrated according to the supplier's directions. After 30 min equilibration at 37 °C with gentle agitation, the compounds were added to the cells to give the final concentration of 1 μM. After incubation periods of 0, 15, 30, 60, 90, and 120 min at 37 °C, samples were removed and mixed with ice-cold stop solution (methanol containing an analytical internal standard). Stopped reactions were kept on ice for at least 10 min. The samples were filtered by centrifugation for 1 min at 500 rcf, and 4 °C and the supernatants were analyzed by LC-MS/MS using Cyprotex generic conditions. Data were calculated as the remaining percentage of parent compound by setting the peak area ratio (analyte/internal standard) at 0 min as 100%. Data were fit to a first-order decay model to determine half-life ($t_{1/2}$). From a plot of the natural logarithm (ln) of peak area against time, the slope of the line was determined. Subsequently, half-life and intrinsic clearance (CL_{int}) were calculated using the following equations: elimination rate constant k = (−slope); half-life $t_{1/2} = 0.693/k$; CL_{int} [μL/min/10^6 cells] = $(V * 0.693)/t_{1/2}$, where V is the incubation volume [μL] divided by the number of cells. The results are summarized in Figure S11 and Table S8 (SI).

Method B (79, 80, and 87 (MUR-2425)). Cryopreserved human hepatocytes were purchased from BioIVT (New York, USA), cryopreserved male CD-1 mouse hepatocytes, and pooled male Sprague−Dawley rat hepatocytes were obtained from TPCS. The hepatocytes were thawed, centrifuged at 100*g* for 5 min, the thawing medium was aspirated, and the cells were resuspended in serum-free incubation medium (William's E Medium supplemented with GlutaMAX (both purchased from Gibco Thermo Fisher Scientific, Waltham, Massachusetts, USA) at a cell density of 0.5×10^6 cells/mL. A portion of the cell suspension was boiled for 5 min to serve as the negative control. Both viable and boiled hepatocytes were dispensed in a 96-well plate to a cell density of 0.1×10^6 cells/well and preincubated for 10 min at 37 °C before the test compound (**79**, **80**, MUR-2425) and the positive control verapamil were added in a final concentration of 1 μM and a final DMSO concentration of 0.01%. After incubation periods of 0, 15, 30, 60, 90, and 120 min at 800 rpm, 5% CO_2, and 37 °C, aliquots of 25 μL were quenched with 400 μL of cold acetonitrile containing the internal standards tolbutamide, ketoprofen, and labetalol. After vortexing at 1000 rpm for 12 min followed by centrifugation for 30 min at 3220*g* and 4 °C, 120 μL of the supernatant were diluted by 120 μL ultrapure water and analyzed via LC-MS/MS according to Pharmaron Bioanalytical Method A with the modification of applying a negative multiple reaction monitoring mode with an ion spray voltage of −4500 V for **79**. The assay was performed in duplicate. The relative peak area of the test compound referred to the internal standard was determined from the extracted ion chromatogram and gives the percentage of remaining compound as the ratio of the relative peak area at the respective time point and the relative peak area at the time point 0 min. The slope value k was obtained by linear fit of the natural logarithm of remaining percentage plotted against incubation time. The *in vitro* half-life ($t_{1/2}$) was determined from the slope value as $t_{1/2} = -0.693/k$. The in vitro intrinsic clearance CL_{int} was calculated from $CL_{int} = k*V/N$ where V is the incubation volume (0.2 mL) and N is the number of hepatocytes per well (0.1×10^6 cells). The results are summarized in Figure 5E, Figure S11 and Table S8 (SI).

Metabolic Stability in Human and Mouse Liver S9 Fractions

Method A (67 (MUR-2424)). Human or mouse S9 fractions (final protein concentration 1 mg/mL; in 0.1 M phosphate buffer containing 3 mM $MgCl_2$, 25 μg/mg alamethicin; pH 7.4), and test compound (MUR-2424) or controls (midazolam, umbilliferone; final substrate concentration 3 μM; final DMSO concentration 0.3%) are preincubated at 37 °C prior to the addition of cofactors (final concentration of 1 mM NADPH) to initiate the reaction. A minus cofactor control incubation is included at 45 min for each compound tested, where 0.1 M phosphate buffer is added instead of cofactors. At predetermined time points (0, 5, 15, 30, and 45 min), an aliquot was removed from each experimental and control reaction and mixed with an equal volume of ice-cold acetonitrile containing an internal standard to stop the reaction and precipitate proteins. The samples were filtered by centrifugation for 1 min at 500 rcf, and 4 °C and the

Downloaded from pubs.acs.org/jmcmar/article-pdf/doi/10.1021/acs.jmedchem.6c01371/6909867/acs.jmedchem.6c01371.pdf by UNIV REGENSBURG user on 17 November 2026

https://doi.org/10.1021/acs.jmedchem.6c01371
J. Med. Chem. XXXX, XXX, XXX−XXX

supernatants were analyzed by LC-MS/MS using Cyprotex generic conditions. Data were calculated as remaining % of parent compound by setting the peak area ratio (analyte/internal standard) at 0 min as 100%. Data were fit to a first-order decay model to determine half-life ($t_{1/2}$). From a plot of natural logarithm (ln) of peak area against time, the slope of the line was determined. Subsequently, half-life and intrinsic clearance (CL_{int}) were calculated using the following equations: elimination rate constant (k) = (−slope); half-life ($t_{1/2}$) = 0.693/k; CL_{int} [μL/min/mg protein] = 0.693/($t_{1/2}$ * $c_{protein}$). The results are summarized in Figure S9 and Table S8 (SI).

Method B (79, 80, and 87 (MUR-2425)). Gender pooled human liver S9 fractions, male IGS SD rat liver S9 fractions, and male CD-1 mouse liver S9 fractions were purchased from Xenotech (Kansas City, USA). Liver S9 fractions were added to a 96-well incubation plate to a final concentration of 1 mg/mL together with 100 mM phosphate buffer, 1 mM NADPH, and 5 mM $MgCl_2$ ($MgCl_2$ was not added for experiments with **79**, **80**). Negative control samples were prepared by adding ultrapure H_2O instead of NADPH. The mixture was warmed for 10 min at 37 °C before the reaction was started by the addition of the test compound (**79**, **80**, MUR-2425) or the positive control verapamil in a final concentration of 1 μM (final DMSO concentration of 0.01%). After incubation periods of 0, 15, 30, 45, and 60 min at 37 °C, 25 μL aliquots were quenched with 4−5 volumes of cold methanol containing the internal standards tolbutamide, labetalol, and ketoprofen. After centrifugation for 30 min at 3220*g*, 100 μL of the supernatant were diluted with ultrapure water and analyzed via LC-MS/MS according to Pharmaron Bioanalytical Method A (for rat samples of **80** and all samples of **79**) or according to Pharmaron Bioanalytical Method B (for mouse and human samples of **79** and for all samples of MUR-2425). The assay was performed in duplicate, negative controls were prepared in singlicate. The relative peak area of the test compound referred to the internal standard was determined from the extracted ion chromatogram and gives the percentage of remaining compound as the ratio of the relative peak area at the respective time point and the relative peak area at the time point 0 min. The slope value k was obtained by linear fit of the natural logarithm of remaining percentage plotted against incubation time. The *in vitro* half-life ($t_{1/2}$) was determined from the slope value as $t_{1/2}$ = −0.693/k. The in vitro intrinsic clearance CL_{int}, was calculated as CL_{int} = k*V/m where V is the incubation volume and m is the amount of protein per well. The results are summarized in Figure 5E, Figure S11, and Table S8 (SI).

Metabolic Stability in Human and Mouse Liver Microsomes (79, 80, and 87 (MUR-2425))

Pooled human male and female liver microsomes and pooled male Sprague−Dawley rat liver microsomes were purchased from Discovery Life Science (Huntsville, USA), pooled male CD-1 mouse liver microsomes were purchased from Xenotech (Kansas City, USA). The microsomes were placed in 0.6 mL microtubes in a 96-well rack to a final assay concentration of 0.5 mg/mL in 100 mM phosphate buffer. NADPH was added to each well in a final concentration of 1 mM. In negative control wells, phosphate buffer was added instead of NADPH. The mixture was prewarmed at 37 °C for 5−10 min before the reaction was started by the addition of the test compound (**79**, **80**, MUR-2425) or the positive control verapamil in a final compound concentration of 1 μM (final DMSO concentration of 0.01% (**79**, **80**) or 0.5% MUR-2425). After incubation periods of 0, 15, 30, 45, and 60 min at 37 °C, reactions were quenched with 4 volumes of cold acetonitrile containing the internal standards tolbutamide, labetalol, and ketoprofen. After centrifugation for 45 min at 3220 *g*, 80 μL of the supernatant were diluted with ultrapure water and analyzed via LC-MS/MS according to Pharmaron Bioanalytical Method B with the modification of using a Waters ACQUITY UPLC Protein BEH C4 column (300 Å, 1.7 μM 2.1 × 50 mm) and a negative multiple reaction monitoring mode with an ion spray voltage of −4500 V for the analysis of **79**. The assay was performed in duplicate; negative controls were prepared in singlicate. The relative peak area of the test compound referred to the internal standard was determined from the extracted ion chromatogram and gives the percentage of remaining compound as the ratio of the relative peak area at the respective time point and the relative peak area at the time point 0 min. The slope value k was obtained by linear fit of the natural logarithm of remaining percentage plotted against incubation time. The *in vitro* half-life ($t_{1/2}$) was determined from the slope value as $t_{1/2}$ = −0.693/k. The *in vitro* intrinsic clearance CL_{int}, was calculated as CL_{int} = k*V/m where V is the incubation volume and m is the amount of protein per well. The results are summarized in Figure 5E, Figure S11, and Table S8 (SI).

Metabolite Identification of 79, 80, and 87 (MUR-2425) in Human, Rat, Dog, Monkey, Minipig, and Mouse Hepatocytes

Male CD-1 mouse hepatocytes and male SD rat hepatocytes were purchased from TPCS, male Gottingen minipig hepatocytes and gender-mixed human hepatocytes were purchased from BioIVT (Shanghai, China), male beagle hepatocytes were purchased from Milecell Biotechnology Inc. (Sugar Land, USA), and male cynomolgus hepatocytes were purchased from the Research Institute for Liver Diseases (RILD, Shanghai, China). For **79** and **80**, the study was conducted with the disodium-salt form. For MUR-2425, the study was conducted with the disodium salt form (human, rat, dog, monkey, and minipig) or the TFA salt form (mouse).

The test compound (**79**, **80**, MUR-2425) was incubated with the respective hepatocytes in a final concentration of 10 μM and 1.0 × 10^6 cells/mL for 0, 120, and 240 min at 37 °C. After the incubation period, samples were quenched with 3 volumes of acetonitrile containing 0.01−0.1% formic acid, followed by centrifugation for 30 min at 16,000*g*. 600 μL of supernatant were transferred to clean tubes and placed in an evaporator under a steady nitrogen stream at RT until dry. Dried residues were reconstituted with 100 μL of acetonitrile:H_2O solution (1:4 (v/v)) and vortexed before they were analyzed via LC-UV-MS/MS on a Vanquish UHPLC system (Thermo Fisher Scientific) equipped with an Orbitrap Exploris 480 (**79**) or a Thermo Scientific Q Exactive Plus (**80**, MUR-2425) (both Thermo Fisher Scientific, USA). A XSelect HSS T3 XP column (100 Å, 2.5 μ, 2.1 × 100 mm; Waters, Milford, USA) was used as the stationary phase and a linear gradient of 0.1% formic acid in water (A) and 0.1% formic acid in acetonitrile (B) with a flow rate of 0.5 mL/min was applied. Positive and negative ions were detected using a spray voltage of 3.5 kV/-2.5 kV (**79**, **80**) or 4.0 kV/-3.6 kV (MUR-2425) and an auxiliary gas temperature of 350 °C and an automatic gain control (AGC) of 1−3 × e^6. The remaining percentage of the test compound was calculated based on the MS response of the parent drug in 240 min samples relative to t_0 samples. The relative peak area of each metabolite was determined from extracted ion chromatograms of 240 min samples. The results are summarized in Figure 5F, Figure S12 and Table S9 (SI).

Identification of CYP Isoforms That Participate in the Metabolism of MUR-2425

MUR-2425 was dissolved in acetonitrile at a concentration of 400 μM. Working solutions of positive CYP substrates were prepared as described in the following: phenacetin (CYP1A2) at 4000 μM, bupropion (CYP2B6) at 8000 μM, amodiaquine (CYP2C8) at 800 μM, diclofenac (CYP2C9) at 2000 μM, (*S*)-mephenytoin (CYP2C19) at 8000 μM, bufuralol (CYP2D6) at 2000 μM and midazolam (CYP3A) at 800 μM. Working solutions of positive CYP inhibitors were prepared as described in the following: furafylline (CYP1A2) at 4000 μM, thio-TEPA (CYP2B6) at 4000 μM, montelukast (CYP2C8) at 4000 μM, tienilic acid (CYP2C9) at 8000 μM, (+)-*N*-3-benzylnirvanol (CYP2C19) at 4000 μM, quinidine (CYP2D6) at 1000 μM and troleandomycin (CYP3A) at 8000 μM. A master solution containing human liver microsomes (final concentration 0.5 mg/mL), phosphate buffer (100 mM, pH 7.4), and NADPH solution (10 mM in phosphate buffer) was prepared. For samples with mechanism-based inhibitor (furafylline, thio TEPA, tienilic acid or troleandomycin), 1 μL of inhibitor solution was added to the master solution with NADPH before preincubation. Then 1 μL of substrate or test compound was added to the master solution (with

Downloaded from pubs.acs.org/jmcmar/article-pdf/doi/10.1021/acs.jmedchem.6c01371/6909867/acs.jmedchem.6c01371.pdf by UNIV REGENSBURG user on 17 November 2026

https://doi.org/10.1021/acs.jmedchem.6c01371
J. Med. Chem. XXXX, XXX, XXX−XXX

NADPH and inhibitor) to start the reaction. For samples with other inhibitors (montelukast, (+)-*N*-3-benzylnirvanol, or quinidine), 1 μL of inhibitor solution and 1 μL of substrate or MUR-2425 were added to the master solution (with NADPH and inhibitor) to start the reaction. For the samples without inhibitor, 1 μL of acetonitrile and 1 μL of substrate or test compound were added to the master solution with NADPH to start the reaction. The incubation mixture was mixed on a whirly mixer for 10 s and incubated at 37 °C. The experiment was performed in duplicate. For the samples of negative control, 1 μL of acetonitrile and 1 μL of substrates or MUR-2425 were added to the master solution without NADPH and mixed on a whirly mixer for 10 s. This experiment was performed in singlicate. 6. At 0, 15, 30, 45, and 60 min, the incubation mixture was mixed on a whirly mixer for 10 s and 50 μL of incubated mixture were transferred to a separate "Quenching plate" containing 400 μL of cold quench solution (acetonitrile containing internal standards imipramine, labetalol, ketoprofen and tolbutamide), which was sealed with a lid and mixed on a whirly mixer for 10 min. Afterward the samples were centrifuged at 3220 *g* and 4 °C for 60 min to precipitate proteins before 100 μL of the supernatant were transferred to a new 96-well plate with 100 μL ultrapure water for LC-MS/MS analysis according to Pharmaron Bioanalytical Method A.

Assessment of Induction Potential of CYP1A2, CYP2B6, and CYP3A4 by MUR-2425 in Human Hepatocytes

Human hepatocytes from male and female Caucasian donors were purchased from BioIVT (NY, USA). Cells were thawed, centrifuged, and thawing medium was aspirated before they were resuspended in plating medium to a seeding density of 0.55×10^6 cells/mL. 100 μL/well were transferred to each well of a collagen I-coated 96-well plate. Plates were incubated at 37 °C with 5% CO_2 and 95% relative humidity for 4−6 h. Medium was exchanged for incubation medium containing Matrigel 0.25 mg/mL and incubated for another 18 h. At the day of the experiment, stock solutions of MUR-2425 and positive control inducers (omeprazole for CYP1A2, phenobarbital for CYP2B6 and rifampicin for CYP3A4) at 1000-fold of the final concentration were prepared in DMSO and diluted with incubation medium to respective working concentrations (1 and 10 μM for MUR-2425, 50 μM for omeprazole, 1000 μM for phenobarbital and 10 μM for rifampicin). A 25 μM solution of chlorpromazine in incubation medium was prepared as a cytotoxicity control. 0.5% DMSO in incubation medium was used as a negative control. The medium in the 96-well hepatocyte plates was replaced with 125 μL of toxicity control, DMSO control, positive inducer, and MUR-2425 solutions, each in triplicate, and incubated for 72 h. Cell morphology was observed and medium with respective controls or test compound was replaced daily. After the incubation period, dosing medium was aspirated and replaced with incubation medium. Cell viability was screened using the CellTiter-Fluor Cell Viability Assay (Promega) according to the manufacturer's instructions. Afterward, stock solutions of respective substrates of the CYP enzymes were prepared and diluted with incubation medium to working concentrations. A phenacetin and bupropion stock solution was prepared in DMSO at 1000-fold or 500-fold working concentration (phenacetin 100 μM, CYP1A2 substrate; bupropion 500 μM, CYP2B6 substrate), and a testosterone stock solution was prepared in methanol at 1000-fold working concentration (200 μM, CYP3A4 substrate). Medium was removed from the 96-well hepatocyte plate and replaced with 125 μL of substrate solution, and hepatocytes were incubated for another 30 min. Immediately after the incubation period, 100 μL samples were transferred to a new 96-well plate and mixed with 3 volumes of methanol containing internal standards labetalol, diclofenac, and imipramine and centrifuged at 3200*g* for 30 min. 100 μL of the supernatant was mixed with 100 μL of ultrapure water. 9- or 10-point calibrations were prepared for the metabolites of phenacetin (acetaminophen), bupropion (hydroxybupropion), and testosterone (6β-hydroxytestosterone) in DMSO at 1000-fold of the highest calibration concentration. 2 μL of 100-fold stock solutions were added to 198 μL incubation medium and mixed with 3 volumes of methanol containing the internal standards. Calibration samples were centrifuged at 3200*g* for 30 min and a 100 μL aliquot of the supernatant was mixed with 100 μL of ultrapure water. LC-MS/MS analysis was performed according to Pharmaron Bioanalytical Method A. Peak areas of marker metabolites were determined from extracted ion chromatograms by using Analyst 1.5.2 software from ABI Inc. CYP activity was expressed as pmol/min/million cells, where pmol is defined as the amount of metabolite formed during the reaction. The number of hepatocytes per well (*N*) is related to the seeding density. The fold-induction enzyme activity was determined by the ratio: Fold of induction = CYP activity$_{(induced)}$/CYP activity$_{(vehicle)}$. The percent adjusted positive control was determined by % positive control = (fold induction$_{test\ compound}$ − 1/fold induction$_{positive\ control}$ − 1) * 100%. The results are summarized in Figure S13 (SI).

Inhibition of CYP1A2, CYP2A6, CYP2B6, CYP2C8, CYP2C9, CYP2C19, CYP2D6, CYP2E1, and CYP3A4 by MUR-2425 in Human Liver Microsomes

Pooled human liver microsomes from female and male donors (Discovery Life Sciences, USA) were prepared at a final concentration of 0.2 mg/mL in phosphate buffer (100 mM). A master solution containing microsomes in phosphate buffer and the respective substrate was prepared and prewarmed to 37 °C for 5 min. 9-point serial dilutions of MUR-2425 or the respective positive controls were added at final assay concentrations ranging from 0 to 50 μM. The following combinations of substrates and positive controls were used for the respective CYP isoforms, final assay concentrations of substrates are given in square brackets: for CYP1A2 phenacetin [40 μM] and furafylline, for CYP2A6 coumarin [2 μM] and tranylcypromine, for CYP2B6 bupropion [50 μM] and ketoconazole, for CYP2C8 paclitaxel [5 μM] and quercetin, for CYP2C9 tolbutamide [200 μM] and sulfaphenazole, for CYP2C19 mephenytoin [50 μM] and N-3-benzylnirvanol, for CYP2D6 dextromethorphan [10 μM] and quinidine, for CYP2E1 chlorzoxazone [50 μM] and disulfiram and for CYP3A4 midazolam [5 μM] and testosterone [50 μM] were used as substrates and ketoconazole as positive control. The reaction was started by addition of NADPH in a final concentration of 1 mM and carried out at 37 °C. After 20 min, the reaction was stopped for CYP isoforms 1A2, 2B6, 2C9, 2C19, 2D6, and 2E1, after 10 min for isoform 2C8 and testosterone-mediated CYP3A4, and after 5 min for isoform 2A6 and midazolam-mediated CYP3A4, by the addition of 2 volumes of cold methanol containing internal standards imipramine, labetalol and ketoprofen. The assay plate was centrifuged at 3200*g* for 60 min to precipitate protein. Aliquots of 100 μL of the supernatant were diluted with 100 μL ultrapure water. The formation of metabolites was analyzed via LC-MS/MS according to Pharmaron Bioanalytical Method A, with the change that a negative multiple reaction monitoring mode with an ion spray voltage of 45,500 V was applied in case of the CYP2A6- and CYP2E1-catalyzed reactions (marker metabolites: hydroxycoumarin and hydroxychloroxazone, respectively). A decrease in the formation of the metabolites in peak area relative to vehicle control is used to calculate an IC_{50} value by using Excel XLfit. All experiments were performed in duplicate. The results are summarized in Figure S14 (SI).

hERG Safety Evaluation of MUR-2425

SyncroPatch 384i/384 Assay. The potential inhibitory effect of MUR-2425 on human Ether-à-go-go-related gene (hERG) channel was evaluated with an automated patch-clamp system on a SyncroPatch 384 instrument (Nanion, Munich, Germany) in CHO hERG-DUO cells stably expressing hERG channel (purchased from B'SYS GmbH (Witterswill, Switzerland)). The cells were cultured in medium consisting of F12 (HAM) medium, 10% FBS, 100 U/mL Penicillin-Streptomycin, 100 μg/mL Hygromycin and 100 μg/mL G418 at 37 °C, 5% CO_2 and were split using StemPro Accutase about three times a week, maintaining about 80% confluence. Internal and external test solutions were composed as follows: internal KF 110 solution (10 mM EGTA, 10 mM HEPES, 10 mM KCl, 10 mM NaCl, 110 mM KF; pF adjusted to 7.4 with KOH), external [-] Ca2+ [-] Mg2+ solution (140 mM NaCl, 4 mM KCl, 5 M D-Glucose, 10 mM

Downloaded from pubs.acs.org/jmcmar/article-pdf/doi/10.1021/acs.jmedchem.6c01371/6909867/acs.jmedchem.6c01371.pdf by UNIV REGENSBURG user on 17 November 2026

https://doi.org/10.1021/acs.jmedchem.6c01371
J. Med. Chem. XXXX, XXX, XXX−XXX

HEPES, pH adjusted to 7.4 with NaOH), external NMDG 60 solution (80 mM NaCl, 60 mM NMDG, 4 mM KCl, 2 mM $CaCl_2$, 1 mM $MgCl_2$, 5 mM D-Glucose, 10 mM HEPES; pH adjusted to 7.4 with HCl). Serial dilution of the test compound MUR-2425 and the positive control cisapride were prepared in DMSO diluted 500-fold with NMDG60 Ca10 solution (80 mM NaCl, 60 mM NMDG, 4 mM KCl, 10 mM $CaCl_2$, 1 mM $MgCl_2$, 5 mM D-Glucose, 10 mM HEPES; pH adjusted to 7.4 with HCl) to final assay concentration of 60, 20, 6.66, 2.22, and 0.74 μM. After stabilizing the baseline for at least 5 min, hERG current in the presence of the test compound at the individual working concentration was recorded for no less than 5 min to reach steady state. If a steady state was not reached within 10 min, the averaged peak current of the last 5 sweeps was used for the steady state value. Afterward, 5 sweeps were measured. Data were defined as acceptable for initial seal resistance of >100 MΩ, access resistance of <25 MΩ, stable leak currents <50% of the control peak tail current at any time, hERG peak tail current amplitude greater than prepulse current amplitude, absolute amplitude of peak tail current of >300 pA, and a rundown of peak tail current amplitude of <30%. The percent current inhbition was calculated on Datacontrol 384 software using the following equation: peak current inhibition = (1 − (Peak tail $current_{compound}$ − Peak tail $current_{positive\ control}$/Peak tail $current_{vehicle}$ − Peak tail $current_{positive\ control}$). Percentages of hERG inhibition against compound concentrations were fit to a sigmoidal dose−response curve with variable slope using Graphpad Prism 8.0 for determination of IC_{50} values. Two independent measurements give IC_{50} values of >30 μM for MUR-2425 and 0.021 μM for the positive control cisapride. The results are summarized in Figure S15 (SI).

FLIPR Assay. CHO hERG-DUO cells stably expressing hERG channel (purchased from B'SYS GmbH (Witterswill, Switzerland) were cultured in F12 (HAM) medium containing 10% FBS, 100 U/mL Penicillin-Streptomycin, 100 μg/mL Hygromycin and 100 μg/mL G418 at 37 °C, 5% CO_2 and were split using StemPro Accutase about three times a week, maintaining about 80% confluence. One day prior to the assay, cells were seeded into 15000 cells/well in culture medium to a 384-well cell plate and incubated at 37 °C/5% CO_2 overnight. The assay was performed on a Fluorometric Imaging Plate Reader (FLIPR, Molecular Device, San Jose, USA) using the corresponding FLIPR Potassium Assay Kit (Molecular Device, San Jose, USA) according to the manufacturer's instructions. 3-fold serial dilutions of the test compound MUR-2425 and the positive control dofetilide were prepared in DMSO and diluted with assay buffer to the highest final assay concentration of 10 μM (dofetilide) and 30 μM (MUR-2425). Based on the normalized fluorescence units RFU = $F_{max} - F_{min}$ while F_{max} and F_{min} are the maximum and minimum of the potassium signal during a defined time window, the percentage of hERG inhibition was calculated as follows: inhibition = (1 − ($RFU_{compound}$ − $RFU_{vehicle}$)/($RFU_{control}$ − $RFU_{vehicle}$). Percentages of hERG inhibition against compound concentrations were fit to a sigmoidal dose−response curve with variable slope using Graphpad Prism 8.0 for determination of IC_{50} values. Two independent measurements give IC_{50} values of >30 μM for MUR-2425 and 0.08 μM for the positive control dofetilide. The results are summarized in Figure S15 (SI).

Off-Target Evaluation of MUR-2425. Off-target safety evaluation of MUR-2425 was performed by Eurofins Panlabs, Inc. (Taipei City, Taiwan) using the SafetyScreen87PLUS Panel. The activity of MUR-2425 at 116 safety-relevant off-targets was tested at 10 μM in different enzyme, radioligand binding, and functional assays. IC_{50} values were determined by a nonlinear, least-squares regression analysis using MathIQ (ID Business Solutions Ltd., UK). K_i values were calculated using the equation of Cheng and Prusoff[52] using the observed IC_{50} of the tested compound, the concentration of radioligand employed in the assay, and the historical values for the K_D of the ligand (obtained experimentally at Eurofins Panlabs, Inc.). The experiments were performed in duplicate and are summarized in Figure S16 (SI).

In Vivo Pharmacokinetic Studies of 67 (MUR-2424) in Female CD-1 Mice

The studies were conducted according to the NeoSome IACUC policies and Operational Guidelines as approved by the IACUC membership, NeoSome Safety Officers, and Attending Veterinarian (approval no. NLS24-006). All efforts were made to minimize animal suffering and the number of animals used, in strict compliance with the 3Rs (replacement, reduction, and refinement) principles.

For the determination of in vivo pharmacokinetics in plasma, brain, and liver tissue, MUR-2424 was administered via intravenous (iv) and subcutaneous (sc) injection of 10 mg/kg to female CD-1 mice. The study was performed in triplicate, meaning that in case of sc administration brain, plasma, and liver samples of three individual animals for every dose were collected at time points of 0.25, 0.5, 1, 2, 4, 8, and 24 h postdosing. In case of iv administration, brain and plasma samples of three individual animals for every dose were collected at time points of 0.083, 0.25, 0.5, 1, 2, 4, 8, and 24 h postdosing. MUR-2424 was formulated at 2 mg/mL in PBS and administered in a volume of 5 mL/kg via subcutaneous or intravenous tail vein injection. At desired time points, three mice for each administration route were euthanized by CO_2 inhalation. Blood was collected through cardiac puncture into K_2EDTA collection tubes, inverted several times to ensure thorough mixing, and kept on wet ice until centrifugation (5 min, 8000 rpm at 4 °C). Plasma was decanted into labeled tubes. The brains and livers were removed, weighed, and stored at −80 °C until further use. Brain and liver samples (50−70 mg) were placed in Precellys tubes (0.5 mL tube containing ceramic beads) and diluted with buffer at a ratio of 1 g of tissue to 3 mL of buffer. The tissue was homogenized on 10 s cycles (6500 rpm) in a Precellys 24 sample homogenizer. The homogenates were either diluted 1 to 9 with plasma and then analyzed against plasma calibration standards or analyzed undiluted against matrix-matched calibration standards that have been prepared from control tissue homogenized the same way. Calibration standards (1.9 to 4000 ng/mL), blanks, zeros (internal standard only), quality control samples (20, 200, and 2500 ng/mL), and test samples were mixed with organic solvent (methanol or acetonitrile) containing a mixture of three generic internal standards at a ratio of 3/1 to precipitate proteins. After centrifugation (10 min, 4 °C, 5000*g*) and filtration, the samples were analyzed by LC-MS/MS using Cyprotex generic conditions and quantified based on a 7-point calibration curve. All procedures were performed according to Institutional Animal Care and Use Committee (IACUC) policies and guidelines as well as standards of the Office of Laboratory Animal Welfare (OLAW). The results are summarized in Figure S17 and Table S10 (SI).

In Vivo Pharmacokinetic Studies of 79, 80, and 87 (MUR-2425) in CD-1 Mice

All procedures related to animal handling, care, and treatment in this study are performed according to Animal Care and Use Protocols (AUP, PK-M-07182025, PK-M-07182026) and approved by the Institutional Animal Care and Use Committee (IACUC) of Pharmaron following the guidance of the Association for Assessment and Accreditation of Laboratory Animal Care (AAALAC). Pharmaron's IACUC policies are in compliance with laws and regulations of local government for animal research, and also in compliance with the guidelines of the Guide for the Care and Use of Laboratory Animals ("The Guide"). Pharmaron adheres to the "3R" principle (Replacement, Reduction, and Refinement) for animal welfare management.

For the determination of *in vivo* pharmacokinetics in plasma and brain tissue, compounds **79** and **80** were administered via subcutaneous (sc) injection of 3,10 or 30 mg/kg bodyweight to male and female CD-1 mice. MUR-2425 was administered per oral (po) in doses of 10 and 50 mg/kg and via subcutaneous (sc) injection of 0.3, 1, 3, 10, or 30 mg/kg. The studies were designed in triplicate, meaning that brain and plasma samples of three individual animals for every sex, dose, and administration route were collected at time points of 0.083, 0.25, 0.5, 1, 2, 4, 8, and 24 h postdosing. For compounds **79** and **80**, all formulations were prepared with the disodium salt form. For MUR-2425, the formulations for po dosing of and for sc dosing of

Downloaded from pubs.acs.org/jmcmar/article-pdf/doi/10.1021/acs.jmedchem.6c01371/6909867/acs.jmedchem.6c01371.pdf by UNIV REGENSBURG user on 17 November 2026

https://doi.org/10.1021/acs.jmedchem.6c01371
J. Med. Chem. XXXX, XXX, XXX−XXX

3, 10, and 30 mg/kg were prepared with the TFA salt form. Additionally, 0.3, 1, 3, 10, and 30 mg/kg sc studies were conducted with the disodium salt form of MUR-2425. The formulations were obtained by dissolving the compound in PBS (pH 7.4) to a concentration of 0.3, 1, 3, or 5 mg/mL. Brain samples were prepared for homogenization by adding deionized water in a ratio of 1:4 (m/m). Aliquots of plasma samples and brain homogenates were diluted with blank plasma or brain homogenate, and proteins were precipitated by the addition of quench solution (acetonitrile or acetonitrile with 0.1% formic acid) containing a mixture of internal standards. Samples were vortexed for 30 s and centrifuged at 4 °C and 4000 rpm for 15 min. The supernatant was diluted three times with water and quantitatively analyzed via LC-MS/MS. For quantification, 10-point (**79**, MUR-2425) or 9-point (**80**) calibration curves covering concentrations from 0.1 ng/mL to 1000 ng/mL were prepared separately for plasma and brain samples by adding the test compound (diluted in MeCN/H_2O 1/1 (v/v) to blank plasma and blank brain homogenates. Quality control samples in a range of 1 ng/mL-800 ng/mL (**79**, **80**) and in a range of 0.3 ng/mL-800 ng/mL (MUR-2425) were prepared for both plasma and brain samples on the day of analysis independently and in the same way as calibration standards. LC-MS/MS analysis of **79**, **80** and the 0.3 mg/kg and 1 mg/kg sc studies of MUR-2425 was performed using a Shimadzu Triple Quad 7500+ instrument equipped with an ESI interface with a Raptor Bipnehyl column (2.7 μ, 90 Å, 30 × 3.0 mm; Restek, Bellefonte, USA) as stationary phase and 0.1% formic acid and 5% MeCN in water and 0.1% formic acid and 5% water in acetonitrile as mobile phase. LC-MS/MS analysis of 3, 10, and 30 mg/kg sc studies and po studies of MUR-2425 was performed on a Shimadzu Triple Quad 6500+ instrument equipped with an ESI interface using a Phenomenex Synergi Polar-RP column (2.5 μ, 100 Å, 50 × 3.0 mm, Phenomenex Ltd., Aschaffenburg, Germany) as stationary phase and 95% water with 10 mM ammonium acetate and 95% acetonitrile with 10 mM ammonium acetate as mobile phase. The plot of the concentration in plasma and brain samples against the time gives the area under the curve (AUC_{last_plasma} and AUC_{last_brain}) and subsequently the brain/plasma ratio as $AUC_{last_brain}/AUC_{last_plasma}$. The slope value k was obtained by linear fit of the natural logarithm of the concentration against the time. The plasma and brain half-life ($t_{1/2_plasma}$ and $t_{1/2_brain}$) was determined from the slope value as $t_{1/2} = -0.693/k$. The limit of quantification for **79** was 0.2 ng/mL in plasma and 1 ng/mL in brain samples. The limit of quantification for **80** was 1 ng/mL in plasma, 2.5 ng/mL in male brain samples, and 5 ng/mL in female brain samples. The limit of quantification for MUR-2425 was 0.1−0.5 ng/mL in plasma and 1 ng/g in brain samples. PK parameters were estimated by a noncompartmental model with the calculation model of "Linear up log down" using WinNonlin 8.6 and WinNonlin 8.3.1. No abnormal clinical symptoms were observed during the entire experiments. The results are summarized in Figure 6, Figure S18−S19 and Tables S11−S12 (SI).

Crystallography

The recombinant protein was prepared and purified as previously described.[53] The ligand−protein complex was obtained by cocrystallization using an Art Robbins Phoenix liquid handler. The plates were automatically imaged with a JANSi imager UVEX. Crystals suitable for X-ray diffraction were harvested, and data were collected at NSLSII 17-ID-1 beamline (Long Island, NY). Data sets were processed with XDS.[54] The structure was solved by molecular replacement with phaser[55] using PDB ID 8VP4 as the search model. Iterative refinement and modeling building were done using the PHENIX[56] suite and COOT.[57] Clear electron density map (2Fo-Fc) as well as Fo−Fc omit map corresponding to the ligand enabled unambiguous placement in the active site. Crystallographic statistics are summarized in Table S12 in the SI, and the final coordinates and structure factors have been deposited in the Protein Data Bank under accession code 9ZEY, 9Z4S, and 9Z4T, respectively. The results are summarized in Table S13 (SI).

Data Analysis

Statistical analyses were performed using GraphPad Prism version 11.0.2 (GraphPad Software, La Jolla, CA). The IC_{50} was calculated by fitting the dose−response data with four-parameter variable slope nonlinear regression. Since neither representative aldehyde nor representative nitrile inhibitors exhibited a dependence of their IC_{50} values on preincubation time (Table S14), both noncovalent and covalent binding to the enzyme were considered to reach rapid equilibrium within the time frame of the fluorometric enzyme assay. Consequently, the IC_{50} values were converted to K_i and the corresponding pK_i values using the Cheng−Prusoff equation[52] to represent the inhibitory potency of the reversible covalent inhibitors. $P < 0.05$ was considered statistically significant.

■ ASSOCIATED CONTENT

Supporting Information

The Supporting Information is available free of charge at https://pubs.acs.org/doi/10.1021/acs.jmedchem.6c01371.

CNS MPO scores and calculated physicochemical properties (Tables S1−S2), tau cleavage assay results of compound (***R***)-**87** (Figure S1), chemical stability of compounds **64**, **67** (MUR-2424), **79**, **80**, **84**, and **87** (MUR-2425) (Figures S2−S7), *in Vitro* ADMET data of compounds **67** (MUR-2424), **79**, **80**, and **87** (MUR-2425) (Figures S8−S16, Tables S3−S9), PK data of compounds **67** (MUR-2424), **79**, **80** and **87** (MUR-2425) (Figures S17−S19, Tables S10−S12), structures of compounds **1**−**87**, (Figures S20−S122), NMR spectra of intermediates (**Int1**-**Int2**) and building blocks (**BB1**-**BB2**) (Figures S123−S129), NMR spectra of aldehydes (compound **8**−**67**) (Figures S130−S249), NMR spectra of nitriles (compound **68**−**87**) (Figures S250−S388), RP-HPLC chromatograms of aldehydes (compound **8**−**67**) (Figures S389−S450), RP-HPLC chromatograms of nitriles (compound **68**−**87**) (Figures S451−S492), crystallography (Table S13), Fluorometric cpCasp2 assay results for prolonged preincubation time (Table S14, Figure S493), and experimental details for the synthesis of **BB1**-**BB2**, compounds **8**−**63**, **65**−**66**, **68**−**86**, and (***R***)-**87** (Scheme S1) (PDF)

Molecular Formula Strings of compounds **1**−**87** (CSV)

Accession Codes

Atomic coordinates and reflection data for crystallographic complexes of JF1cpCasp2 with (Quin)(hE)G(Dab)D-CHO (**41**, PDB ID: 9ZEY), (2-Me-Idc)(hE)VP*D-CHO (**67**, MUR-2424, PDB ID: 9Z4S), and (2-Me-Idc)(hE)VP*D-CN (**87**, MUR-2425, PDB ID: 9Z4T) have been deposited into the Protein Data Bank. Authors will release the atomic coordinates upon article publication.

■ AUTHOR INFORMATION

Corresponding Authors

Michael A. Walters − *Department of Medicinal Chemistry, Institute for Therapeutics Discovery and Development, University of Minnesota, Minneapolis, Minnesota 55414, United States;* orcid.org/0000-0001-5650-9277; Email: mwalters@umn.edu

Steffen Pockes − *Department of Pharmaceutical & Medicinal Chemistry, Institute of Pharmacy, University of Regensburg, 93053 Regensburg, Germany;* orcid.org/0000-0002-2211-9868; Email: steffen.pockes@ur.de

https://doi.org/10.1021/acs.jmedchem.6c01371
J. Med. Chem. XXXX, XXX, XXX−XXX

Downloaded from pubs.acs.org/jmcmar/article-pdf/doi/10.1021/acs.jmedchem.6c01371/6909867/acs.jmedchem.6c01371.pdf by UNIV REGENSBURG user on 17 November 2026

Authors

Bernadette Vallaster − *Department of Pharmaceutical & Medicinal Chemistry, Institute of Pharmacy, University of Regensburg, 93053 Regensburg, Germany*

Lisa Forster − *Department of Pharmaceutical & Medicinal Chemistry, Institute of Pharmacy, University of Regensburg, 93053 Regensburg, Germany*

Merlin Bresinsky − *Department of Pharmaceutical & Medicinal Chemistry, Institute of Pharmacy, University of Regensburg, 93053 Regensburg, Germany;* Present Address: Bionorica SE, Neumarkt, Germany

Lukas Wirth − *Department of Pharmaceutical & Medicinal Chemistry, Institute of Pharmacy, University of Regensburg, 93053 Regensburg, Germany;* Present Address: Heidolph Scientific Products GmbH, Schwabach, Germany.

Jessica L. Fuller − *Department of Medicinal Chemistry, Institute for Therapeutics Discovery and Development, University of Minnesota, Minneapolis, Minnesota 55414, United States;* Present Address: Bio-Techne Corporation, Minneapolis, MN, USA.

Ke Shi − *College of Biological Sciences, University of Minnesota, Nanoliter Crystallization Facility, Minneapolis, Minnesota 55455, United States;* orcid.org/0000-0003-4175-3714

Ian P. Lapcinski − *Department of Neurology, University of Minnesota, Minneapolis 55455, United States;* Present Address: University of California Los Angeles, Los Angeles, CA, USA.

Peng Liu − *Department of Neurology, University of Minnesota, Minneapolis 55455, United States;* orcid.org/0000-0003-2615-1213

Deepti Mudaliar − *Department of Medicinal Chemistry, Institute for Therapeutics Discovery and Development, University of Minnesota, Minneapolis, Minnesota 55414, United States*

Alexander Hubmann − *Department of Pharmaceutical & Medicinal Chemistry, Institute of Pharmacy, University of Regensburg, 93053 Regensburg, Germany*

Jonas Daschner − *Department of Pharmaceutical & Medicinal Chemistry, Institute of Pharmacy, University of Regensburg, 93053 Regensburg, Germany*

Herwig Pongratz − *Department of Pharmaceutical & Medicinal Chemistry, Institute of Pharmacy, University of Regensburg, 93053 Regensburg, Germany*

Marlisa Ködel − *Department of Pharmaceutical & Medicinal Chemistry, Institute of Pharmacy, University of Regensburg, 93053 Regensburg, Germany;* Present Address: TU Wien, Vienna, Austria.

Mu Yang − *Department of Medicinal Chemistry, Institute for Therapeutics Discovery and Development, University of Minnesota, Minneapolis, Minnesota 55414, United States;* orcid.org/0000-0002-3041-8235

Karen H. Ashe − *Department of Neurology, University of Minnesota, Minneapolis 55455, United States*

Complete contact information is available at: https://pubs.acs.org/10.1021/acs.jmedchem.6c01371

Author Contributions

#B.V. and L.F. contributed equally to this work. The manuscript was written through contributions of all authors. All authors have given approval to the final version of the manuscript. K.H.A., M.A.W., and S.P.: resources; M.A.W. and S.P.: conceptualization; B.V., L.F., M.B., L.W., I.P.L., P.L., J.L.F., K.S., D.M., A.H., J.D., H.P., M.K., and M.Y.: formal analysis; B.V., L.F., M.B., L.W., I.P.L., P.L., J.L.F., K.S., D.M., A.H., J.D., H.P., M.K., and M.Y.: investigation; B.V., L.F., K.S., P.L., and S.P.: writing——original draft; B.V., L.F., K.S., P.L., A.H., and S.P.: visualization; K.H.A., M.A.W., and S.P.: funding acquisition; all authors: writing——review and editing; K.H.A., M.A.W., and S.P.: supervision; and M.A.W. and S.P.: project administration.

Funding

This work was funded by NIH grant R01AG062199 (Ashe, Walters; subaward to Pockes), and the Lucas Brothers Foundation (Caspase-2 Inhibitors to Reverse Cognitive Decline, Ashe). S.P. thanks the German Research Foundation DFG for research grant PO 2563/3-1 and Heisenberg professorship PO 2563/4-1. S.P. was also supported by the Fonds der Chemischen Industrie (No. 661688) and Alzheimer Forschung Initiative e.V. (AFI, International Training Grant for M.B.)

Notes

This research did not involve human participants.

The authors declare the following competing financial interest(s): KHA, MWA, and SP are founders and shareholders of Myriel, Inc., which is developing caspase-2 inhibitors to treat Alzheimer's disease and related dementias.

■ ACKNOWLEDGMENTS

The authors thank Vivien Czipper and Julia Blüml for excellent technical assistance. The TOC graphic was created with Biorender.com.

■ ABBREVIATIONS USED

AAALAC, Assessment and Accreditation of Laboratory Animal Care; AFC, 7-amino-4-trifluoromethylcoumarin; ARIA, amyloid-related imaging abnormalities; AU, absorption units; AUP, Animal care and Use Protocol; BB, building block; BeI, 1*H*-benzo[*d*]imidazole-2-carboxylic acid; CAA, 2-cyclohexylacetic acid; Casp1, caspase-1; Casp2, caspase-2; Casp3, caspase-3; Casp6, caspase-6; Casp7, caspase-7; Casp9, caspase-9; Cha, (*S*)-2-amino-3-cyclohexylpropanoic acid; CHAPS, 3-[(3-cholamidopropyl)dimethylammonio]-1-propanesulfonate; Chg, (*S*)-2-amino-2-cyclohexylacetic acid; CL, clearance; cmpd, compound; CNS MPO, central nervous system multiparameter optimization; CPA, 3-cyclohexylpropanoic acid; cpCasp2, circular permutated caspase-2; ctrl, control; Dab, diaminobutyric acid; DAD, diode array detector; di-Na, disodium; DIPEA, *N*,*N*-diisopropylethylamine; D_2O, deuterium oxide; 4-F-F, 4-fluoro-L-phenylalanine; EGTA, ethylene glycol-bis(2-aminoethyl ether)-*N*,*N*,*N*′,*N*′-tetraacetic acid; FLIPR, fluorometric imaging plate reader; 4-F-PPA, 3-(4-fluorophenyl)propanoic acid; FTD, frontotemporal dementia; HATU, [O-(7-azabenzotriazol-1-yl)-*N*,*N*,*N*′,*N*′-tetramethyluronium-hexafluorphosphat]; HBSS, Hanks′ balanced salt solution; HD, Huntington′s disease; hE, homoglutamic acid; HEPES, 4-(2-hydroxyethyl)-1-piperazinethanesulfonic acid; IACUC, Institutional Animal Care and Use Committee; Idc, *S*-indoline-2-carboxylic acid; Ind, indole-2-carboxylic acid; IP, immuno precipitation; Isa, 2,3-dihydro-1*H*-indene-5-sulfonic acid; K_2EDTA, dipotassium ethylenediaminetetraacetic acid; LBD, Lewy body dementia; LiHMDS, lithiumbis(trimethylsilyl)amide; LOQ, limit of quantification; LY, lucifer yellow; MCI, mild cognitive impairment; MDCK, Madin-

Downloaded from pubs.acs.org/jmcmar/article-pdf/doi/10.1021/acs.jmedchem.6c01371/6909867/acs.jmedchem.6c01371.pdf by UNIV REGENSBURG user on 17 November 2026

Darby Canine Kidney; MDR1, multidrug resistance protein1; MeCN, acetonitrile; 4-Me-F, 4-methyl-L-phenylalanine; 2-Me-Idc, (*S*)-2-methylindoline-2-carboxylic acid; MeOD, methanol-d_4; 4-Me-PPA, 3-(4-methylphenyl)propionic acid; MES, 2-(*N*-morpholino)ethanesulfonic acid; MetID, metabolite identification; MRM^+, multiple reaction monitoring; MWCO, molecular weight cutoff; NMDG, N-methyl-D-glucamine; 4-OH-PPA, 3-(4-hydroxyphenyl)propanoic acid; Ω, ohm; Oic, octahydro-1*H*-indole-2-carboxylic acid; OLAW, Office of Laboratory Animal Welfare; P*, (1*R*,2*S*,5*S*)-6,6-dimethyl-3-azabicyclo[3.1.0]hexane-2-carboxylic acid; PAA, 2-phenylacetic acid; PDD, Parkinson's disease with dementia; PMSF, phenylmethylsulfonyl fluoride; 3PPA, 3-phenylpropionic acid; PTFE, polytetrafluoroethylene; PTM, post-translational modification; Quin, quinaldic acid; (*S*)-Me-THIQ, (*S*)-6-methyl-1,2,3,4-tetrahydroisoquinoline-1-carboxylic acid; SARS-CoV-2, severe acute respiratory syndrome coronavirus 2; *rac*, racemic; Rec, recovery; RFU, relative fluorescent units; RP, reversed phase; RT, retention time; SD, standard deviation; SEM, standard error of the mean; SI, Supporting Information; SI-HP, silica high-purity; SPPS, solid phase peptide synthesis; STD, standard; TEER, transepithelial electrical resistance; THIQ, (*S*)-1,2,3,4-tetrahydroisoquinoline-1-carboxylic acid; t_0, dead time or time point zero; t_R, retention time; TPSA, topological polar surface area; WB, Western blotting

REFERENCES

(1) Yiannopoulou, K. G.; Papageorgiou, S. G. Current and Future Treatments for Alzheimer's Disease. *Ther. Adv. Neurol. Disord.* **2013**, *6* (1), 19−33.

(2) Cummings, J.; Osse, A. M. L.; Cammann, D.; Powell, J.; Chen, J. Anti-Amyloid Monoclonal Antibodies for the Treatment of Alzheimer's Disease. *BioDrugs* **2024**, *38* (1), 5−22.

(3) Vigneswaran, S.; Vijverberg, E. G. B.; Barkhof, F.; van de Giessen, E.; Lemstra, A. W.; Pijnenburg, Y.; Teunissen, C. E.; van der Flier, W. M.; van Harten, A. C. "Real-World" Eligibility for Anti-Amyloid Treatment in a Tertiary Memory Clinic Setting. *Alzheimer's Dement.* **2025**, *21* (6), No. e70375.

(4) Smith, B. R.; Nelson, K. M.; Kemper, L. J.; Leinonen-Wright, K.; Petersen, A.; Keene, C. D.; Ashe, K. H. A Soluble Tau Fragment Generated by Caspase-2 Is Associated with Dementia in Lewy Body Disease. *Acta Neuropathol. Commun.* **2019**, *7* (1), No. 124.

(5) Brown-Suedel, A. N.; Bouchier-Hayes, L. Caspase-2 Substrates: To Apoptosis, Cell Cycle Control, and Beyond. *Front. Cell Dev. Biol.* **2020**, *8*, No. 610022.

(6) Kurokawa, M.; Kornbluth, S. Caspases and Kinases in a Death Grip. *Cell* **2009**, *138* (5), 838−854.

(7) Pozueta, J.; Lefort, R.; Ribe, E. M.; Troy, C. M.; Arancio, O.; Shelanski, M. Caspase-2 Is Required for Dendritic Spine and Behavioural Alterations in J20 APP Transgenic Mice. *Nat. Commun.* **2013**, *4* (1), No. 1939.

(8) Julien, O.; Wells, J. A. Caspases and Their Substrates. *Cell Death Differ.* **2017**, *24* (8), 1380−1389.

(9) Salazar, I. L.; Caldeira, M. V.; Curcio, M.; Duarte, C. B. The Role of Proteases in Hippocampal Synaptic Plasticity: Putting Together Small Pieces of a Complex Puzzle. *Neurochem. Res.* **2016**, *41* (1−2), 156−182.

(10) Poreba, M.; Strózyk, A.; Salvesen, G. S.; Drag, M. Caspase Substrates and Inhibitors. *Cold Spring Harb. Perspect. Biol.* **2013**, *5* (8), No. a008680.

(11) Chéreau, D.; Kodandapani, L.; Tomaselli, K. J.; Spada, A. P.; Wu, J. C. Structural and Functional Analysis of Caspase Active Sites. *Biochemistry* **2003**, *42* (14), 4151−4160.

(12) Liu, P.; Ashe, K. H. The Molecular Implications of a Caspase-2-Mediated Site-Specific Tau Cleavage in Tauopathies. *Neural Regener. Res.* **2021**, *16* (9), 1774.

(13) Liu, P.; Smith, B. R.; Huang, E. S.; Mahesh, A.; Vonsattel, J. P. G.; Petersen, A. J.; Gomez-Pastor, R.; Ashe, K. H. A Soluble Truncated Tau Species Related to Cognitive Dysfunction and Caspase-2 Is Elevated in the Brain of Huntington's Disease Patients. *Acta Neuropathol. Commun.* **2019**, *7* (1), No. 111.

(14) Troy, C. M.; Shelanski, M. L. Caspase-2 and Tau—a Toxic Partnership? *Nat. Med.* **2016**, *22*, 1207.

(15) Sladky, V. C.; Villunger, A. Uncovering the PIDDosome and Caspase-2 as Regulators of Organogenesis and Cellular Differentiation. *Cell Death Differ.* **2020**, *27* (7), 2037−2047.

(16) Zhao, X.; Kotilinek, L. A.; Smith, B.; Hlynialuk, C.; Zahs, K.; Ramsden, M.; Cleary, J.; Ashe, K. H. Caspase-2 Cleavage of Tau Reversibly Impairs Memory. *Nat. Med.* **2016**, *22* (11), 1268.

(17) Miles, M. A.; Kitevska-Ilioski, T.; Hawkins, C. J. Old and Novel Functions of Caspase-2. In *International Review of Cell and Molecular Biology*; Elsevier, 2017; Vol. *332*, pp155−212 DOI: 10.1016/bs.ircmb.2016.12.002.

(18) Steuer, E. L.; Kemper, L. J.; Hlynialuk, C. J.; Leinonen-Wright, K.; Montonye, M. L.; Lapcinski, I. P.; Forster, C. L.; Ashe, K. H.; Liu, P. Blocking Site-Specific Cleavage of Human Tau Delays Progression of Disease-Related Phenotypes in Genetically Matched Tau-Transgenic Mice Modeling Frontotemporal Dementia. *J. Neurosci.* **2022**, *42* (23), 4737−4754.

(19) Duan, A. R.; Jonasson, E. M.; Alberico, E. O.; Li, C.; Scripture, J. P.; Miller, R. A.; Alber, M. S.; Goodson, H. V. Interactions between Tau and Different Conformations of Tubulin: Implications for Tau Function and Mechanism. *J. Mol. Biol.* **2017**, *429* (9), 1424−1438.

(20) Fath, T.; Eidenmüller, J.; Brandt, R. Tau-Mediated Cytotoxicity in a Pseudohyperphosphorylation Model of Alzheimer's Disease. *J. Neurosci.* **2002**, *22* (22), 9733−9741.

(21) Gong, C.-X.; Liu, F.; Grundke-Iqbal, I.; Iqbal, K. Post-Translational Modifications of Tau Protein in Alzheimer's Disease. *J. Neural Transm.* **2005**, *112* (6), 813−838.

(22) Teravskis, P. J.; Oxnard, B. R.; Miller, E. C.; Kemper, L.; Ashe, K. H.; Liao, D. Phosphorylation in Two Discrete Tau Domains Regulates a Stepwise Process Leading to Postsynaptic Dysfunction. *J. Physiol.* **2021**, *599* (9), 2483−2498.

(23) Liu, P.; Smith, B. R.; Montonye, M. L.; Kemper, L. J.; Leinonen-Wright, K.; Nelson, K. M.; Higgins, L.; Guerrero, C. R.; Markowski, T. W.; Zhao, X.; Petersen, A. J.; Knopman, D. S.; Petersen, R. C.; Ashe, K. H. A Soluble Truncated Tau Species Related to Cognitive Dysfunction Is Elevated in the Brain of Cognitively Impaired Human Individuals. *Sci. Rep.* **2020**, *10*, No. 3869.

(24) Carroll, J. B.; Southwell, A. L.; Graham, R. K.; Lerch, J. P.; Ehrnhoefer, D. E.; Cao, L.-P.; Zhang, W.-N.; Deng, Y.; Bissada, N.; Henkelman, R. M.; Hayden, M. R. Mice Lacking Caspase-2 Are Protected from Behavioral Changes, but Not Pathology, in the YAC128 Model of Huntington Disease. *Mol. Neurodegener.* **2011**, *6* (1), No. 59.

(25) Tiwari, M.; Herman, B.; Morgan, W. W. A Knockout of the Caspase 2 Gene Produces Increased Resistance of the Nigrostriatal Dopaminergic Pathway to MPTP-Induced Toxicity. *Exp. Neurol.* **2011**, *229* (2), 421−428.

(26) Poreba, M.; Groborz, K.; Navarro, M.; Snipas, S. J.; Drag, M.; Salvesen, G. S. Caspase Selective Reagents for Diagnosing Apoptotic Mechanisms. *Cell Death Differ.* **2019**, *26* (2), 229−244.

(27) Poreba, M.; Rut, W.; Groborz, K.; Snipas, S. J.; Salvesen, G. S.; Drag, M. Potent and Selective Caspase-2 Inhibitor Prevents MDM-2 Cleavage in Reversine-Treated Colon Cancer Cells. *Cell Death Differ.* **2019**, *26* (12), 2695−2709.

(28) Bresinsky, M.; Strasser, J. M.; Vallaster, B.; Liu, P.; McCue, W. M.; Fuller, J.; Hubmann, A.; Singh, G.; Nelson, K. M.; Cuellar, M. E.; Wilmot, C. M.; Finzel, B. C.; Ashe, K. H.; Walters, M. A.; Pockes, S. Structure-Based Design and Biological Evaluation of Novel Caspase-2 Inhibitors Based on the Peptide AcVDVAD-CHO and the Caspase-2-Mediated Tau Cleavage Sequence YKPVD314. *ACS Pharmacol. Transl. Sci.* **2022**, *5* (1), 20−40.

(29) Bresinsky, M.; Strasser, J. M.; Hubmann, A.; Vallaster, B.; McCue, W. M.; Fuller, J.; Singh, G.; Nelson, K. M.; Cuellar, M. E.;

Downloaded from pubs.acs.org/jmcmar/article-pdf/doi/10.1021/acs.jmedchem.6c01371/6909867/acs.jmedchem.6c01371.pdf by UNIV REGENSBURG user on 17 November 2026

Finzel, B. C.; Ashe, K. H.; Walters, M. A.; Pockes, S. Characterization of Caspase-2 Inhibitors Based on Specific Sites of Caspase-2-Mediated Proteolysis. *Arch. Pharm.* **2022**, *355*, No. e2200095.
(30) McStay, G. P.; Salvesen, G. S.; Green, D. R. Overlapping Cleavage Motif Selectivity of Caspases: Implications for Analysis of Apoptotic Pathways. *Cell Death Differ.* **2008**, *15* (2), 322−331.
(31) Boxer, M. B.; Quinn, A. M.; Shen, M.; Jadhav, A.; Leister, W.; Simeonov, A.; Auld, D. S.; Thomas, C. J. A Highly Potent and Selective Caspase 1 Inhibitor That Utilizes a Key 3-Cyanopropanoic Acid Moiety. *ChemMedChem* **2010**, *5* (5), 730.
(32) Maillard, M. C.; Brookfield, F. A.; Courtney, S. M.; Eustache, F. M.; Gemkow, M. J.; Handel, R. K.; Johnson, L. C.; Johnson, P. D.; Kerry, M. A.; Krieger, F.; Meniconi, M.; Muñoz-Sanjuán, I.; Palfrey, J. J.; Park, H.; Schaertl, S.; Taylor, M. G.; Weddell, D.; Dominguez, C. Exploiting Differences in Caspase-2 and −3 S2 Subsites for Selectivity: Structure-Based Design, Solid-Phase Synthesis and in Vitro Activity of Novel Substrate-Based Caspase-2 Inhibitors. *Bioorg. Med. Chem.* **2011**, *19* (19), 5833−5851.
(33) Singh, G.; Liu, P.; Yao, K. R.; Strasser, J. M.; Hlynialuk, C.; Leinonen-Wright, K.; Teravskis, P. J.; Choquette, J. M.; Ikramuddin, J.; Bresinsky, M.; Nelson, K. M.; Liao, D.; Ashe, K. H.; Walters, M. A.; Pockes, S. Caspase-2 Inhibitor Blocks Tau Truncation and Restores Excitatory Neurotransmission in Neurons Modeling FTDP-17 Tauopathy. *ACS Chem. Neurosci.* **2022**, *13* (10), 1549−1557.
(34) Forster, L.; Vallaster, B.; Hubmann, A.; Bresinsky, M.; Fuller, J. L.; Shi, K.; Lapcinski, I. P.; Liu, P.; Yang, M.; Strasser, J. M.; Nelson, K. M.; John, K.; Mudaliar, D.; Wirth, L.; Daschner, J.; Pongratz, H.; Ashe, K. H.; Walters, M. A.; Pockes, S. Potent and Selective Caspase-2 Inhibitors: Biological Profiling, Structural Characterization, and Challenges of Molecular Instability *J. Med. Chem.* **2026**, DOI: 10.1021/acs.jmedchem.6c01370.
(35) Gampe, C.; Verma, V. A. Curse or Cure? A Perspective on the Developability of Aldehydes as Active Pharmaceutical Ingredients. *J. Med. Chem.* **2020**, *63* (23), 14357−14381.
(36) Brogi, S.; Ibba, R.; Rossi, S.; Butini, S.; Calderone, V.; Gemma, S.; Campiani, G. Covalent Reversible Inhibitors of Cysteine Proteases Containing the Nitrile Warhead: Recent Advancement in the Field of Viral and Parasitic Diseases. *Molecules* **2022**, *27*, 2561.
(37) Gehringer, M.; Laufer, S. A. Emerging and Re-Emerging Warheads for Targeted Covalent Inhibitors: Applications in Medicinal Chemistry and Chemical Biology. *J. Med. Chem.* **2019**, *62* (12), 5673−5724.
(38) Otto, H.-H.; Schirmeister, T. Cysteine Proteases and Their Inhibitors. *Chem. Rev.* **1997**, *97* (1), 133−172.
(39) Augeri, D. J.; Robl, J. A.; Betebenner, D. A.; Magnin, D. R.; Khanna, A.; Robertson, J. G.; Wang, A.; Simpkins, L. M.; Taunk, P.; Huang, Q.; Han, S.-P.; Abboa-Offei, B.; Cap, M.; Xin, L.; Tao, L.; Tozzo, E.; Welzel, G. E.; Egan, D. M.; Marcinkeviciene, J.; Chang, S. Y.; Biller, S. A.; Kirby, M. S.; Parker, R. A.; Hamann, L. G. Discovery and Preclinical Profile of Saxagliptin (BMS-477118): A Highly Potent, Long-Acting, Orally Active Dipeptidyl Peptidase IV Inhibitor for the Treatment of Type 2 Diabetes. *J. Med. Chem.* **2005**, *48* (15), 5025−5037.
(40) Owen, D. R.; Allerton, C. M.; Anderson, A. S.; Aschenbrenner, L.; Avery, M.; Berritt, S.; Boras, B.; Cardin, R. D.; Carlo, A.; Coffman, K. J.; et al. An Oral SARS-CoV-2 Mpro Inhibitor Clinical Candidate for the Treatment of COVID-19. *Science* **2021**, *374* (6575), 1586−1593.
(41) Schweizer, A.; Briand, C.; Grütter, M. G. Crystal Structure of Caspase-2, Apical Initiator of the Intrinsic Apoptotic Pathway. *J. Biol. Chem.* **2003**, *278* (43), 42441−42447.
(42) Chauvier, D.; Ankri, S.; Charriaut-Marlangue, C.; Casimir, R.; Jacotot, E. Broad-Spectrum Caspase Inhibitors: From Myth to Reality? *Cell Death Differ.* **2007**, *14* (2), 387−391.
(43) Chauvier, D.; Renolleau, S.; Holifanjaniaina, S.; Ankri, S.; Bezault, M.; Schwendimann, L.; Rousset, C.; Casimir, R.; Hoebeke, J.; Smirnova, M.; Debret, G.; Trichet, A.-P.; Carlsson, Y.; Wang, X.; Bernard, E.; Hébert, M.; Rauzier, J.-M.; Matecki, S.; Lacampagne, A.; Rustin, P.; Mariani, J.; Hagberg, H.; Gressens, P.; Charriaut-Marlangue, C.; Jacotot, E. Targeting Neonatal Ischemic Brain Injury with a Pentapeptide-Based Irreversible Caspase Inhibitor. *Cell Death Dis.* **2011**, *2* (9), e203.
(44) Algera, R. F.; Allais, C.; Baldwin, A. F.; Becirovic, H.; Bowles, P.; Brown, A. R.; Buske, J. M.; Clarke, H. J.; Do, N. M.; Doyle, K.; Fifer, J.; Gray, K.; Happe, A.; Hardink, M.; Hubbell, A. K.; James, C.; Khadamkar, H. P.; Magano, J.; McInturff, E. L.; Mustakis, J.; Ozbuyukkaya, G.; Piper, J. L.; Place, D. W.; Ragan, J. A.; Rauschenberger, B.; Reyes, G.; Shehadeh, R.; Stanchina, C.; Stanley, M.; Weekly, R. M.; Weinstein, E.; Weisenburger, G. A.; Wood, E.; Yayla, H. G.; Yu, S. Synthesis of Nirmatrelvir: Development of an Efficient, Scalable Process to Generate the Western Fragment. *Org. Process Res. Dev.* **2023**, *27* (12), 2240−2249.
(45) Bosc, E.; Anastasie, J.; Soualmia, F.; Coric, P.; Kim, J. Y.; Wang, L. Q.; Lacin, G.; Zhao, K.; Patel, R.; Duplus, E.; Tixador, P.; Sproul, A. A.; Brugg, B.; Reboud-Ravaux, M.; Troy, C. M.; Shelanski, M. L.; Bouaziz, S.; Karin, M.; El Amri, C.; Jacotot, E. D. Genuine Selective Caspase-2 Inhibition with New Irreversible Small Peptidomimetics. *Cell Death Dis.* **2022**, *13* (11), No. 959.
(46) Cheewawisuttichai, T.; Hurst, R. D.; Brichacek, M. Transformation of Aldehydes into Nitriles in an Aqueous Medium Using O-Phenylhydroxylamine as the Nitrogen Source. *Carbohydr. Res.* **2021**, *502*, No. 108282.
(47) Cserjan-Puschmann, M.; Lingg, N.; Engele, P.; Kröß, C.; Loibl, J.; Fischer, A.; Bacher, F.; Frank, A.-C.; Öhlknecht, C.; Brocard, C.; et al. Production of Circularly Permuted Caspase-2 for Affinity Fusion-Tag Removal: Cloning, Expression in *Escherichia Coli*, Purification, and Characterization. *Biomolecules* **2020**, *10* (12), 1592.
(48) Fang, B.; Boross, P. I.; Tozser, J.; Weber, I. T. Structural and Kinetic Analysis of Caspase-3 Reveals Role for S5 Binding Site in Substrate Recognition. *J. Mol. Biol.* **2006**, *360* (3), 654−666.
(49) Wager, T. T.; Hou, X.; Verhoest, P. R.; Villalobos, A. Central Nervous System Multiparameter Optimization Desirability: Application in Drug Discovery. *ACS Chem. Neurosci.* **2016**, *7* (6), 767−775.
(50) Tang, Y.; Wells, J. A.; Arkin, M. R. Structural and Enzymatic Insights into Caspase-2 Protein Substrate Recognition and Catalysis. *J. Biol. Chem.* **2011**, *286* (39), 34147−34154.
(51) Denault, J.-B.; Salvesen, G. S. Expression, Purification, and Characterization of Caspases. *Curr. Protoc. Protein Sci.* **2002**, *30* (1), 21.13.1−21.13.15.
(52) Cheng, Y.; Prusoff, W. H. Relationship between the Inhibition Constant (K1) and the Concentration of Inhibitor Which Causes 50 per Cent Inhibition (I50) of an Enzymatic Reaction. *Biochem. Pharmacol.* **1973**, *22* (23), 3099−3108.
(53) Fuller, J. L.; Shi, K.; Pockes, S.; Finzel, B. C.; Ashe, K. H.; Walters, M. A. Reengineering of Circularly Permuted Caspase-2 to Enhance Enzyme Stability and Enable Crystallographic Studies. *ACS Chem. Biol.* **2025**, *20* (4), 845−857.
(54) Kabsch, W. XDS. *Acta Crystallogr., Sect. D: Biol. Crystallogr.* **2010**, *66* (Pt 2), 125−132.
(55) McCoy, A. J.; Grosse-Kunstleve, R. W.; Adams, P. D.; Winn, M. D.; Storoni, L. C.; Read, R. J. Phaser Crystallographic Software. *J. Appl. Crystallogr.* **2007**, *40* (Pt 4), 658−674.
(56) Adams, P. D.; Afonine, P. V.; Bunkóczi, G.; Chen, V. B.; Davis, I. W.; Echols, N.; Headd, J. J.; Hung, L.-W.; Kapral, G. J.; Grosse-Kunstleve, R. W.; et al. PHENIX: A Comprehensive Python-Based System for Macromolecular Structure Solution. *Acta Crystallogr., Sect. D: Biol. Crystallogr.* **2010**, *66* (2), 213−221.
(57) Emsley, P.; Lohkamp, B.; Scott, W. G.; Cowtan, K. Features and Development of Coot. *Acta Crystallogr., Sect. D: Biol. Crystallogr.* **2010**, *66* (4), 486−501.

Downloaded from pubs.acs.org/jmcmar/article-pdf/doi/10.1021/acs.jmedchem.6c01371/6909867/acs.jmedchem.6c01371.pdf by UNIV REGENSBURG user on 17 November 2026